Earth-Science Reviews 238 (2023) 104323

Contents lists available at ScienceDirect

Earth-Science Reviews

journal homepage: www.elsevier.com/locate/earscirev

What role does anoxia play in exceptional fossil preservation? Lessons from the taphonomy of the Posidonia Shale (Germany)

A.D. Muscente [a], Olivia Vinnes [a], Sinjini Sinha [b], James D. Schiffbauer [c,d], Erin E. Maxwell [e], Günter Schweigert [e], Rowan C. Martindale [b,*]

[a] Department of Geology, Cornell College, 600 First Street SW, Mount Vernon, Iowa 52314, USA
[b] Department of Geological Sciences, The University of Texas at Austin, 2275 Speedway, Austin, TX 78712, USA
[c] Department of Geological Sciences, University of Missouri, 101 Geological Sciences Building, Columbia, MO 65211, USA
[d] X-ray Microanalysis Laboratory, University of Missouri, 1 Geological Sciences Building, Columbia, MO 65211, USA
[e] Staatliches Museum für Naturkunde, Rosenstein 1, 70191 Stuttgart, Germany

ARTICLE INFO

Keywords:
Oceanic Anoxic Event
Redox
Lagerstätte
Geomicrobiology
Sedimentology
Palaeontology

ABSTRACT

Konservat-Lagerstätten—deposits with exceptionally preserved fossils of articulated multi-element skeletons and soft tissues—offer the most complete snapshots of ancient organisms and communities in the geological record. One classic example, the Posidonia Shale in southwestern Germany, contains a diverse array of fossils preserved during the ~183 Ma Toarcian Oceanic Anoxic Event. Seminal work on this deposit led to the hypothesis that many Konservat-Lagerstätten were preserved in stagnant basins, where anoxic conditions limited soft tissue degradation. To date, however, no studies have thoroughly investigated the geomicrobiological processes that drove fossil mineralization in the Posidonia Shale. As a result, the role of anoxia in its exceptional preservation remains uncertain. Here, we address these issues by reviewing the geology of the Posidonia Shale; describing the mineralization of its fossils; and synthesizing novel and existing data to develop a new model for the paleoenvironment and taphonomy of the Lagerstätte. Although shells and carbonate skeletal elements were preserved as pyritized and carbonaceous fossils, non-biomineralized tissues were primarily preserved via phosphatization (transformation of remains into calcium phosphate minerals). Unambiguous examples of phosphatization include ammonite shells, crustacean carapaces, ichthyosaur remains, coprolites, and coleoid gladii, mantle tissues, and ink sacs. Phosphatized crustaceans and coleoids contain cracks filled with pyrite, sphalerite, and aluminosilicate minerals. Such cracks were likely generated during burial compaction, which fractured phosphatized tissues, exposed their organic matter to focused microbial sulfate reduction, and thereby led to formation of, and infilling by, sulfide and clay minerals. These observations indicate that phosphatization happened early in diagenesis, prior to burial compaction and microbial sulfate reduction, beneath (sub)oxic bottom water, and corroborate the hypothesis that the animals were preserved during ephemeral pulses of oxygenation in the basin and/or within environments located along boundaries of anoxic water bodies. Overall, our findings support the view that anoxic bottom water does not directly promote exceptional preservation; in fact, it may impede it. Konservat-Lagerstätten, particularly "stagnation deposits", tend to form in (sub)oxic depositional environments with steep redox gradients and/or high sedimentation rates. Under these conditions, organisms are rapidly buried below the redox boundary, where their mineralization is promoted by focused geomicrobiological processes, and degradation is limited by the supply of oxidants in the microenvironments around them.

1. Introduction

In the marine fossil record, remains of labile (non-biomineralized) tissues are considerably rarer than biomineralized elements, like shells, bones, and teeth (Muscente et al., 2017). This bias is a consequence of physical, chemical, and biological processes that affect the bodies of organisms around the time of death. Predation, scavenging, and various other physical forces contribute to transport, breakage, and disarticulation of delicate morphological features and multi-element skeletons (Allison and Briggs, 1991). Labile tissues, including integuments that

* Corresponding author.
E-mail address: Martindale@jsg.utexas.edu (R.C. Martindale).

https://doi.org/10.1016/j.earscirev.2023.104323
Received 16 June 2022; Received in revised form 2 January 2023; Accepted 12 January 2023
Available online 23 January 2023

cover skeletal elements as well as the connective tissues that bind them, readily decay and decompose under the influence of microbial metabolic activities (Allison and Briggs, 1991; Briggs, 2003). These processes lead to complete degradation of all tissues, muscles, and organs in most cases. Consequently, most marine animals (perhaps 80% to 90%) leave no identifiable remains (Briggs, 1991; Sperling, 2013) resulting in the overrepresentation of biomineralizing organisms that only represent a fraction of total biodiversity (Schopf, 1978; Allison and Briggs, 1991; Valentine, 1989; Shaw et al., 2021).

Konservat-Lagerstätten are geologic deposits with fossils that exhibit minimal alteration from degradation (Seilacher, 1970); the 'exceptionally preserved fossils' in such deposits variably include remains of labile tissues and articulated multi-element skeletons (Seilacher and Westphal, 1971; Seilacher et al., 1985). Because such fossils are rare or absent in most deposits, Konservat-Lagerstätten represent significant sources of paleontological information, both in terms of quality and quantity. They provide relatively complete pictures of the biodiversity and ecology of ancient ecosystems as well as the complex morphologies of ancient organisms (Allison, 1988a). For these reasons, Konservat-Lagerstätten are substantially researched by paleontologists, paleobiologists, and sedimentary geologists.

Exceptional preservation occurs where the bodies of deceased organisms survive degradation long enough to become buried in sediment, and in cases of labile tissue preservation, experience geomicrobiological and other authigenic and diagenetic processes that transform them into recalcitrant materials and minerals that can endure over geologic timescales (Briggs, 2003). Trends in occurrences of exceptionally preserved fossils suggest that their preservation depends on phenomena that can be expressed at local, regional, and global scales (Allison and Briggs, 1993; Muscente et al., 2017). Such phenomena influence the physical forces, geochemical gradients, and biological processes that contribute to soft tissue degradation (e.g., predation, scavenging, and microbial decay), and in some cases, may directly promote fossil mineralization. Local and regional factors that affect preservational potential include water circulation (Seilacher et al., 1985), topography and/or bathymetry (Muscente et al., 2017), climate (Allison and Briggs, 1993; Briggs, 2003), sediment composition and provenance (Anderson et al., 2018), sedimentation rate (Brett et al., 2012; Schiffbauer et al., 2014b), and sedimentary processes related to transport, deposition, and bioturbation (Brett et al., 2012). Global secular changes in the composition of seawater and frequency or prevalence of geomicrobiological agents (e.g., sediment-mixing animals and microbial mats) over Earth history may have also affected the potential for exceptional fossil preservation (Allison, 1988a; Allison and Briggs, 1993; Butterfield, 2003; Muscente et al., 2017). Due to the wide variety of factors that affect fossil degradation and mineralization, the drivers of exceptional preservation in many Konservat-Lagerstätten are not straightforward.

Redox conditions set the stage for exceptional preservation in marine settings. In the modern ocean, the concentration of dissolved oxygen varies with depth, such that the lowest levels occur in the oxygen minimum zone (water depths between 200 and 1000 m) and within the sediment (Levin, 2003). Whereas anoxic (~0 mg O_2 per liter), suboxic (0–0.2 mg O_2 per liter), and dysoxic (0.2–2 mg O_2 per liter) conditions are localized to the oxygen minimum zone and intermediate to deep sediment, oxic conditions (>2 mg O_2 per liter) typically prevail in all other environments (Rhoads and Morse, 1971; Tyson and Pearson, 1991). Oxic and anoxic water masses are separated by redox gradients, including the gradual decline in oxygen concentration that begins at the sediment-water interface and extends downward into pore water environments (discussed in Muscente et al., 2017). Environments along these gradients are inhabited by successions of microbial communities stratified from the water column down into the sediment. These microorganisms utilize different oxidants for respiration in order of availability and decreasing energy yield: O_2 > NO_3 > Mn(IV) > Fe(III) > SO_4 > CO_2 (van Gemerden, 1993; Lyons et al., 1996; Briggs, 2003). These metabolic pathways have different rates of degradation, and anaerobic processes (those which occur under anoxic conditions) produce chemical by-products (e.g., H_2S and CO_3^{2-}) that can serve as ionic building blocks for mineral precipitation and fossil preservation under some circumstances (discussed in Muscente et al., 2017). Exceptional fossil preservation occurs under redox conditions where decomposition of organic material does not proceed to completion and/or the rate of mineralization exceeds the speed of degradation (e.g., Butterfield, 2003; Muscente et al., 2017).

Marine Konservat-Lagerstätten are thought to form in settings with low levels of oxygen. Most marine Lagerstätten were preserved prior to the late Paleozoic (Muscente et al., 2017), when oceanic oxygen levels were relatively low and anoxic bottom waters were widespread (Dahl et al., 2010; Gill et al., 2011; Sperling et al., 2015; Edwards et al., 2017). During the Mesozoic and Cenozoic, exceptional fossil preservation primarily occurred in marine environments during Oceanic Anoxic Events (OAEs), or brief (~1 Ma) episodes of oxygen minimum zone expansion in the ocean (Jenkyns, 2010; Takashima et al., 2006). Konservat-Lagerstätten were deposited during OAEs in both the Jurassic (e.g., Doyle, 1990; Röhl et al., 2001; Ansorge, 2003; Riccardi, 2005; Williams et al., 2015; Martindale et al., 2017; Muscente et al., 2019; Sinha et al., 2021) and Cretaceous (e.g., Feldmann et al., 1999; Ifrim et al., 2007; Li et al., 2008; Martill et al., 2011; Klug et al., 2012). The hypoxic-to-anoxic conditions that developed during OAEs may have enhanced exceptional preservation in several ways. In some marine regions OAEs likely limited aerobic microbial degradation and reduced the abundance of predators, scavengers, and sediment-mixing animals, which require high concentrations of oxygen. These conditions may have also influenced geochemical cycles in ways that favored mineralization of labile remains (Muscente et al., 2019; Sinha et al., 2021). Therefore, OAEs likely contributed to exceptional preservation, not simply by limiting the destruction of soft tissues, but also by promoting their transformation into recalcitrant minerals (minerals that persisted in the fossil record).

The circumstances that led to Konservat-Lagerstätten formation during OAEs remain ambiguous. During each event, the boundary between oxic and anoxic water was variably positioned, at times and places, above and below the sediment-water interface. Exceptional preservation may have occurred in environments where anoxic conditions remained limited to the sediment, where they extended up into the water column, or both (Seilacher et al., 1985). Because microorganisms with anaerobic metabolic pathways can degrade organic matter as rapidly as aerobic organisms (Allison, 1988b), bottom water anoxia may not have guaranteed survival of soft tissues. Localization of the oxic/anoxic boundary to sediment, on the other hand, may have established focused geomicrobiological processes and sedimentary microenvironments conducive to fossil mineralization (Allison, 1988b; Briggs et al., 1996; Muscente et al., 2015a; Guan et al., 2017). If so, exceptional preservation during Mesozoic OAEs may have been limited to environments located along the boundaries of anoxic water masses and/or times with fluctuating redox conditions that favored establishment of steep redox gradients across the sediment-water interface (Muscente et al., 2019; Sinha et al., 2021). This may imply that the geographic and stratigraphic distributions of Konservat-Lagerstätten reflect temporal and spatial patterns in redox gradients during OAE events.

The marine Posidonienschiefer Formation (Fm.) of western Europe contains several Konservat-Lagerstätten related to the Early Jurassic OAE (Riegraf et al., 1984; Ansorge, 2003). Its most famous deposit—the 'Posidonia Shale Konservat-Lagerstätte'—crops out as black oil shales in the state of Baden-Württemberg of southwestern Germany (Hauff, 1921; Hauff and Hauff, 1981; Röhl et al., 2001). The Posidonia Shale contains a variety of exceptionally preserved fossils, including gladii, ink sacs, and tentacles of coleoids (Přikryl et al., 2012; Jenny et al., 2019; Klug et al., 2021a); articulated exoskeletons of crustaceans (Schweigert et al.,

2003; Schweigert, 2013; Klug et al., 2021b); articulated bodies of crinoids attached to driftwood (Hess, 1999; Matzke and Maisch, 2019); and fully articulated skeletons of large vertebrates, such as ichthyosaurs, crocodylomorphs, plesiosaurs, pterosaurs, and fishes (Hauff, 1921; Urlichs et al., 1979; Hauff and Hauff, 1981; Riegraf et al., 1984; Lingham-Soliar, 2001; van Loon, 2013; Dick, 2015; Lindgren et al., 2018; Eriksson et al., 2022; Maxwell et al., 2022). Some of the vertebrate fossils are preserved with remains of embryos, skin, digestive tracts, and stomach contents (Urlichs et al., 1979; Hauff and Hauff, 1981). The Konservat-Lagerstätte also contains an abundance of ammonites, bivalves, and belemnites (Hauff, 1921; Urlichs et al., 1979; Riegraf et al., 1984; Seilacher et al., 1976; Seilacher, 1980); rare gastropods, brachiopods, echinoderms, serpulids, ostracods, and foraminifers (Hauff, 1921; Riegraf et al., 1984; Schmid-Röhl and Röhl, 2003); and various types of trace fossils, including burrows (Izumi, 2012; Izumi et al., 2014; Rodríguez-Tovar, 2021), coprolites (Seilacher et al., 1985), and regurgitated stomach contents often called speiballen (Thies and Hauff, 2012). These fossils were primarily preserved in organic-rich mud beneath the Tethys Ocean during the ~183 Ma Toarcian OAE (TOAE). Various observations indicate that fossilization occurred in environments with oxygen deficient water masses (Schouten et al., 2000; Röhl et al., 2001; Röhl and Schmid-Röhl, 2005; Dickson et al., 2017; Them et al., 2018), and the Posidonia Shale deposit itself was the basis of the hypothesis that Konservat-Lagerstätten tend to form in stagnant basins with restricted water circulation (Seilacher and Westphal, 1971; Seilacher et al., 1985). The Posidonia Shale, therefore, provides an ideal opportunity to explore the effects of ocean deoxygenation on exceptional preservation.

To date, no studies have thoroughly described the mineralization of fossils in the Posidonia Shale. It is generally thought that bivalves consist of calcite, except where their internal and external surfaces are lined with pyrite (Seilacher et al., 1976; Riegraf et al., 1984). Purportedly, ammonite shells were dissolved during diagenesis, leaving behind their outer organic layers (periostraca), which were compressed during burial and subsequently replaced by pyrite (Schmid-Röhl, 2021). Such fossils may exemplify the preservational process of pyritization in which geomicrobiological activities cause pyrite to form within, and ultimately replace, tissues (Briggs et al., 1996; Schiffbauer et al., 2014b; Guan et al., 2017). In recent years, various works have highlighted soft tissue remains that experienced a similar process—phosphatization—which converted them into apatite minerals (Briggs et al., 1993; Schiffbauer et al., 2014a; Muscente et al., 2015a). Phosphatized fossils of the Posidonia Shale include ichthyosaur skin and integument (Lingham-Soliar, 2001; Lindgren et al., 2018); coleoid gladii and ink sacs (Jenny et al., 2019; Klug et al., 2021a, 2021b; Sinha et al., 2021); crustacean exoskeletons (Schweigert et al., 2003; Sinha et al., 2021); and coprolites (Seilacher et al., 1985). Reports also indicate that some pyritized and phosphatized fossils contain sulfur-bearing minerals such as barite and sphalerite, along with aluminosilicate minerals and carbonaceous materials (Sinha et al., 2021), including a compact form of lignite called "jet" (Urlichs et al., 1979; Seilacher et al., 1985). To date, the paragenesis of these minerals and materials has not been described fully; therefore, our understanding of the taphonomy of the Posidonia Shale remains incomplete.

In this paper, we review the sedimentology, stratigraphy, and geochemistry of the Posidonia Shale with emphasis on its age, depositional environment, and diagenetic history. We also review the occurrence of exceptionally preserved fossils in the Posidonienschiefer Fm. providing detailed descriptions of the compositions, mineralogies, and microstructures of these fossils. Synthesizing these datasets, we reconstruct the preservational environment of the Posidonia Shale Konservat-Lagerstätte and provide a new taphonomic model based on geomicrobiological processes and redox gradients. This work provides a critical analysis of the role that anoxia plays in exceptional preservation, and sheds light on the origins of 'stagnation deposits' (Seilacher and Westphal, 1971; Seilacher et al., 1985).

2. Previous work on the Posidonienschiefer Formation

2.1. Regional geology

Lower Jurassic rocks were deposited in multiple basins (e.g., the Paris, Yorkshire/Cleveland, Northwestern German, and Southwestern German basins) beneath the European Epicontinental Sea on the northwestern side of the Tethys Ocean (Fig. 2) (Thierry, 2000; Röhl et al., 2001; Röhl and Schmid-Röhl, 2005; McCann, 2008; Ullmann et al., 2020; Müller et al., 2020). Water circulation among basins was influenced by sea level, climate, and landmass locations. The sediment of the Posidonienschiefer Fm. accumulated within the Southwestern German Basin, between the Bohemian, Rhenish, and Central massifs at latitudes around 30°N to 35°N (Galasso et al., 2021, and references therein). Oriented belemnite rostra at Holzmaden (Brenner, 1976) and Dotternhausen (Röhl et al., 2001; Röhl and Schmid-Röhl, 2005) suggest that westerly bottom currents predominated in the area. The currents may have also been influenced by basinal contours during the Toarcian *Hildoceras bifrons* biozone (Brenner and Seilacher, 1978). The Posidonienschiefer Fm. and similar, coeval units, such as the Jet Rock Fm. (England), Schistes Carton Fm. (France), Grandcourt Fm. (Belgium), and Rietheim Member of Staffelegg Fm. (Reisdorf et al., 2011) record widespread deposition of bituminous facies, such as black shales and oil shales, across the European Epicontinental Sea during the Toarcian (Fig. 2B) (McCann, 2008). Insects and other exceptionally preserved fossils (Ansorge, 2003) have been reported from outcrops in many of these areas (e.g., Braunschweig and Mistelgau).

The Swabian Alb, also known as the 'Swabian Jura' or 'Swabian Alps', represents an extension of the Jura Mountains between France and Switzerland (Fig. 1B). These mountains give their name to the Jurassic System as a whole, and the Swabian Alb is often credited as the 'birthplace' of zonal stratigraphy (Urlichs, 1977), as some of the first lithostratigraphic and biostratigraphic divisions of the geologic record emerged from seminal work in this area. Buch (1839) divided the Jurassic of Germany into three lithostratigraphic units—the Schwarzer Jura ("Black Jurassic", in which the Posidonienschiefer is found), Brauner Jura ("Brown Jurassic"), and Weißer Jura ("White Jurassic")—based on predominant rock colors (roughly corresponding to Lower, Middle, and Upper Jurassic).

The Posidonienschiefer Fm. received its name from Quenstedt (1843), who described it as the "Posidonienschiefer mit Stinksteinen" (or "Posidonia Slate with stinking stones") as it contained many bivalve fossils belonging to the family Posidoniidae, including *Bositra buchi* (formerly *Posidonia ornata*) and *Steinmannia bronni* (formerly *Posidonia bronni* var. *magna*). The formation belongs to the Lias Group of western and northern Europe, and crops out in northeastern and southwestern Germany, southern Luxembourg, northwestern Austria, and the Netherlands. Exceptionally preserved marine animals occur primarily in the state of Baden-Württemberg, Germany (Fig. 1A), where the Posidienschiefer Fm. crops out in the northwestern foreland of the Swabian Alb (Fig. 1B), a northeast-to-southwest trending mountain belt that spans from Nördlingen to Waldshut (Riegraf et al., 1984). These outcrops represent the classically defined 'Posidonia Shale Konservat-Lagerstätte' (e.g., Seilacher et al., 1985).

Most of the exceptionally preserved fossils have been collected from quarries in the central part of the Swabian Alb; areas around Dotternhausen (Fig. 1C) and Holzmaden (Fig. 1D) have received the most attention from professional geologists and fossil collectors (e.g., Hauff, 1921; Hauff and Hauff, 1981; Schmid-Röhl, 2021). Hauff (1921) reported fossils from dozens of locations near Holzmaden, Ohmden, Zell unter Aichelberg, and Bad Boll; most were quarries that are now closed. Nonetheless, quarries remain active in the area, particularly near the villages of Holzmaden and Ohmden as well as Dotternhausen and nearby Dormettingen. Historically, the Posidonienschiefer Fm. has been a major source of raw materials and was regularly mined for fuel, cement, and stone slabs. Thus, our current understanding of the Posidonia Shale

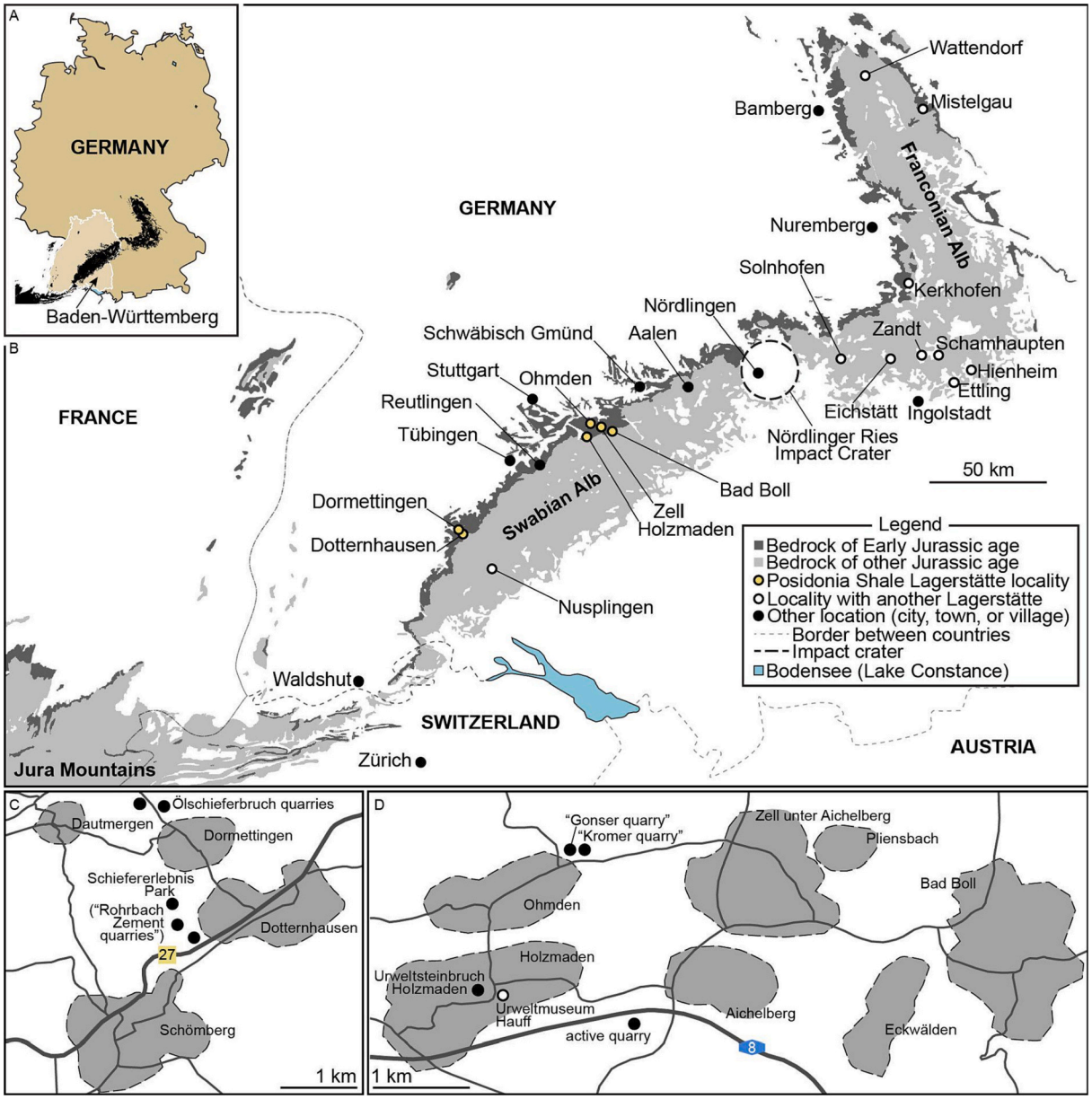

Fig. 1. Maps of the Posidonia Shale. (A) Map of Germany; the state of Baden-Württemberg and mountain ranges are highlighted. (B) Map showing outcrops of Lower Jurassic strata in the Swabian Alb, Franconian Alb, and Jura Mountains of southern Germany, northwestern Switzerland, and southeastern France, based on illustrations in various works (e.g., Urlichs, 1977; Riegraf et al., 1984; Riegraf, 1985; Röhl et al., 2001; etc.). (C) Map of the villages, municipalities, fossil localities, and major roads around Dotternhausen and Dormettingen. In this area, fossils are preserved at various locations, including the active Ölschieferbruch and "Rohrbach Zement" quarries (Röhl and Schmid-Röhl, 2005) as well as the Schiefererlebnis Park; all of which are now owned and operated by the Holcim (Süddeutschland) GmbH company (Schmid-Röhl, 2021). (D) Map of the villages, municipalities, roads, fossil localities, and museums around Holzmaden and Ohmden.

Konservat-Lagerstätte comes from centuries of work on its geology and palaeontology.

Subsequently, Quenstedt (1843, p. 122) adopted these units (today in the ranking of groups) and subdivided the Schwarzer Jura (Schwarzjura Group) into multiple lithologic units. Quenstedt (1843) did not assign names to these lithologic units, but instead, described them in chapters labeled with Greek letters between alpha (α) and zeta (ζ), which were subsequently adopted as identifiers for the strata (e.g., Hauff, 1921; Urlichs, 1977; Riegraf et al., 1984). According to Quenstedt's nomenclature, the Posidonienschiefer Fm. represents the epsilon (ε) unit of the Schwarzer Jura, Unterer Jura, or Lower Jurassic (Quenstedt, 1843). Only recently has the use of the Greek identifiers been formally abandoned and replaced by formation names (Mönnig et al., 2018).

2.2. Lithostratigraphy

In the central Swabian Alb, the Posidonienschiefer Fm. overlies the Amaltheenton Fm. and lies below the Jurensismergel Fm. (Fig. 3). In this area, it is roughly 5 to 15 m thick (Urlichs, 1977; Riegraf et al., 1984), and informally divided into three members (Quenstedt, 1858; Hauff, 1921): Member I (εI), Member II (εII), and Member III (εIII). The major lithological components are clay minerals (aluminum phyllosilicates), quartz, pyrite, and organic matter in addition to fecal pellets and coccoliths, which represent the bulk of the carbonate material (Riegraf et al., 1984). In general, Member I consists of non-laminated terrigenous and calcareous mudstones ('marls') and contains few benthic fossils or bioturbated layers (Riegraf et al., 1984; Röhl et al., 2001). Member II, which represents the local expression of the TOAE (Dickson et al., 2017;

Them et al., 2018), is composed of black, bituminous microlaminated 'oil shales' containing exceptionally preserved fossils but few benthic body or trace fossils (Hauff, 1921; Röhl et al., 2001). Member III also consists of black shale and calcareous mudstone, but the shales include shell beds along with evidence of bioturbation and fossils of benthic animals (Röhl et al., 2001; Schmid-Röhl et al., 2002). All three members also contain limestone interbeds (Fig. 3).

Over the centuries, quarriers have subdivided the Posidonienschiefer Fm. and geologists subsequently adapted these names for their own research (Quenstedt, 1858; Hauff, 1921; Riegraf et al., 1984). One of the most practical stratigraphic schemes was developed by Hauff (1921), who enumerated the strata between Holzmaden and Ohmden (Fig. 3). This scheme commonly appears in the literature, as many of Hauff (1921) 'beds' are easy to identify and can be correlated across the Swabian Alb (e.g., the Unterer Stein and Oberer Stein). Even so, no system of subdivision accurately describes every section, as some beds and units are missing in places (Riegraf et al., 1984). For example, the sections near Holzmaden and Dotternhausen (Figs. 1, 4)—the two areas that have received the most attention for their fossils and sedimentary geology—have notable differences in the upper part of Member II (Fig. 3).

At the boundary between the Amaltheenton and Posidonienschiefer formations, interbedded mudstones and limestones are replaced by blue-gray mudstones of the 'Blaugraue Mergel' (Röhl and Schmid-Röhl, 2005), the lowest layer of Member I (εI). This unit consists of two or three layers of mudstone, including the Blaugraue Mergel and Aschgraue Mergel (Riegraf et al., 1984), separated by two layers of relatively hard yet bituminous black shale (Fig. 3): the Tafelfleins and Seegrasschiefer (Riegraf et al., 1984). By weight percentage, the mudstones are roughly 30–35% carbonate minerals and 65–70% terrigenous material (mostly clay minerals). Depending on the bed, pyrite and organic matter can each represent up to 10% (Riegraf et al., 1984; Röhl et al., 2001). By comparison, the black shales are distinguished by higher pyrite and organic matter content, representing a combined 10–30% by weight, with the remainder largely split between carbonate and terrigenous material (Röhl et al., 2001). Around Dotternhausen (Röhl et al., 2001), the Tafelfleins and Seegrasschiefer are separated by a layer of mudstone, which pinches out toward the northeast around Holzmaden and Ohmden (Fig. 3); there, the Seegrasschiefer directly overlies the Tafelfleins (Hauff, 1921). Except for the Tafelfleins, layers in Member I are non-laminated and highly bioturbated. Although black shales contain very few benthic invertebrate body fossils, the mudstones host a diverse array of benthic body fossils, and trace fossils occur in both mudstones and shales (Röhl et al., 2001). Indeed, the Seegrasschiefer derives its name from the trace fossil *Phymatoderma granulatum*, a subhorizontal branching burrow system that resembles seagrass (Izumi, 2012; Izumi et al., 2014).

The abrupt lithologic transition between the gray mudstones of the Aschgraue Mergel and the overlying black shales of Member II (εII) may reflect a major change in sea level, redox conditions, paleoclimate, and ocean circulation (Röhl et al., 2001; Schmid-Röhl et al., 2002; Röhl and Schmid-Röhl, 2005). The dominant lithology in Member II is black, bituminous oil shale intercalated with limestone beds or "banks". Pyrite concretions, discs, suns, and flowers are common in Member II (Seilacher, 2001), which contains more pyrite and organic matter; the total organic carbon (TOC) is typically less that 1% in Member I versus 4–16% in Member II, and pyrite is typically around 2–3% in Member I versus 8–16% in Member II (Röhl et al., 2001). Member II also contains the largest fecal pellets in the formation (Röhl and Schmid-Röhl, 2005). Although the oil shales near the top of Member II lack distinct laminations (Riegraf et al., 1984), the shales in the lower part of the unit have wavy and lenticular microlaminations of submillimetric scale (Riegraf et al., 1984; Röhl et al., 2001). Light-colored laminae are dominated by carbonate material (coccolith debris, particularly *Schizosphaerella*) and fecal pellets, whereas dark laminae are composed of clay minerals, pyrite, and organic matter (Riegraf et al., 1984). Limestone interbeds also contain clay (10–20%), pyrite (<2%), and bitumen (<2%) in addition to coccolith debris and micritic and sparitic cements (Riegraf et al., 1984; Röhl et al., 2001).

Member II (εII) can be divided into lower ("Unterer Schiefer"), middle ("Mittlerer Schiefer") and upper ("Oberer Schiefer") oil shale units, separated by well-laminated, laterally extensive limestones that serve as regional marker beds (Figs. 3, 4; Urlichs, 1977; Riegraf et al., 1984). The lowest oil shale unit is comprised of the Koblenzer, Hainzen, Fleins (or Schieferfleins), and Unterer Schiefer layers (in ascending order, Hauff, 1921); although the term Unterer Schiefer sometimes refers to all these layers (sensu Pannkoke, 1965), it most commonly refers to the uppermost one of four (sensu Hauff, 1921; Fig. 3). All four layers are evident in sections across the Swabian Alb (Fig. 1) and contain abundant, non-diverse benthic fauna (Hauff, 1921; Riegraf et al., 1984) and are anecdotally known as the best horizons for exceptionally preserved fossils (Hauff, 1921); the Fleins and Unterer Schiefer have yielded some of the most noteworthy coleoids and crustaceans (Riegraf et al., 1984) along with ichthyosaur skin and muscle remains (Heller, 1966; Martin et al., 2021). The various layers differ with respect to color, hardness, stratification, and composition (e.g., bitumen content); all Member II units have microlaminations (Röhl et al., 2001) except for the Koblenzer layer, which is inconsistently laminated and contains faint signs of bioturbation (Riegraf et al., 1984). The Hainzen and Fleins layers are sometimes difficult to distinguish but in general, the Fleins is a relatively hard layer that splits into four slabs of roughly equal thickness, which are used as natural stones for interior decoration and construction (Riegraf et al., 1984). The Unterer Schiefer (sensu Hauff, 1921) has the greatest amount of organic matter, with TOC values as high as 16% (Röhl et al., 2001; Dickson et al., 2017).

The Mittlerer Schiefer and Oberer Schiefer consist of layers of oil shale (>10% TOC), bituminous mudstone (1–10% TOC), and limestone not present at all localities (Fig. 3). The oil shale and bituminous mudstone layers contain less organic matter and pyrite, but more carbonate, than those in the underlying Unterer Schiefer (Riegraf et al., 1984; Röhl et al., 2001; Dickson et al., 2017; Fig. 4). The Mittlerer Schiefer and Unterer Schiefer are separated by the Unterer Stein (Fig. 4), a diagenetic, well-laminated limestone that is laterally extensive across the Swabian Alb (Urlichs, 1977; Riegraf et al., 1984); the Unterer Stein consists of oil shale with lenticular (Röhl et al., 2001) or indistinct lamination (Riegraf et al., 1984), depending on the section. The major strata in the Mittlerer Schiefer include the Schieferklotz, a layer of oil shale known for marine reptiles (Dick, 2015), and the Steinplatte (Fig. 4), a non-laminated diagenetic limestone that sometimes appears yellow in outcrop due to weathering and occurs in sections (Riegraf et al., 1984). Near Holzmaden and Ohmden (Fig. 1), the Mittlerer Schiefer also contains the Wolke oil shale and the Gelbe Platte ("yellow plate"), a limestone that turns yellow during weathering (Hauff, 1921; Riegraf et al., 1984); these layers do not occur at Dotternhausen and Dormettingen (Fig. 3). The Mittlerer Schiefer is overlain by the Oberer Stein (Fig. 4), which is a well-laminated and laterally extensive diagenetic limestone that serves as a regional marker (Fig. 3; Urlichs, 1977; Riegraf et al., 1984).

The Oberer Schiefer exhibits spatial variation in lithology (Urlichs, 1977; Riegraf et al., 1984; Röhl et al., 2001), which hinders correlation; at Dotternhausen and Dormettingen (Fig. 3), it consists of oil shale with lenticular lamination, mudstone with indistinct lamination, and beds of non-laminated limestone like the Obere Bank and the Inoceramenbank (Röhl et al., 2001). The unit's lithology changes toward Holzmaden and Ohmden (Fig. 3), where it is primarily represented by the Falchen and other unnamed shales with irregular and indistinct lamination (Hauff, 1921; Riegraf et al., 1984). In both areas, the Oberer Schiefer includes robust evidence of diverse benthic life in addition to sediment starvation and condensation (Riegraf, 1985; Röhl et al., 2001), such as shell beds and "schlacken", which are clay-rich but well-cemented limestone beds (and possible hardgrounds) with time averaged accumulations of invertebrates and vertebrate debris (Heibert, 1988). These bone beds

occur at multiple levels, and include bivalve and ammonite shells, belemnites, fish scales, as well as bones and teeth of vertebrates (Riegraf et al., 1984). Such layers may represent winnowed lag deposits or hiatuses in sedimentation (Heibert, 1988).

The uppermost unit of the Posidienschiefer Fm.—Member III—is represented by the Wilder Schiefer. Depending on the section, it may consist of bituminous and calcareous mudstone (Röhl et al., 2001) or black shale (Hauff, 1921; Urlichs, 1977; Riegraf et al., 1984). In all cases, it lacks distinct lamination and contains greater amounts of carbonate and lesser amounts of organic matter than the shales in Member II (Riegraf et al., 1984; Röhl et al., 2001). Limestone interbeds include layers of "Nagelkalk" consisting of limestone with cone-in-cone structures (Seilacher, 2001). Shell beds, schlacken, bioturbation, and assemblages of diverse benthic fauna are also relatively common in the Wilder Schiefer, particularly near the top of the unit, where an erosional surface separates it from the Jurensismergel Fm. (Riegraf et al., 1984).

2.3. Biostratigraphy, chemostratigraphy, and relative age of the Lagerstätte

Fossils, including remains of non-biomineralized tissues, occur throughout the Posidonienschiefer Fm. (Hauff, 1921; Riegraf et al., 1984); exceptionally preserved coleoids, crustaceans, fishes, and marine reptiles have been reported from virtually all layers of Member II as well as the Tafelfleins (Member I) and lower Wilder Schiefer (Member III) (e.g., Fig. 3) (Hauff, 1921; Riegraf et al., 1984). Based on observations from local collectors and museum curators, fossils occur in the greatest abundance and highest preservational quality in the Koblenzer, Hainzen, Fleins, and Unterer Schiefer layers. Perhaps correlating with exceptional preservational quality, the most speciose assemblages of coleoids, crustaceans, fishes, and marine reptiles were collected from these layers (Fig. 3), specifically sections near Holzmaden, Ohmden, Bad Boll, and Zell unter Aichelberg (Fig. 1; Hauff, 1921). These taxa are also present in the Tafelfleins, though with lower species diversity (Hauff, 1921). It is possible that the fossils of the Tafelfleins and Wilder Schiefer are either less common or harder to sample than those from Member II; Hauff (1921) reported only the coleoid *Geoteuthis sagittata* and the fish *Dapedium pholidotum* from the Wilder Schiefer, the latter of which has more recently been reported throughout the Posidonia Shale sequence (Urlichs et al., 1979; Thies and Waschkewitz, 2016). In general, the Wilder Schiefer has produced few exceptional fossils, despite representing almost one-third of the section at Holzmaden (Fig. 1) and residing above the water table. While Hauff (1921) assessment is a century old, recent evaluations reported similar distributions of fossils (Riegraf et al., 1984); for example, most coleoids and ichthyosaurs come from the Fleins (Maxwell and Vincent, 2016). Thus, while comparable fossils are found throughout the formation, the greatest abundance and highest fidelity preservation of fossils in the Posidonia Shale Lagerstätte is confined to the lower part of Member II.

The Posidonienschiefer Fm. can be lithologically and biostratigraphically correlated with similar organic-rich black shales that were deposited around the world during the TOAE (Takashima et al., 2006; Jenkyns, 2010; Them et al., 2017a, 2017b; Martindale et al., 2017; Reolid et al., 2021). Biostratigraphy indicates that the Posidonienschiefer Fm. (Fig. 3) spans the uppermost Pliensbachian to the top of the lower Toarcian in the central Swabian Alb (Urlichs, 1977; Riegraf et al., 1984; Riegraf, 1985; Röhl et al., 2001; Maisch, 2021). In the sub-Boreal province of Europe, the lower Toarcian is represented by three chronozones based on ammonite index fossils—*Dactylioceras tenuicostatum, Harpoceras serpentinum*, and *Hildoceras bifrons* biozones (Urlichs, 1977; Page, 2003; Ruebsam and Al-Husseini, 2020) —which are subdivided into ten sub-chronozones. The Pliensbachian/Toarcian boundary corresponds to the contact between the *Pleuroceras spinatum* and *D. tenuicostatum* chronozones (Page, 2003; Ruebsam and Al-Husseini, 2020) within mudstones of the Blaugraue Mergel (Urlichs, 1977; Riegraf et al., 1984; Riegraf, 1985; Röhl et al., 2001). All overlying strata in Member I, as well as the lowest layers of Member II (the Koblenzer, Hainzen, and Fleins), belong to the *D. tenuicostatum* zone, the overlying *H. serpentinum* zone begins in the Unterer Schiefer above the Fleins (Riegraf et al., 1984; Riegraf, 1985). The boundary between the *H. serpentinum* and *H. bifrons* zones falls somewhere in the transition between Members II and III. The shell beds, schlacken, and other condensed units in this transition may represent paraconformities or disconformities that formed during sediment bypass, non-deposition, and/or erosion; however, ammonite biostratigraphy suggests that no subzones are missing (Riegraf et al., 1984; Riegraf, 1985; Röhl and Schmid-Röhl, 2005). The largest stratigraphic gap occurs between the Posidonienschiefer and the stratigraphically condensed Jurensismergel formations (Röhl and Schmid-Röhl, 2005). At Dormettingen, a disconformity separates strata of the *Peronoceras fibulatum* subzone (truncated), from rocks of upper Toarcian age, indicating the absence of the uppermost subzone of the lower Toarcian, the *Catacoeloceras crassum* subchronozone (Maisch and Matzke, 2017). In most other sections the *C. crassum* subzone is recorded in the lowermost bed of the Jurensismergel Fm. (Maisch, 2021). Together, these observations imply that the Posidonia Shale Lagerstätte primarily occurs within the *Dactylioceras semicelatum*, *Harpoceras exaratum*, and *Harpoceras elegans* subchronozones (Fig. 3), and accumulated through, more or less continuous sedimentation (Röhl and Schmid-Röhl, 2005). Biostratigraphic ages have recently been corroborated by *Re*-Os ages (183.0 ± 2.0 Ma) from the Dormettingen section (Fig. 1) (van Acken et al., 2019).

Data on the carbon isotope ($\delta^{13}C$) chemostratigraphy of the Posidonienschiefer Fm. provides additional constraints on the age of the Lagerstätte. These constraints are most evident in the organic carbon isotope ($\delta^{13}C_{org}$) record. Most samples from the Posidonienschiefer Fm. have $\delta^{13}C_{org}$ values around −25 per mil (‰) based on the Vienna Pee Dee Belemnite standard (V-PDB), but a contiguous interval in the lower half of Member II consists of oil shales that have values as low as −32.5‰ V-PDB (Fig. 5). At Dotternhausen, this negative $\delta^{13}C_{org}$ excursion spans from the *D. semicelatum* subzone (*D. tenuicostatum* zone) to the *H. elegans* subzone (*H. serpentinum* zone) but is limited to the oil shale of Member II (Schouten et al., 2000). The $\delta^{13}C_{org}$ value drops to −32‰ at base of the Koblenzer layer, and remains low up to the Mittlerer Schiefer, where it gradually increases back to −25‰ (Schouten et al., 2000; Dickson et al., 2017). This negative carbon isotope excursion is apparent in both organic and inorganic (carbonate) carbon records (Küspert, 1982; Schouten et al., 2000; Dickson et al., 2017), and can be correlated with similar patterns in the $\delta^{13}C$ profiles of Toarcian sections around the world (Al-Suwaidi et al., 2010; Caruthers et al., 2011; Gröcke et al., 2011; Suan et al., 2011; Kemp and Izumi, 2014; Them et al., 2017a). In all sections with reported chemostratigraphic data, the negative $\delta^{13}C$ excursion occurs in the *D. semicelatum*, *H. exaratum*, and/or *H. elegans* subzones, or equivalent units (Ruebsam and Al-Husseini, 2020), and usually in association with black shales (Jenkyns, 2010). Accordingly, the excursion has been interpreted to reflect a major perturbation in the global carbon cycle during the TOAE (Jenkyns, 1985, 1988, 2010). The chemostratigraphy of the Posidonia Shale is often used to correlate units and redox conditions across outcrops and so is an important component of the age model.

2.4. Terrestrial influence

Posidonienschiefer Fm. palynomorphs and organic macerals from the Swabian Alb support the interpretation of a marine setting with little terrestrial influence. The most common palynomorphs are unicellular green algae (Chlorophyta: Prasinophyceae) and ellipsoidal/spherical microfossils, likely remains of algae and/or pollen (Prauss et al., 1991). Dinoflagellates and acritarchs are also common in Members I and III, but definitive fossils of spores and pollen grains are rare, particularly in Member II. Macerals are dominated by lamalginite (produced by algae) and bituminite (produced by algae, zooplankton, and bacteria); vitrinite, inertinite, sporinite, and other macerals from plants are rare

(Prauss et al., 1991). Galasso et al. (2021) note five palynofacies in the Dormettingen section, which correspond to paleoecological turnovers; notably terrestrial organic matter decreases at the end of the *D. tenuicostatum* zone (above the Fleins). Most of the Posidonia Shale wood occurs as large tree-trunks covered by epibionts, like stalked crinoids and bivalves (Hess, 1999; Matzke and Maisch, 2019). The epibionts indicate that the wood drifted into the depositional environments, potentially across large distances. Fossils of other terrestrial organisms, like plants and insects, are preserved at localities in the Northern German Basin (Fig. 2B) and Franconian Alb (Fig. 1B) (Ansorge, 2003). In contrast, terrestrial fossils are rare in the strata exposed along the Swabian Alb, where insects are restricted to the Unterer Stein (e.g., Ansorge, 2003) and washed-out remains of terrestrial vertebrates are also extremely rare (e.g., *Ohmdenosaurus* Wild, 1978). During the Toarcian, the depositional environment of the Posidonia Shale Lagerstätte was presumably located too far away from coastlines for abundant terrestrial fauna.

2.5. Redox conditions

Redox proxy data indicate that bottom water anoxia existed in the Southwestern German Basin during the depositional history of the Posidonienschiefer Fm. (Schouten et al., 2000; Röhl et al., 2001; Röhl and Schmid-Röhl, 2005; Dickson et al., 2017; Them et al., 2018; Wang et al., 2021; Ajuaba et al., 2022). Data include measurements of iron species (Them et al., 2018), molybdenum isotopes (Dickson et al., 2017), thallium isotopes (Them et al., 2018), nitrogen isotopes (Wang et al., 2021), and redox-sensitive biomarkers (Schouten et al., 2000; Ajuaba et al., 2022), in addition to other lithological and geochemical indicators (Röhl et al., 2001; Röhl and Schmid-Röhl, 2005; Rodríguez-Tovar, 2021). Workers commonly cite high organic matter content, presence of microlaminations, occurrence of exceptionally preserved fossils, and abundance of pelagic and planktonic fossils relative to large benthic body and trace fossils (including bioturbation) as evidence of bottom water anoxia (e.g., Röhl et al., 2001; Hess, 1999). Nevertheless, the origins of some of these features, including exceptionally preserved fossils, remain a matter of debate, and interpretations are often circular in nature.

Geochemical proxies for redox conditions can reflect global perturbations in environmental conditions. Thallium isotope ratios, ε^{205}Tl, are reliably recorded in sulfide-bearing minerals and organic matter and vary over time and space in relation to the extent of seafloor oxygenation (Owens et al., 2017). Expansion of anoxic water masses can reduce the global burial rate of manganese oxides, which preferentially adsorb ^{203}Tl over ^{205}Tl (Nielsen et al., 2017), yielding an increase in seawater ε^{205}Tl that becomes reflected in buried sulfides and organic matter. At Dotternhausen (Fig. 5), oil shales near the base of Member II (e.g., the Koblenzer, Hainzen, and Fleins) have greater values of ε^{205}Tl than the black shales (i.e., the Tafelfleins and Seegrasschiefer) of Member I, which suggests the global expansion of oxygen-minimum zones and anoxic water masses in the marine realm (Them et al., 2018). This interpretation is consistent with the onset of the TOAE during the *D. semicelatum* subchronozone (Jenkyns, 1985, 1988, 2010). The repeated fall and rise of ε^{205}Tl values across the rest of the Dotternhausen strata, specifically peaks in the Unterer Schiefer and Mittlerer Schiefer (Fig. 5), may be indicative of multiple deoxygenation events or secular variation in ocean oxygenation (Them et al., 2018).

Molybdenum isotopes, specifically the concentration ratio reported as $\delta^{98/95}$Mo, support variable oxygenation following the nadir of the δ^{13}C excursion. Under anoxic conditions, molybdenum reacts with reduced sulfur species (e.g., H_2S or HS^-) produced by anaerobic processes, leading to the formation and burial of molybdenum-sulfide minerals, such as thiomolybdate (Siebert et al., 2003; Nakagawa et al., 2012). When conditions become oxic or suboxic, manganese-oxyhydroxide minerals can form and adsorb molybdenum onto their surfaces, which favors the lighter isotopes (^{95}Mo) over ^{98}Mo. Thus, bottom-water anoxia causes a decrease in $\delta^{98/95}$Mo (Dickson et al., 2017). The Posidonienschiefer Fm. at Dotternhausen (Fig. 5) records an increase of $\delta^{98/95}$Mo values across the lower Toarcian; $\delta^{98/95}$Mo generally increases from the Seegrasschiefer (Member I) to the top of the formation with notable steps in the *H. elegans* and *H. falciferum* subzones (Dickson et al., 2017). This trend may represent diminishing burial of molybdenum-sulfide relative to manganese-oxyhydroxide over the course of the TOAE (Dickson et al., 2017), and implies a global change

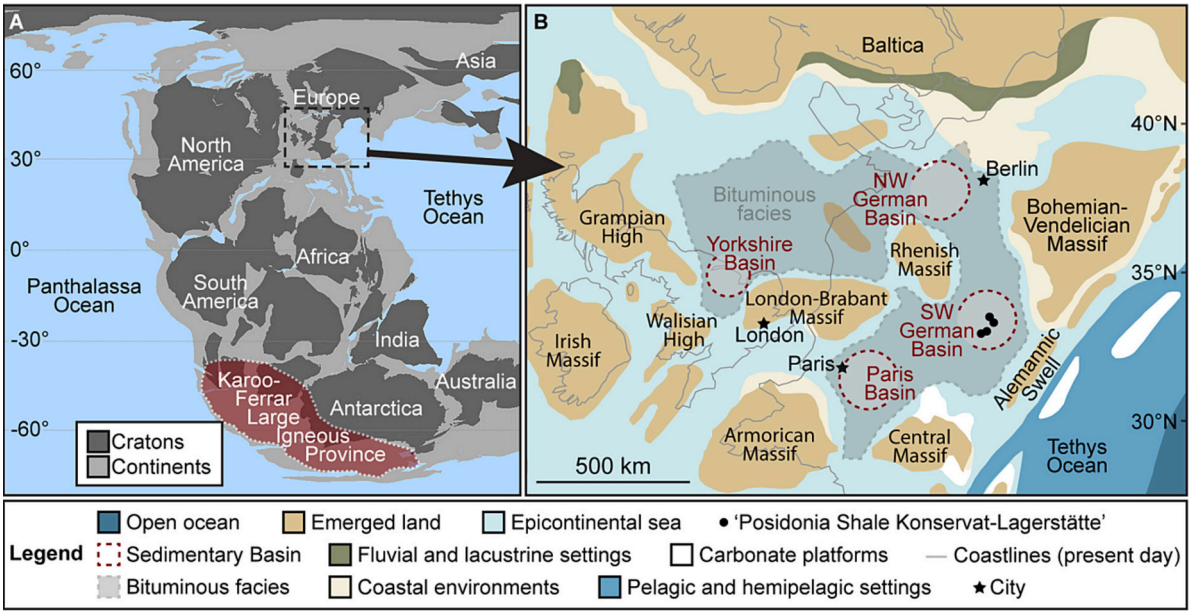

Fig. 2. Palaeogeography of the Posidonia Shale Konservat-Lagerstätte. (A) Paleogeographic map of the world during the ~183 Ma Toarcian Oceanic Anoxic Event (TOAE), produced in GPlates (Müller et al., 2018) using the model of Merdith et al. (2021). Map illustrates the location of Karoo-Ferrar Large Igneous Province, cratons, and continents. (B) Synthesis of paleogeographic maps of the European Epicontinental Sea during TOAE published in various works (Thierry, 2000; Röhl et al., 2001; Röhl and Schmid-Röhl, 2005; Ullmann et al., 2020; Müller et al., 2020). This map illustrates locations of depositional basins relative to emerged land, bituminous facies, and depositional environments.

from relatively euxinic to oxic conditions in marine environment beginning during the *D. semicelatum* subchronozone. That said, the Seegrasschiefer lies stratigraphically below the negative $\delta^{13}C$ excursion (Fig. 5), and therefore, pre-dates the canonical TOAE onset. In addition, molybdenum isotopes do not include signs of multiple pulses of deoxygenation, unlike the thallium isotopes. These results may reflect the different sensitivities of the proxies to regional and local phenomena (Dickson et al., 2017; Them et al., 2018).

Whereas molybdenum and thallium isotopes purportedly capture global trends in seafloor oxygenation, other proxies measure local redox conditions. Sedimentary rocks tend to have high weight percentages of organic matter and sulfur (mainly in sulfide minerals) when deposited below anoxic waters (Leventhal, 1983; Raiswell and Berner, 1985). In the Posidonienschiefer Fm., TOC values typically range from 0.2% to 16% and the weight percentages of total sulfur (TS) vary from 0.2% to 13%. TOC and TS are positively correlated with a positive intercept (Röhl et al., 2001), which suggests local anoxic conditions were common in the Southwestern German Basin during the early Toarcian (Röhl et al., 2001; Röhl and Schmid-Röhl, 2005). Nitrogen isotope ($\delta^{15}N$) values from the Dotternhausen section (Fig. 1) indicated the presence of discrete basins with local stratification and anoxia. (Wang et al., 2021). In these regions, nitrogen was limited due to denitrification and/or anammox, so Wang et al. (2021) suggest that Molybdenum-based nitrogen fixation was common. Biomarkers confirm an abundance of diazotrophic cyanobacteria (Ajuaba et al., 2022).

Organic macerals and biomarkers provide additional evidence of anoxia. In the Swabian Alb, Posidonienschiefer organic macerals are dominated by bituminite, often derived from the anaerobic degradation of algae, zooplankton, and bacteria (Prauss et al., 1991). Biomarkers in the organic matter include derivatives of carotenoids, such as isorenieratane, which is produced by sulfur bacteria with anaerobic (and phototrophic) metabolic pathways; thus, its concentration is a proxy for photic zone euxinia and the presence of free sulfide (Sinninghe Damsle et al., 1993). Most layers of the Posidonienschiefer Fm. have high concentrations of isorenieratane, except for strata beneath the negative carbon isotope excursion in the *D. tenuicostatum* zone (Schouten et al., 2000). Biomarkers and other organic compounds from the Dormettingen section (Fig. 1) also record conditions of photic zone anoxia and intervals of oxygenation during the carbon isotope excursion, with the most severe conditions just above the Unterer Stein (Ajuaba et al., 2022). Thus, biomarkers indicate that benthic marine environments experienced a change from relatively oxic to more euxinic (anoxic and sulfidic) conditions during the *D. semicelatum* subchronozone (Schouten et al., 2000), reaching the most severe deoxygenation at the top of the *H. exaratum* zone (Ajuaba et al., 2022).

Redox conditions also influence the forms of iron in sedimentary rocks (Raiswell and Canfield, 1998; Poulton and Raiswell, 2002). Total iron (Fe_T) includes the iron in clay minerals, pyrite (Fe_{py}), and highly reactive iron phases (Fe_{HR}), like carbonate, sulfide, and (oxyhydr)oxide minerals. The weight percentages and ratios of these iron species depend on redox conditions with oxic, euxinic (anoxic with sulfide), and ferruginous (anoxic with iron) water columns leaving different geochemical signatures. Sedimentary rocks deposited beneath anoxic (ferruginous or euxinic) water masses have Fe_{HR}/Fe_T values greater than 0.38 (Poulton and Canfield, 2011); however, factors such as episodic sedimentation can modify this threshold (Raiswell et al., 2018). Values of Fe_{py}/Fe_T less or greater than 0.7 represent ferruginous and euxinic water masses, respectively. Posidonienschiefer Fm. iron speciation data indicate that most iron is present in highly reactive phases, specifically pyrite. At Dotternhausen (Fig. 5), the mean Fe_{HR}/Fe_T is 0.93 (minimum = 0.40) and mean Fe_{py}/Fe_T is 0.89 (minimum = 0.60) (Them et al., 2018), which implies that anoxic—typically euxinic but sometimes ferruginous—bottom water was present throughout the depositional history of the Posidonienschiefer Fm. In contrast to the other proxies, iron speciation data suggest that anoxic conditions existed prior to the start of the TOAE during the *D. semicelatum* subchronozone (Them et al., 2018); these data may indicate that Dotternhausen was located near an oxygen minimum zone prior to the TOAE.

Paleoecological data can further illuminate redox history (Kauffman, 1978, 1981; van Acken et al., 2019; Rodríguez-Tovar, 2021). The unit contains at least 14 distinct intervals of bioturbation with trace fossils of *Phymatoderma*, *Chondrites*, and *Thalassinoides* (Savrda and Bottjer, 1989) along with *Spongeliomorpha*, *Planolites*, and *Rhizocorallium* (Brenner and Seilacher, 1978; Kauffman, 1978, 1981). The trace fossil distributions (Fig. 5) indicate benthic oxygenation until the top of the *D. tenuicostatum* zone, followed by anoxia with brief periods of oxygenated bottom water during the rest of the lower Toarcian interval (van Acken et al., 2019; Rodríguez-Tovar, 2021). Benthic taxa in the Posidonia Shale include bivalves and crustaceans along with rare brachiopods, gastropods, asteroids, ophiuroids, echinoids, holothurians, and serpulids (Riegraf et al., 1984; Röhl et al., 2001; Schmid-Röhl and Röhl, 2003). Although infaunal bivalves are largely restricted to the upper part of Member II and the linguliformean brachiopods (e.g., *Discinisca papyracea*) mainly occur in condensed units (e.g., the Inoceramenbank at Dotternhausen; Röhl et al., 2001), the epifaunal bivalves *Bositra* (formerly *Posidonia*) and *Parainoceramya* (formerly *Inoceramus* and *Pseudomytiloides*) are preserved throughout the formation (Röhl et al., 2001). Many *Parainoceramya* fossils occur on wooden logs; in some cases, logs are covered by thousands of specimens, suggesting that *Parainoceramya* had a pseudoplanktic lifestyle and attached to driftwood in the water column (Hess, 1999). Other *Parainoceramya* fossils are preserved *en masse* in shell beds and pavements above the Oberer Stein (e.g., the Inoceramenbank and condensed units at Dotternhausen; Fig. 3). Recognizing that these beds have organic carbon and total sulfur values with non-positive intercepts, Röhl et al. (2001) argued that they may represent colonization events during seafloor oxygenation. If so, *Parainoceramya* may have been facultatively pseudoplanktic and benthic (Röhl and Schmid-Röhl, 2005; Martindale and Aberhan, 2017). Conversely, *Bositra* was almost certainly a benthic organism (Kauffman, 1981; Schmid-Röhl, 2021). Shell beds in Member III can have dense pavements with tens of thousands of *Bositra* per square-meter with some beds rising to 20,000 individuals per square-meter (Schmid-Röhl, 2021). Large, distinct assemblages of *Bositra* are preserved in the lower part of Member II, the middle of the Oberer Schiefer, and middle and upper layers of Member III (Kauffman, 1981; Röhl et al., 2001). These assemblages differ with respect to their size distributions and growth patterns (Röhl et al., 2001). According to Röhl et al. (2001), the growth of *Bositra* varied with the availability of oxygen on the seafloor, as expected for a benthic mode of life (Caswell et al., 2009).

At Dotternhausen, benthic animal fossils and bioturbated beds occur in all members of the Posidonienschiefer Fm. (Kauffman, 1981). In Member I, benthic fossils are diverse and bioturbated layers generally have ichnofabric indices between 4 and 6, consistent with oxic and suboxic bottom waters (Röhl and Schmid-Röhl, 2005). Evidence of benthic life occurs in discrete zones of Member II, where numerous horizons contain assemblages of tiny (1–2 mm) juvenile bivalves representing benthic colonization events that failed due to low oxygen levels (Röhl et al., 2001). At Dotternhausen, this unit also contains low diversity assemblages dominated by *Bositra*, which may have rapidly reproduced and opportunistically colonized during seafloor oxygenation (Röhl et al., 2001). These assemblages increase in frequency up-section. In addition to monospecific assemblages of *Bositra*, the Mittlerer Schiefer and Oberer Schiefer layers also contain low diversity assemblages with *Parainoceramya*, *Discinisca*, and *Meleagrinella*. Unlike the Unterer Schiefer, they contain ichnofabrics indices of 3 (Röhl and Schmid-Röhl, 2005), which represent thin mixed layers with centimeter-thick piped zones (Röhl et al., 2001). Similar assemblages and bioturbated layers are found in Member III with greater frequency (Röhl and Schmid-Röhl, 2005). Collectively, these paleoecological data corroborate the hypothesis that the upper *D. semicelatum*, *H. exaratum*, and lower *H. elegans* subchronozones represent times of limited ocean oxygenation, when anoxic water masses may have prevented animals from inhabiting the

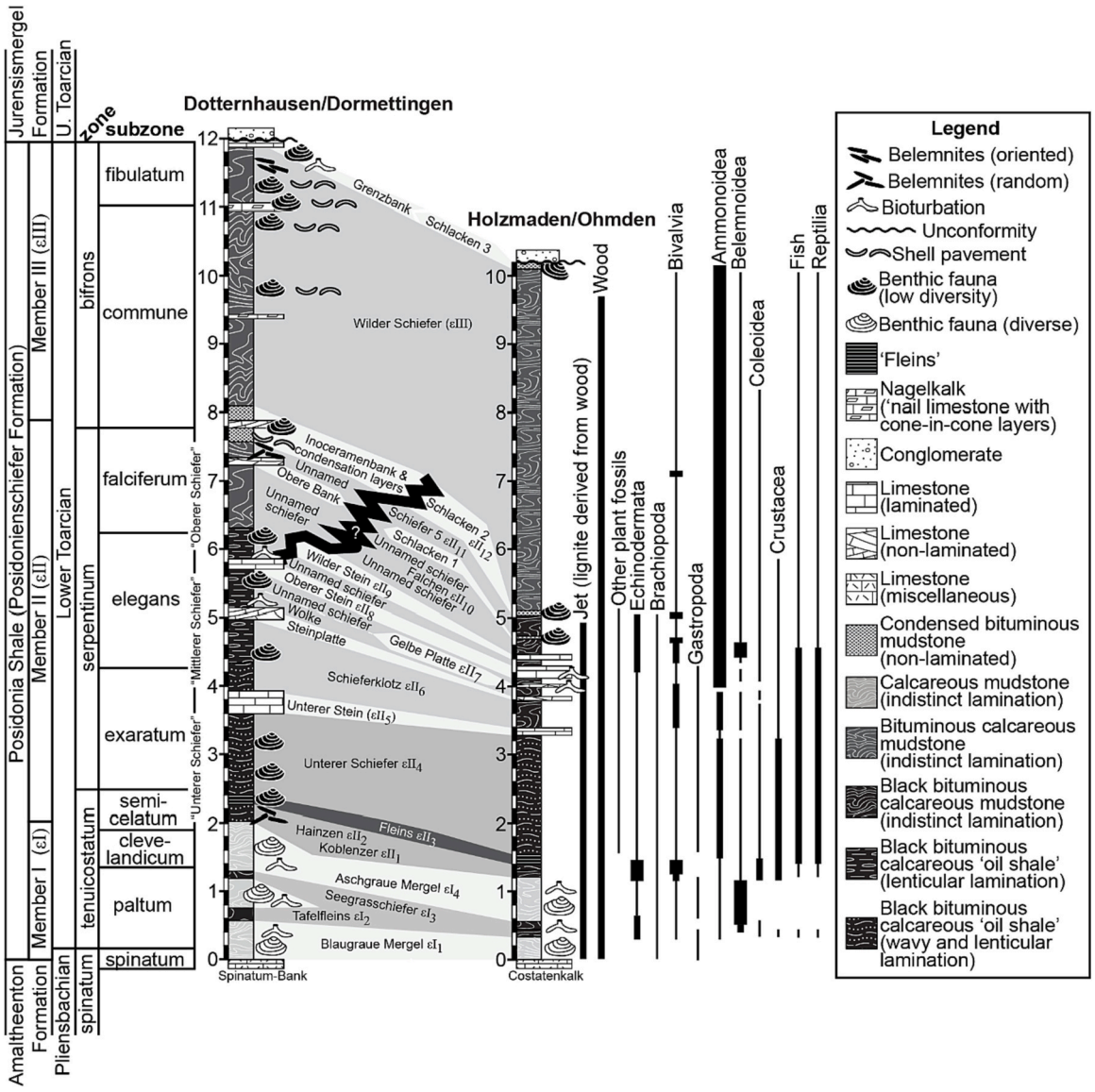

Fig. 3. Stratigraphy of the Posidonia Shale at Dotternhausen, Dormettingen, Holzmaden, and Ohmden. Sedimentary log on left for Dotternhausen (and nearby Dormettingen) comes from Röhl et al. (2001), Schmid-Röhl and Röhl (2003); and Röhl and Schmid-Röhl (2005); sedimentary log on right illustrates the stratigraphy in the area between Ohmden and Holzmaden, as described by Hauff (1921) with thicknesses of units equal to their average values between Reutlingen and Schwäbisch Gmünd. These logs are provided with lithostratigraphic (formation and member), chronostratigraphic (sub-stage), and biostratigraphic (fossil biozone and subzones) units, as interpreted in various works (Röhl et al., 2001; Schmid-Röhl and Röhl, 2003; Röhl and Schmid-Röhl, 2005; Maisch, 2018). Vertical bars illustrate qualitative data on occurrences of various fossils (and variation in their abundance with stratigraphic height) in the Holzmaden-Ohmden area according to Hauff (1921) and Riegraf et al. (1984).

seafloor.

Fossils and geochemical proxies support similar interpretations of redox conditions. Most geochemical proxies suggest that euxinic conditions persisted in benthic environments of the Southwestern German Basin throughout the deposition of the Posidonia Shale Lagerstätte; however, body and trace fossils suggest that anoxic bottom waters were periodically replaced by oxic or suboxic water masses (Kauffman, 1981; Röhl et al., 2001). Similar results were also reported from Toarcian black shales in western Canada (Martindale and Aberhan, 2017; Muscente et al., 2019). The conflicting results suggest that geochemical proxies, like iron speciation and biomarkers, record relatively long-term trends in seawater chemistry (e.g., decades to millenia) rather than short-term (days to years) or ephemeral fluctuations in environmental conditions (Sperling et al., 2016, 2018; Muscente et al., 2019). Considering these nuances, fossils likely provide the most accurate record of changes in redox environments that affected habitat viability and fossil preservation.

2.6. Sea level

Facies patterns in the Posidonienschiefer Fm. may reflect fluctuations in sea level. Against the backdrop of low global sea level in the Early Jurassic (Haq et al., 1988; Hardenbol et al., 1999; Miller et al., 2005; Haq and Al-Qahtani, 2005), Toarcian strata of the *Hildoceras bifrons* and *Haugia variabilis* biozones record a second-order sea level high (Haq, 2017), suggesting a transgression between the late Pliensbachian and middle Toarcian (Haq, 2017). During this transgression, there were third- and fourth-order fluctuations in sea-level, including a forced regression prior to the TOAE (Krencker et al., 2019). Evidence of this forced regression include subaerial exposure surfaces, dolomitized horizons, incised valleys, and other signs of erosion in strata of the upper *Dactylioceras polymorphum* biozone of Morocco and *D. tenuicostatum*

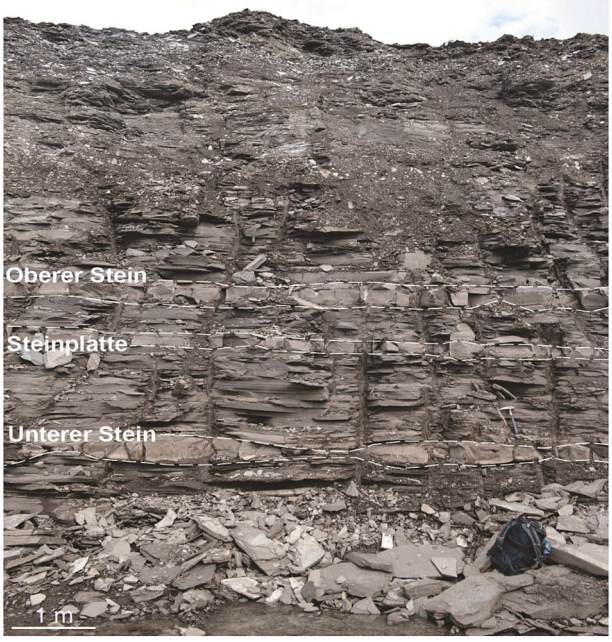

Fig. 4. Field photograph of the Posidonienschiefer Formation exposed in the eastern Ölschieferbruch quarry of the Dormettingen section near Dotternhausen (Fig. 1). The Unterer Stein, Steinplatte, and Oberer Stein layers are labeled.

biozone of Greenland (Krencker et al., 2019), which can be correlated with the upper part of Member I and lowest part of Member II in the Posidonienschiefer Fm.

Efforts to reconstruct the relative sea level curve of the Posidonienschiefer Fm. on the Swabian Alb have focused on lithology, fossil assemblages, organic macerals, and geochemical proxies, such as TOC, total sulfur (TS), and redox-sensitive biomarkers (Röhl et al., 2001; Schmid-Röhl et al., 2002; Röhl and Schmid-Röhl, 2005). At the section near Dotternhausen (Fig. 1), Röhl et al. (2001) and Schmid-Röhl et al. (2002) argued that strata near the bottom of the *Hildoceras serpentinum* biozone—the Koblenzer, Hainzen, Fleins, and Unterer Schiefer layers—represent a lowstand systems tract, and interpreted the strata near the top of the biozone—the Inoceramenbank, schlacken, and other condensed units—as a highstand systems tract. They reasoned that low sea level may have limited ocean circulation, creating stagnant conditions that led to anoxia and deposition of laminated sediment with high TOC content. Subsequently, Röhl and Schmid-Röhl (2005) revised this model to identify systems tracts, interpreting the lower and middle part of Member I as a lowstand systems tract (Fig. 5); the strata between the middle of Member I and the top of Member II as a transgressive systems tract; and Member III as a highstand systems tract. Given reconstructions of global eustatic sea level change (Haq, 2017), these most likely represent a second-order cycle. According to this model, the Inoceramenbank, schlacken, and other condensed units represent maximum flooding (Röhl and Schmid-Röhl, 2005), when sediment starvation or bypass allowed skeletal debris to accumulate (Röhl et al., 2001). Petrographic analysis shows that the schlacken may have undergone rapid carbonate cementation (Heibert, 1988), consistent with low sedimentation and burial rates. Data on palynomorphs and organic macerals also support this model; palynomorphs and organic particulates of terrestrial origin decline in frequency from the lowstand to transgressive system tract, indicating that transgression shifted the depositional environment away from coastlines (Galasso et al., 2021). Assemblages of belemnite rostra at Dotternhausen indicate the transgression also contributed to the stagnation of bottom water; assemblages at the bottom and top of Member II lack preferred orientations, indicating that no bottom currents existed during the upper *D. tenuicostatum* and *H. serpentinum* zones (Röhl and Schmid-Röhl, 2005). Westerly currents or basinal contours subsequently developed during the highstand system tract, resulting in aligned belemnite rostra in Member III (*H. bifrons* zone) (Röhl and Schmid-Röhl, 2005). Overall, these observations indicate that exceptional fossils were preserved during second- and third-order transgressions.

2.7. Paleoenvironmental reconstruction

Lithological, geochemical, and paleoecological data along with paleogeographical reconstructions indicate that the Posidonia Shale was deposited in an enclosed (or semi-enclosed) basin during the early Toarcian. The paucity of terrestrial elements (e.g., plant debris and insect fossils) and presence of microlaminations suggest the Lagerstätte formed far from the coastline in a quiet depositional environment below wave base. Most fossils were preserved during the TOAE when second- and third-order marine transgressions contributed to ocean stagnation and deoxygenation. Euxinic bottom water dominated but pulses of oxygenation periodically allowed for establishment of low-diversity benthic communities, as supported by the presence of trace fossils and bioturbation. Many of the organisms preserved in the Posidonia Shale, however, are pelagic species—including the ammonites, coleoids, fish, and marine reptiles. The crustaceans, brachiopods, and bivalves, on the other hand, were the primary inhabitants of the benthos. As such, it is the expansion of anoxia through the water column that controls the taxonomic composition of the fossil assemblages captured in the Posidonia Shale Lagerstätte.

Together, this paleoenvironmental synthesis still lacks a crucial piece of information: how did (de)oxygenation in the basin and the events of the TOAE influence exceptional fossilization? Although exceptional preservation predates the TOAE negative $\delta^{13}C$ excursion, persists through the event, and continues after the completion of the isotope excursion, the abundance of exceptionally preserved fossils is highest within the TOAE negative $\delta^{13}C$ excursion interval (Figs. 3, 5). Preliminary or taxon-specific research suggests that phosphatization is a chief taphonomic pathway in the Posidonia Shale Konservat-Lagerstätte (Sinha et al., 2021; Eriksson et al., 2022), which requires some degree of oxygenation. Therefore, this work expands the previous taphonomic evaluation to thoroughly assess the taphonomy of a broader suite of Posidonia Shale fossils (both exceptional and ordinary).

3. Material and methods for taphonomic evaluation

3.1. Fossil specimens

A total of 70 fossils were sampled from the Posidonia Shale; taxa include ammonites, belemnites, bivalves, brachiopods, coleoids, crustaceans, and vertebrates, specifically teleost fishes and one thalattosuchian crocodylomorph tooth (Table 1). One coprolite and various pieces of wood were also studied. Most specimens were surface collected from three quarries during the summer of 2019. These quarries (Fig. 1B, C) include the “Kromer quarry” managed by Kurt Kromer in Ohmden (48.65262 N, 9.53996 E); the “Urweltsteinbruch quarry” that belonged to the Fischer Museum in Holzmaden at the time (48.63534 N, 9.52799 E), and the Ölschieferbruch quarry (48.24426 N, 8.76450 E) owned and operated by Holcim (Süddeutschland) GmbH (Schmid-Röhl, 2021) near Dormettingen and Dotternhausen (Fig. 1). Several additional specimens were donated for analysis by the Museum of Natural History in Stuttgart, Germany, and Non-vertebrate Paleontology Laboratory (NPL) at the University of Texas at Austin (UT Austin), USA. In general, specimens were selected because: (1) they are small enough for microscopic study; (2) they exhibit strong definition and contrast relative to the surrounding matrix; (3) they appear representative of the fossils of their type (i.e., the fossilized anatomy and preservation style is similar to most other specimens); and (4) they represent common finds (i.e., the specimens do not include unique fossils with substantial inherent value for research in taxonomy or paleobiology; destructive sampling,

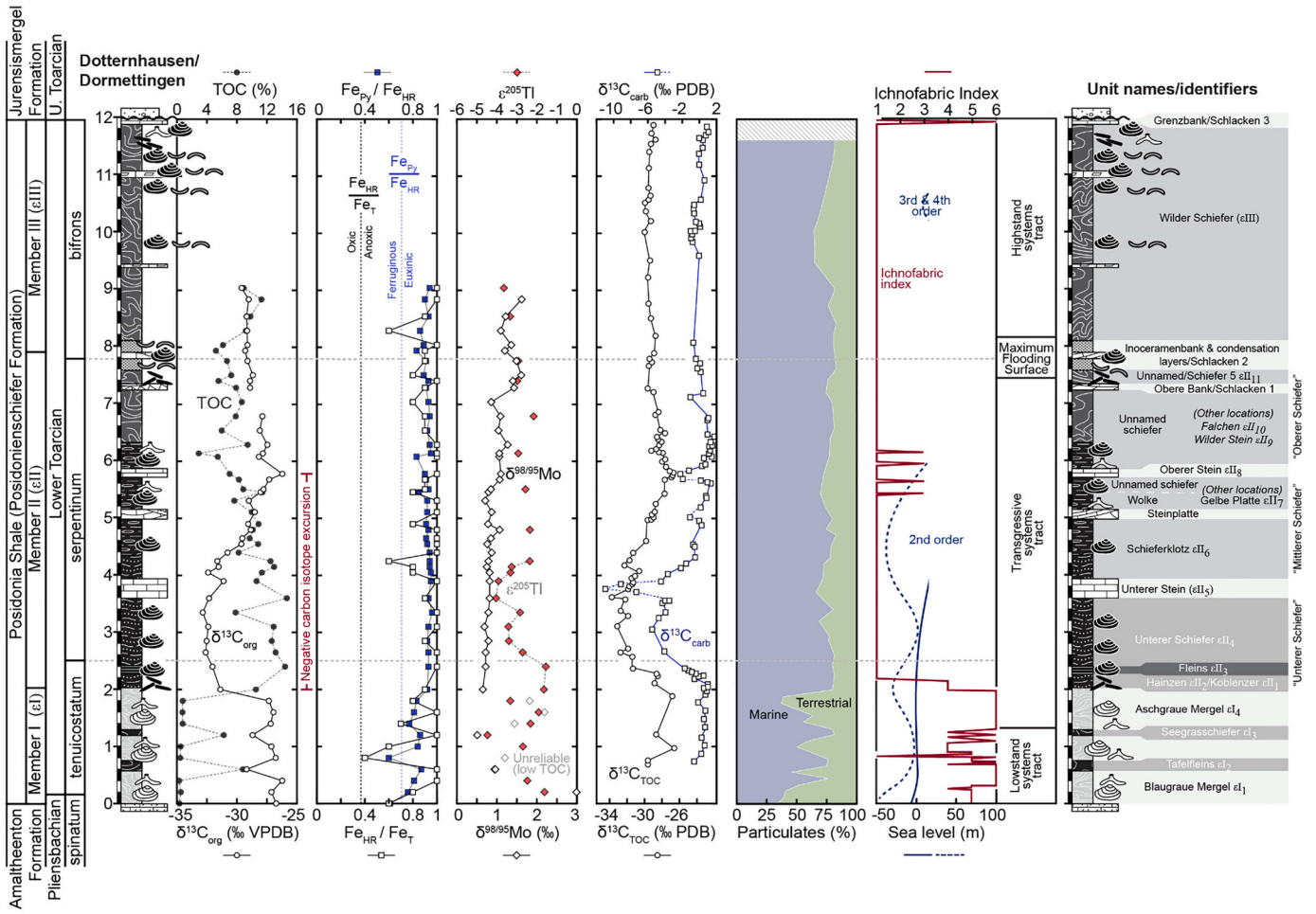

Fig. 5. Geochemical and related data on the Posidonienschiefer Formation. Sedimentary log for Dotternhausen (and nearby Dormettingen) comes from Fig. 3. Data (left to right) include total organic carbon (TOC) with carbon and molybdenum isotope data from Dickson et al. (2017); iron speciation and thallium isotope data from Them et al. (2018); organic and inorganic carbon isotope data from Röhl et al. (2001); percentages of marine and terrestrial particulate organic matter from Galasso et al. (2021); ichnofabric index measurements from Röhl and Schmid-Röhl (2005); relative sea level curves from Haq (2017); and interpretation of sequence stratigraphy and systems tracts from Röhl and Schmid-Röhl (2005). Unit names and identifiers from Fig. 3.

subsampling, or trimming would not be permitted for such fossils). All specimens are now reposited in the NPL.

3.2. Fossil preparation and examination

Specimens were trimmed (dimensions less than 6 cm × 6 cm × 2 cm) to fit inside the three scanning electron microscopy systems employed for this study (see below). Several specimens received additional preparation (i.e., matrix removal, cleaning with water and brushes). The coprolite (specimen number NPL00094456.000) and crocodylomorph tooth (NPL00094455.000) as well as one crustacean (NPL00036039.000), one coleoid ink sac (NPL00094460.000), and all belemnites were cut, polished, and prepared as transverse cross sections. All specimens were photographed with polarized light according to standard reflected light techniques using a Nikon D3200 DSLR camera with 18–55 mm lens and LED light board. They were also examined using a Stemi 508 non-polarized dissecting microscope with Axiocam 208 color Zeiss camera.

3.3. Scanning electron microscopy

Fossils were imaged using variable pressure scanning electron microscopy (SEM) systems, allowing for analysis of native specimens (without conductive coatings applied). To mitigate charging issues, each piece was wrapped in copper or aluminum foil tape, leaving only the fossil(s) exposed, and then grounded to the sample stage (Orr et al., 2002).

This study utilized three variable pressure SEM systems housed in the Materials Analysis, Testing, and Fabrication (MATFab) Facility at the University of Iowa (Hitachi S-3400); the Jackson School of Geoscience at UT Austin (JEOL 6490LV); and the X-ray Microanalysis Laboratory at the University of Missouri (Zeiss Sigma 500VP). Operating conditions were generally similar, using a 20 keV beam accelerating voltage, low chamber vacuum, and working distances constrained between 10 and 15 mm. At the X-ray Microanalysis lab, automated large-area SEM image mosaics were also collected. We collected both secondary (SE) and backscattered (BSE) electron images, showing sample topography and atomic number contrast, respectively.

Pyrite framboids were systematically measured using the BSE images from the JEOL 6490LV SEM. Pyrite framboids are μm-scale, densely packed clusters of euhedral pyrite crystals, commonly found in anoxic, euxinic, and dysoxic environments of modern and ancient sedimentary strata (Butler and Rickard, 2000). They generally form within centimeters below the sediment/water interface (oxic/anoxic boundary) underlying an oxic water column (Wilkin et al., 1996). Pyrite framboid sizes are directly proportional to the amount of time spent in the sulfate reduction zone so their size distributions have been applied to ancient environments to determine redox conditions (Wilkin et al., 1996). The

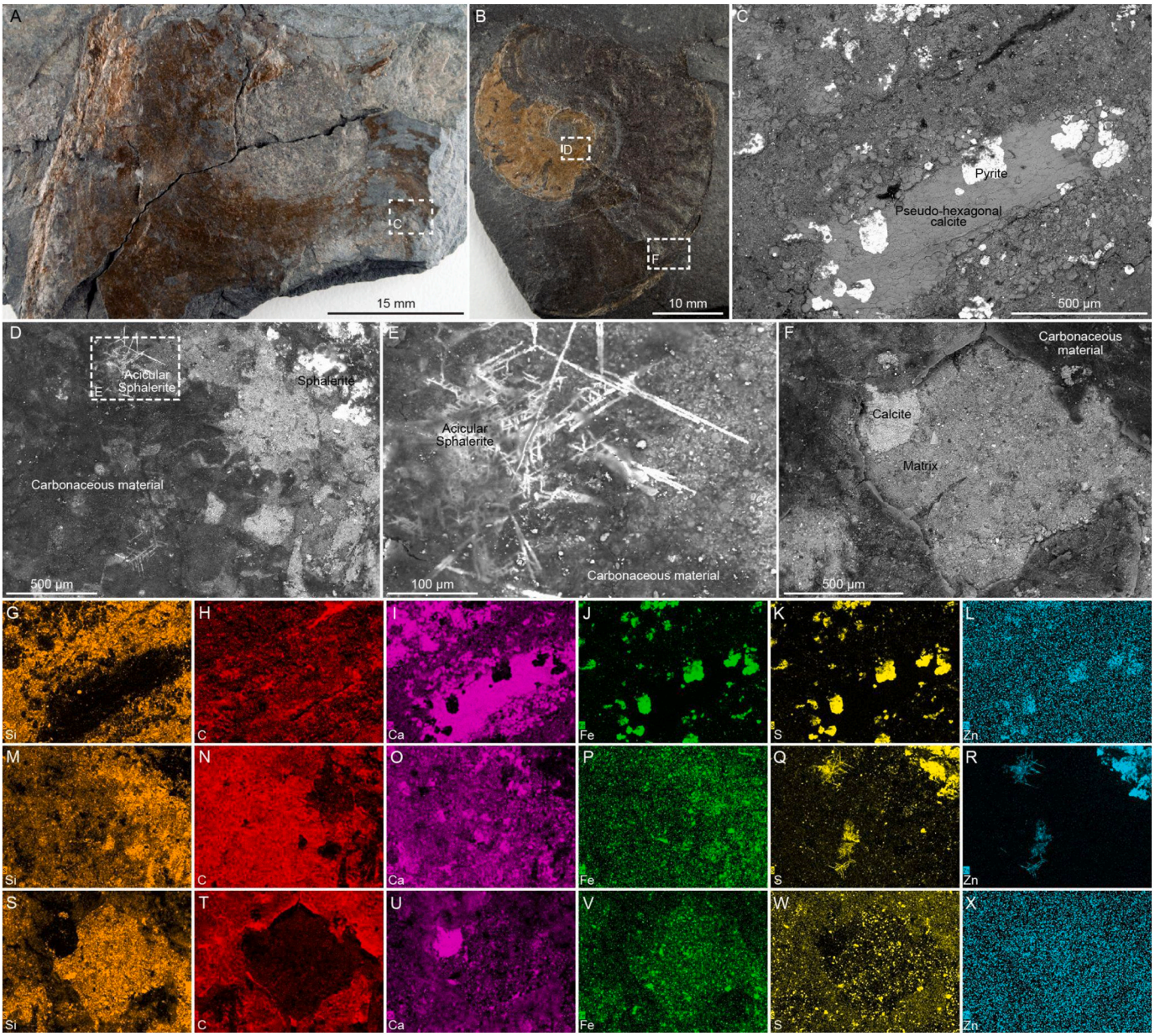

Fig. 6. Ammonites with calcite, pyrite, sphalerite, and carbonaceous material. (A) Reflected light image of fossil (NPL00096929.000) from the Ölschieferbruch Quarry near Dormettingen and Dotternhausen (Posidonienschiefer Fm., upper part of Member II). (B) Reflected light image of fossil (NPL00096930.000) from the Kromer Quarry near Ohmden (Posidonienschiefer Fm., upper part of Member II above Unterer Stein). (C-F) BSE-SEM images acquired in compositional contrast imaging mode. (C) Magnified image of box in (A), showing that the fragmented shell consists of calcite and has been partially replaced by pyrite. (D) Magnified image of box in (B), documenting that the shell primarily consists of carbonaceous material that is encrusted by acicular and anhedral sphalerite. (E) Magnified image of box in (D), illustrating acicular sphalerite crystals. (F) Magnified image of box in (B), showing contrast between carbonaceous and calcitic fossil, diagenetic calcite, and shale matrix. (G-X) EDS elemental maps with elemental labels in the lower left corners. (G-L) Maps of (C). (M-R) maps of (D). (S-X) Maps of (F).

average mean diameter of a framboid from modern euxinic sediments is 5.0 μm, with <4% of framboids >10 μm (Guan et al., 2014), whereas oxic or dysoxic sediments contain framboids with average mean diameters of 7.7 μm, with 10–50% of framboids >10 μm (Wilkin et al., 1996). Here we follow the classification of framboid types from Guan et al. (2014); Posidonienschiefer specimens studied contain types I, II, and III. Type I are spherical aggregates of almost uniform-sized closely packed microcrysts of pyrite with well-defined boundaries, Type II are less closely packed microcrysts of pyrite, with no well-defined spherical boundary, and Type III are isolated or groups of euhedral diagenetic pyrite crystals.

Samples with visible pyrite crystals as well as samples that had a shiny, yellowish luster (i.e., those that appeared pyritized in hand sample) were selected for the framboid analysis. BSE images were collected at the UT Austin facility with an accelerating voltage of 30 keV, spot size of 50–60 nm, and a working distance of 1 mm. Continuous areas were assessed so duplication of counts was not a concern, and only the diameters of Type I framboids were measured for size distribution analyses. Individual framboids were measured along their longest diameter using the on-screen calipers in the Aztec software, following the methods of Wilkin et al. (1996). Although the surface of the framboid used may not necessarily represent its true diameter, the offset error is <10% (Wilkin et al., 1996). To ensure pyrite crystals were measured and not other minerals, point energy dispersive X-ray spectroscopy (EDS) analyses were performed to obtain quantitative concentrations of Fe and S for all selected grains.

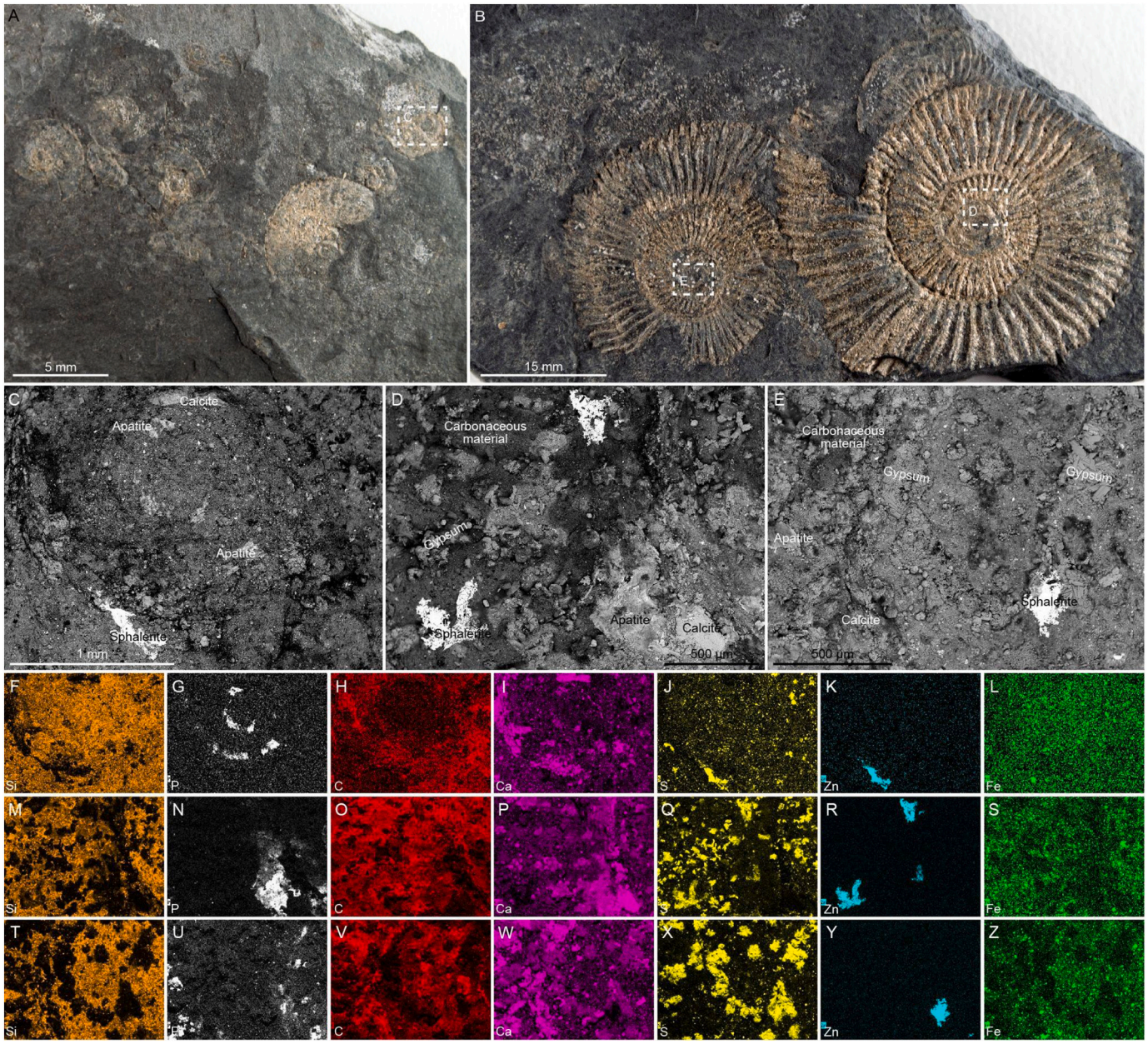

Fig. 7. Partially phosphatized ammonites with calcite, apatite, sphalerite, gypsum and carbonaceous material from the Kromer Quarry near Ohmden (Posidonienschiefer Fm., upper part of Member II above Unterer Stein). (A, B) Reflected light images of fossils (A: NPL00096931.000, B: NPL00096932.000). (C-F) BSE-SEM images acquired in compositional contrast imaging mode. (C) Magnified image of box in (A), showing that the coiled shell consists of calcite and apatite minerals encrusted by acicular sphalerite crystals. (D) Magnified image of box in (B), documenting that the shell primarily consists of carbonaceous material, calcite, and apatite minerals encrusted by acicular sphalerite and rhombohedral gypsum crystals. (E) Magnified image of box in (B), illustrating additional apatite, calcite, gypsum, and sphalerite in the ammonite shell. (F-Z) EDS elemental maps with elemental labels in the lower left corners. (F-L) Maps of (C). (M-S) maps of (D). (T-Z) Maps of (E).

3.4. Energy dispersive X-ray spectroscopy (EDS)

Elemental maps were collected using EDS detectors in the three SEM systems. At the University of Iowa and UT Austin, elemental maps were acquired at an accelerating voltage of 20 keV, probe current at 80 A, spot size of 1.2 µm, and working distances of 12–15 mm for live times of 300 to 1200 seconds (s), yielding X-ray count rates of 40–60 kilocounts per second at the University of Iowa and > 100 kilocounts per second at UT Austin, depending on the sample. On the Zeiss Sigma system at the University of Missouri, EDS maps were collected for 480 s live time using both detectors in tandem with beam accelerating voltage of 20 keV and 40 nA current, ~15 mm working distance, and 120 µm aperture, resulting in acquisition of 300 kilocounts per second.

4. New results: taphonomy of fossils from the Posidonia Shale Konservat-Lagerstätte

4.1. Minerals observed in Posidonia Shale samples

Combined BSE imaging and EDS elemental mapping (Figs. 6–19, S1–72) show that, in addition to carbonaceous materials (e.g., kerogen and lignite), Posidonia Shale fossils commonly contain sulfur-bearing minerals, including pyrite (FeS_2), sphalerite (ZnS_2), barite ($BaSO_4$), and gypsum ($CaSO_4$), as well as minerals belonging to the calcium

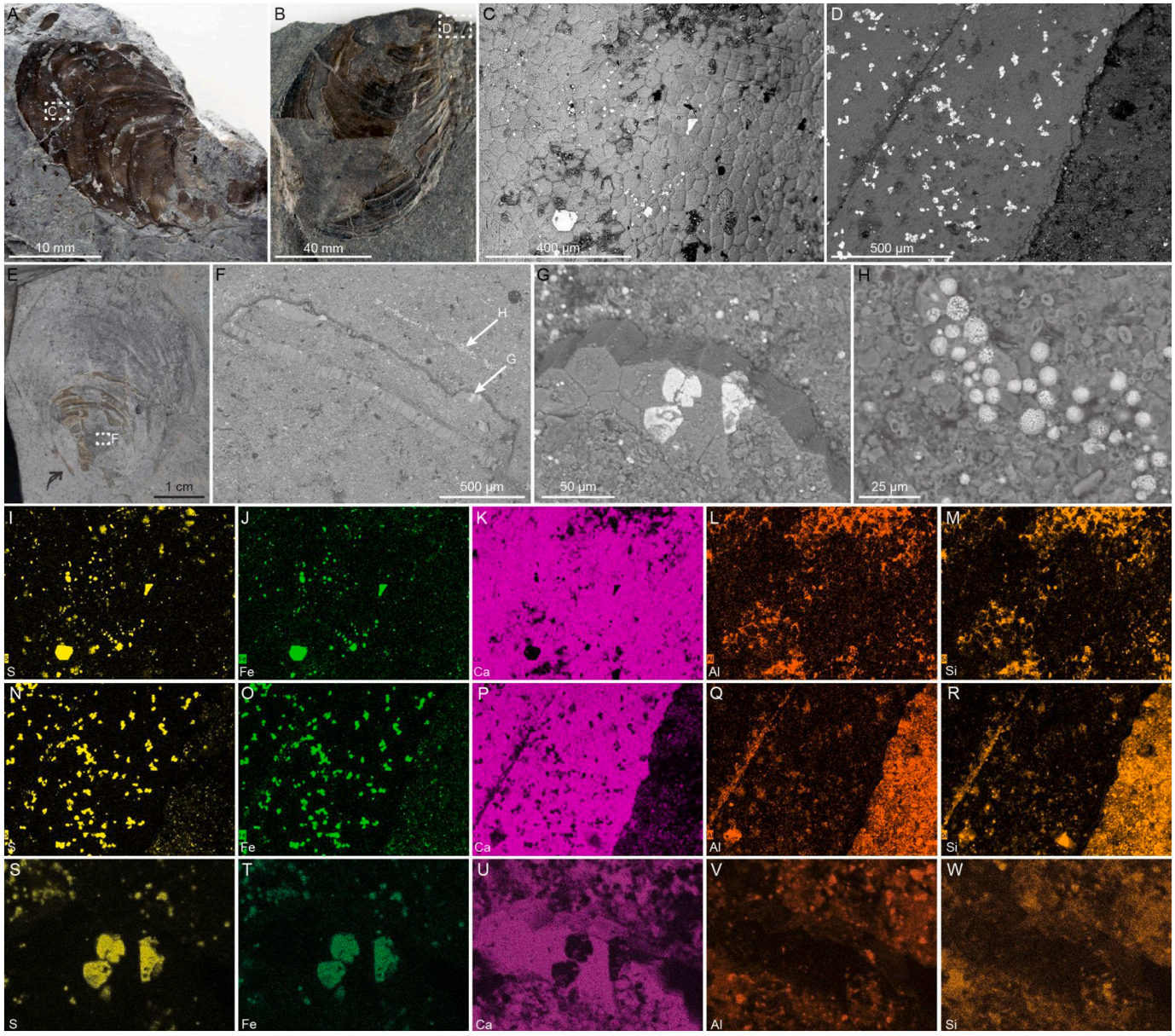

Fig. 8. Bivalves. (A, B) Reflected light images. (A) *Parainoceramya* fossil (NPL00096933.000) from the Kromer Quarry near Ohmden (Posidonienschiefer Fm., upper part of Member II above Unterer Stein). (B) *Parainoceramya* fossil (NPL00096934.000) from the Ölschieferbruch Quarry near Dormettingen and Dotternhausen (Posidonienschiefer Fm., upper part of Member II). (C, D) BSE-SEM image (acquired in compositional contrast imaging mode). (C) Magnified image of box in (A), showing that shell consists of hexagonal plates made of calcite. (D) Magnified image of box in (B), showing hexagonal plates made of calcite located along the edge of a shell. (E) Reflected light image of *Parainoceramya* fossil (NPL00095632.000) from the Posidonienschiefer Fm. (F-H) BSE-SEM image (acquired in compositional contrast imaging mode). (F) Magnified image of box in (E). (G) Magnified image of area indicated by arrow in (F), showing hexagonal plates that have been partially replaced with pyrite. (H) Magnified image of area indicated by arrow in (F), showing pyrite framboidal located in matrix around fossil. (I-W) EDS elemental maps with elemental labels in the lower left corners. (I-M) Maps of (C). (N-R) Maps of (D). (S-W) Maps of (G).

carbonate ($CaCO_3$), apatite ($CaPO_4$), and aluminosilicate groups. With some exceptions (e.g., ammonite shells in Fig. 6B, 7A are partially composed of carbonaceous material encrusted by sphalerite and/or gypsum), the bulk of the fossilized remains consist of calcite and apatite minerals. Pyrite and sphalerite are common, occurring in virtually all fossils, but few (if any) specimens consist entirely of these minerals. Gypsum and barite are comparatively rare in the fossils.

The oil shale and mudstones in which the fossils are preserved largely consist of clay minerals (aluminum phyllosilicates), quartz, pyrite, calcite, and organic matter. The carbonaceous materials in the fossils have the lowest Z values (atomic number) of all components, including the matrix; consequently, in BSE images (Fig. 6F), they appear darker than the mineralized remains and matrix. Carbonaceous material is also evident in EDS elemental maps as regions with high concentrations of C and low concentrations of other elements (Fig. 6G-X). Unlike the carbonaceous material, all the minerals in the fossils have higher Z values than the surrounding matrix, and thus appear brighter in BSE images (Figs. 6C-F; 7C-E). In EDS elemental maps the matrix appears as regions with relatively high concentrations of Al, Si, K, Mg, Na, and occasionally Ca (with low concentrations of most other elements); however, host rock composition of the varies from oil shale to mudstone across the Posionienschiefer Fm. Because elemental maps visualize relative (not absolute) concentration data, the matrix appearance varies based on the other materials in the sample. For example, the concentration of Ca in the matrix appears low (despite its calcareous composition) in EDS elemental maps of fossils consisting of calcite, gypsum,

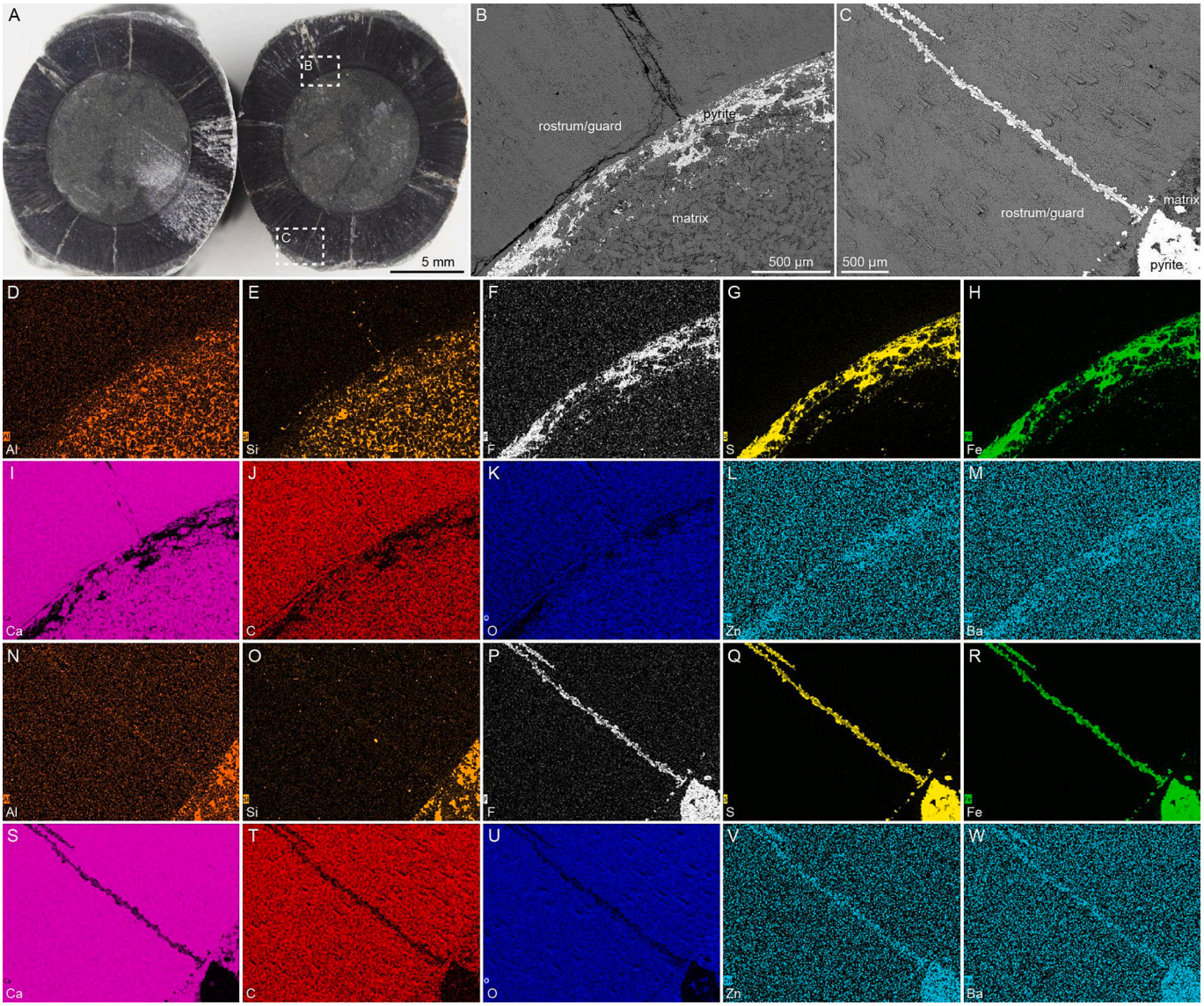

Fig. 9. Belemnite rostrum (NPL00096935.000) from the Ölschieferbruch Quarry near Dormettingen and Dotternhausen (Posidonienschiefer Fm., upper part of Member II). Specimen was cut into transverse cross sections and polished for analysis. (A) Reflected light image. (B, C) BSE-SEM images acquired with compositional contrast imaging mode (note: image and maps in 9C, N-W are shown reflected on a verticle axis, i.e., a mirror image of the area identified in 9A). (B) Image of the box in (A), showing that the rostrum consists of radially oriented calcite crystals and is encrusted by pyrite on its interior surface. (C) Image of the box in (A), illustrating that the rostrum consists of radially oriented calcite crystals, contains cracks filled with pyrite, and has an exterior crust composed of pyrite. (D-W) EDS elemental maps with elemental labels in the lower left corners. (D-M) Maps of (B). (N-W) Maps of (C).

and apatite minerals (e.g., Figs. 8P, 10D, 13U, 14K, U, 17H, R). Likewise, pyrite and organics occur in both the matrix and fossils. For these reasons, the Ca, C, Fe, and S maps represent unreliable images of the matrix, whereas the Al and Si maps provide the best visual representations of the matrix, as the oil shales and mudstones contain abundant aluminum phyllosilicates and quartz.

Some of the minerals in the fossils have similar Z values, which results in low BSE contrast. Under low magnification, calcite, gypsum, and apatite minerals appear nearly identical in grayscale value (e.g., Figs. 7C-E). High magnification images show that gypsum consists of rhombohedral crystals (Fig. 7E), but the crystallographic differences between calcite and apatite minerals are ambiguous; they are mainly distinguished by EDS elemental maps (e.g., Fig. 7F-Z). Apatite minerals are evident from high concentrations of P and Ca (and low concentrations of C, S, and other elements); in contrast, calcite appears as high concentrations of Ca and C (low concentrations of P, S, and other elements) and gypsum is evident where there are high concentrations of Ca and S (and low concentrations of C, P, and other elements). Pyrite, sphalerite, and barite have similar issues; although there is high contrast between these three minerals and others (i.e., apatite, calcite, and gypsum, e.g., Fig. 7C-E), they all tend to appear in BSE images as relatively bright (high Z) materials. High magnification images reveal that some of the pyrite and sphalerite consist of framboids (Fig. S6C) and acicular crystals (Fig. 6D, E), respectively, but in many places, minerals are anhedral, and their crystal habits are ambiguous. Again, EDS elemental maps allow for their differentiation; pyrite appears as defined regions with high concentrations of Fe and S (and low concentrations of Zn, Ba, etc.), sphalerite is evident as distinct regions with high concentrations of Zn and S (and low concentrations of Fe, Ba, etc.), and barite appears as regions with high concentrations of Ba and S (and low concentrations of Fe, Zn, etc.).

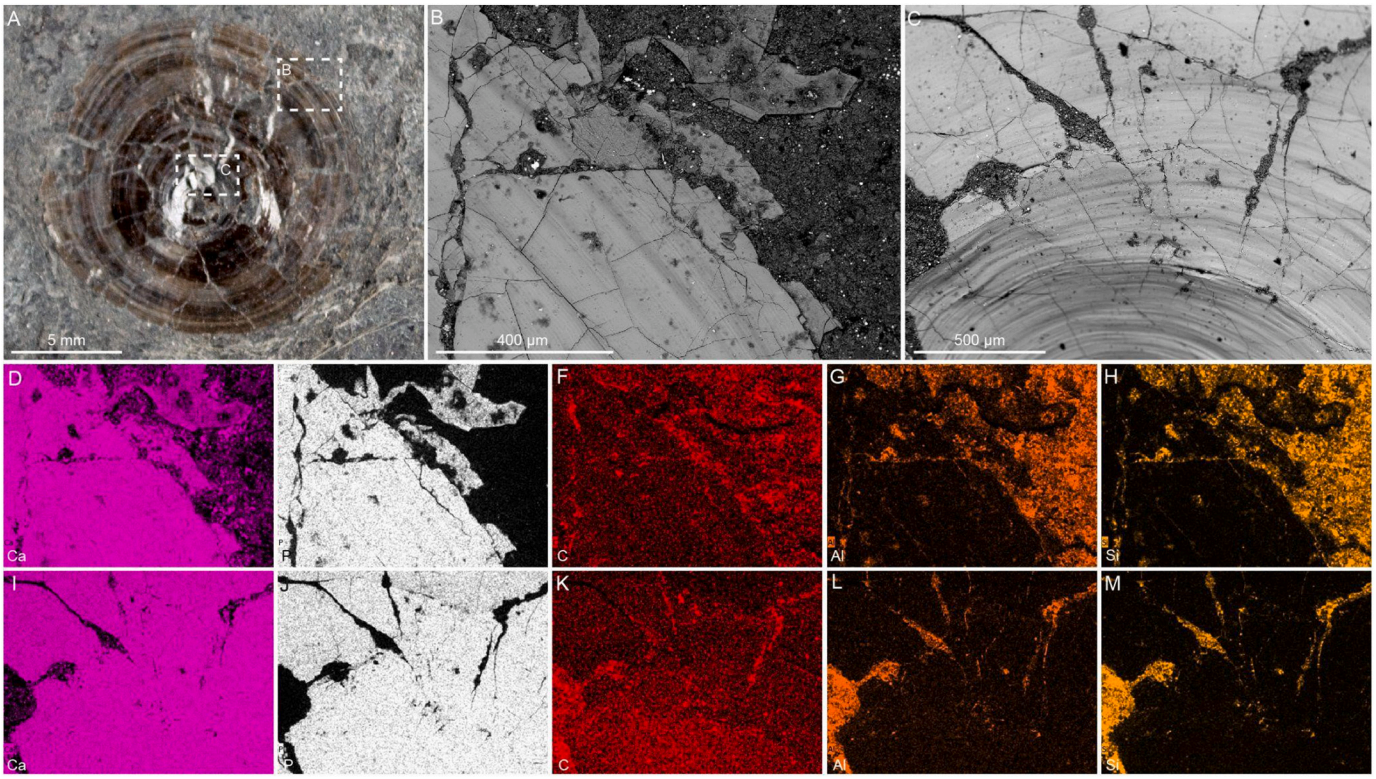

Fig. 10. Linguliformean brachiopod *Discinisca papyracea* (NPL00096936.000) from quarry near Holzmaden (Posidonienschiefer Fm., Member II, Schlacken 2). (A) Reflected light image of shell. (B) BSE-SEM image (acquired in compositional contrast imaging mode) showing edge of phosphatic shell. (C-G) EDS elemental maps of (B) with elemental labels in the lower left corners.

4.2. Ammonites, bivalves, and belemnites

Ammonites, bivalves, and belemnites are the most common macroinvertebrates in the Posidonia Shale (Schmid-Röhl, 2021). Ammonite fossils include shells and aptychi of *Dactylioceras*, *Harpoceras*, *Hildoceras*, *Lytoceras*, and *Phylloceras*. The fossils exhibit substantial variation in appearance; some are slightly iridescent with significant topographic relief (Fig. 6A), whereas others are flat and golden-brown in color (Figs. 6, 7, S1–18). Evidently, they range from collapsed shells (Fig. 6A) to true impressions (Fig. S1). Suture lines are not always apparent but are preserved in fossils of all levels of compaction including true impressions (Fig. 6A, B). Combined BSE and EDS analyses indicate the fossils primarily consist of calcium carbonate (Figs. 6C-F, S2–15) and carbonaceous material (Figs. 6D-F, S16). Carbonaceous material appears in the form of cohesive layers on top of calcium carbonate minerals (Fig. 6D, F), which impart a dimension of depth such that they are not 'carbonaceous compressions' (Butterfield, 1990) or 'organic films' (Muscente and Xiao, 2015b). Calcium carbonate minerals vary among and within specimens. Ammonite fossils with preserved growth lines and topographic relief (Fig. 6A) have 'honeycomb microstructure' (González-Casado et al., 2003), consisting of hexagonal plates of calcium carbonate (Fig. 6C). Other shells (Figs. 6B, S5) can be comprised of two discrete materials with distinct *Z*-contrast or compositional contrast (Figs. 6F, S5C): (1) a low-Z (relatively dark) material that makes up the bulk of the fossils, corresponding to carbonaceous remains, and (2) a high-Z (relatively bright) calcite that occurs in a patchy distribution on interior and exterior surfaces of shells.

Ammonite fossils contain a variety of additional minerals. Pyrite (Figs. 6C, S3, S6–S15) and sphalerite (Figs. 6D-F, 7C-E, S16–18) occur as overgrowth minerals on the surfaces of virtually all ammonites. Some of the fossils (Figs. S7–S14) are partially preserved inside or with pyrite nodules and structures called 'pyrite flowers' (Seilacher, 2001), and others provide evidence that pyrite grew in replacement of hexagonal plates during diagenesis (Fig. S6C). A few shells are also preserved, in part, as apatite minerals (Fig. 7C-E). The apatite minerals primarily occur near the umbilici (centers of the coiled shells), and in some cases, are concentrated on the walls that separate adjacent whorls (Fig. 7F-X), such that shells appear as coils in P elemental maps (Fig. 7C).

Bositra and *Parainoceramya* shells are the most common bivalve fossils in the Posidonia Shale (Schmid-Röhl, 2021). The fossils exhibit appreciable topographic relief, have retained their concentric growth lines (Fig. 8A, B, E), and are composed of calcite and pyrite (Figs. 8, S19–S29). The *Parainoceramya* shells have 'honeycomb microstructure' (pseudohexagonal prisms of calcite) (Fig. 8C); in some places, prisms have been partially replaced by pyrite (Fig. 8D, G). The amount of pyrite varies; some shells contain very little (Figs. 8A, S19) whereas others exhibit extensive pyritization (Figs. 8E, S20–S29).

Belemnite guards (rostra) are common in certain strata of the Posidonienschiefer Fm., particularly above and below the Unterer Schiefer in Member II (Hauff, 1921; Schmid-Röhl, 2021). As is typical for belemnites with rostra preserved in three dimensions, their interior cavities (alveoli) are filled with matrix material (Fig. 9A). The rostra, themselves, consist of radially oriented calcite crystals (Fig. 9B, C), and the interior and exterior surfaces are encrusted by pyrite, and possibly, sphalerite and barite. These minerals also occur as void-filling cements within cracks in the rostra (Fig. 9C).

4.3. Linguliformean brachiopods

Brachiopods are generally rare in the Posidonia Shale (Hauff, 1921), with the most common being shells of the linguliformean *Discinisca papyracea* (Röhl et al., 2001); which are somewhat common in schlacken-type units, including the Inoceramenbank and other condensed units at Dotternhausen (Röhl et al., 2001). *Discinisca papyracea* shells have appreciable topographic relief and concentric growth lines (Fig. 10A-C). Elemental maps show fossils consist of apatite

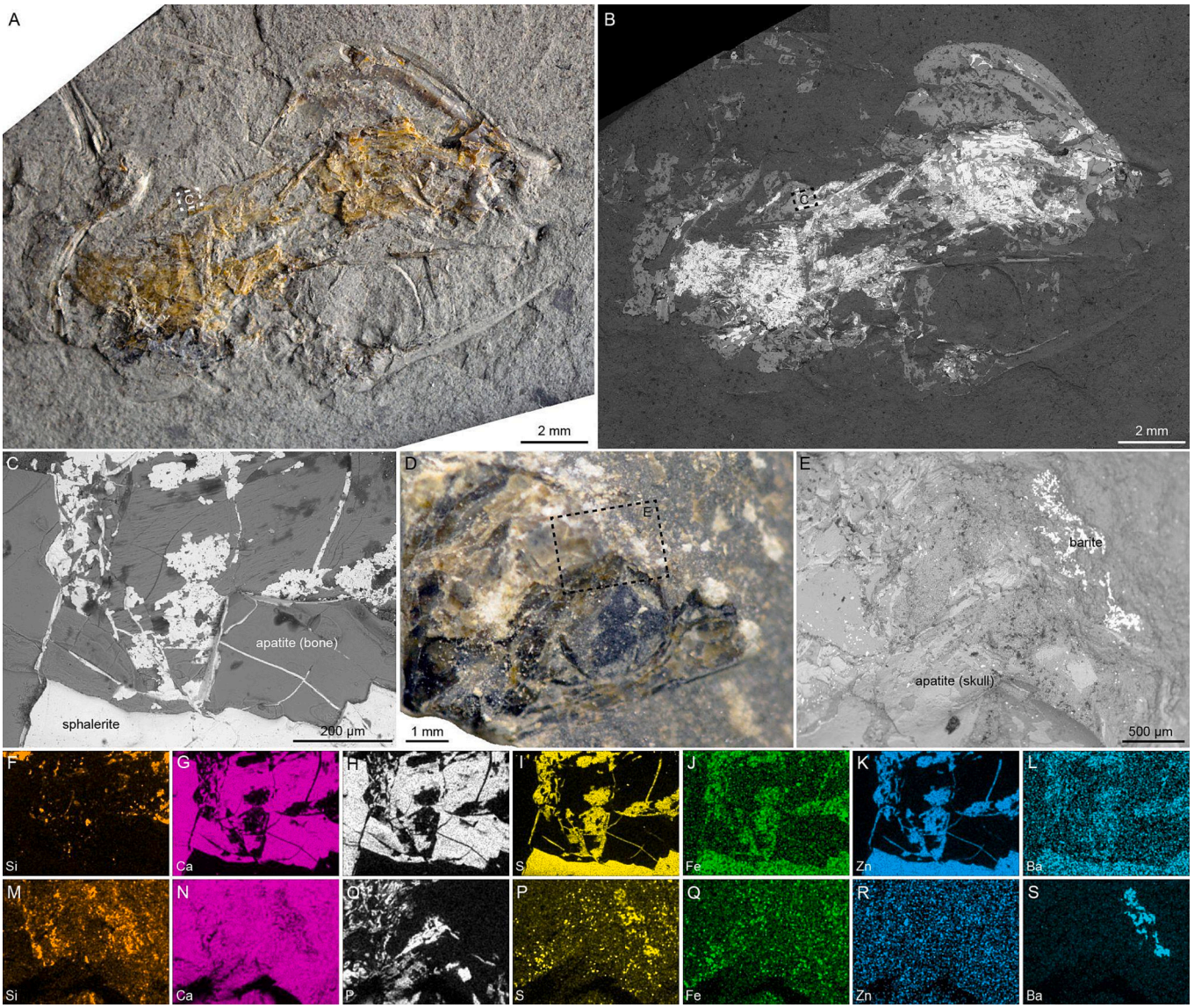

Fig. 11. Fish fossils. (A-C) Body and skull (NPL00036036.000) from the Kromer Quarry near Ohmden (Posidonienschiefer Fm.). (A) Reflected light image showing yellow sphalerite. (B, C) BSE-SEM images acquired with compositional contrast imaging mode. (B) Mosaic image of the entire fossil. (C) Magnified image of boxes in (A, B) showing sphalerite on surfaces and cracks within the bones of the fossil. (D, E) Fish skull from the Ölschieferbruch Quarry near Dormettingen and Dotternhausen (Posidonienschiefer Fm., upper part of Member II). (D) Reflected light image. (E) Magnified image of box in (D) that illustrates barite along periphery of skull. (F-S) EDS elemental maps with elemental labels in the lower left corners. (F-L) Maps of (C). (M-S) Maps of (E).

minerals (Fig. 10D-M).

4.4. Fish

Dozens of fish species are preserved in the Posidonia Shale but compared to other vertebrate taxa (e.g., ichthyosaurs), fish infrequently preserve remains of labile and non-biomineralized tissues (Figs. S30–S34). This study herein examined two small teleost fossils (Fig. 11A, D) represented by skulls and other bones to determine if there were different taphonomic conditions during their formation. The skeletons are generally flat, but SE-SEM shows some three-dimensional relief (Fig. S31C). Combined BSE-SEM and EDS analyses illustrate that the bones primarily consist of apatite minerals (Fig. 11C, D, S30–S34) but are also associated with sphalerite, pyrite, and barite. In one specimen (Fig. 11A-C), the spaces between bones are filled with sphalerite and minor pyrite. These minerals, which appear golden brown in reflected light images (Fig. 11A, B), occur as cements on the surfaces and cracks within the fossil (Figs. 11C, S30–S33). The second specimen—a fish skull (Figs. 11D, S34)—does not contain any noteworthy pyritic or sphaleritic cement, but the matrix around this fossil contains significant amounts of barite (Fig. 11E, M-S).

4.5. Crustaceans

Most crustacean fossils in the Posidonia Shale belong to the decapod *Uncina*, specifically, *Uncina posidoniae* (Schweigert et al., 2003). The fossils represent exoskeletons (carapaces), predominantly crustacean cephalothoraxes and appendages; in most cases, they do not include remains of other labile or non-biomineralized tissues (e.g., muscles). Reflected light images (Figs. 12A, B, 13A, B, 14A, S35-S51) and SE-SEM images (Figs. S48B) show that specimens have topographic relief. Combined BSE-SEM and EDS analyses illustrate that crustacean fossils primarily consist of apatite minerals (Figs. S12C-Y, 13C-Y, 14F-Y, S38, S48, S50, S51) and phosphatic remains appear black in reflected light images (Figs. 12A, B, 13A, B, 14A). Although they have cracks in many places (Figs. 12D, 13C, E, 14C-E), carapaces are preserved with original

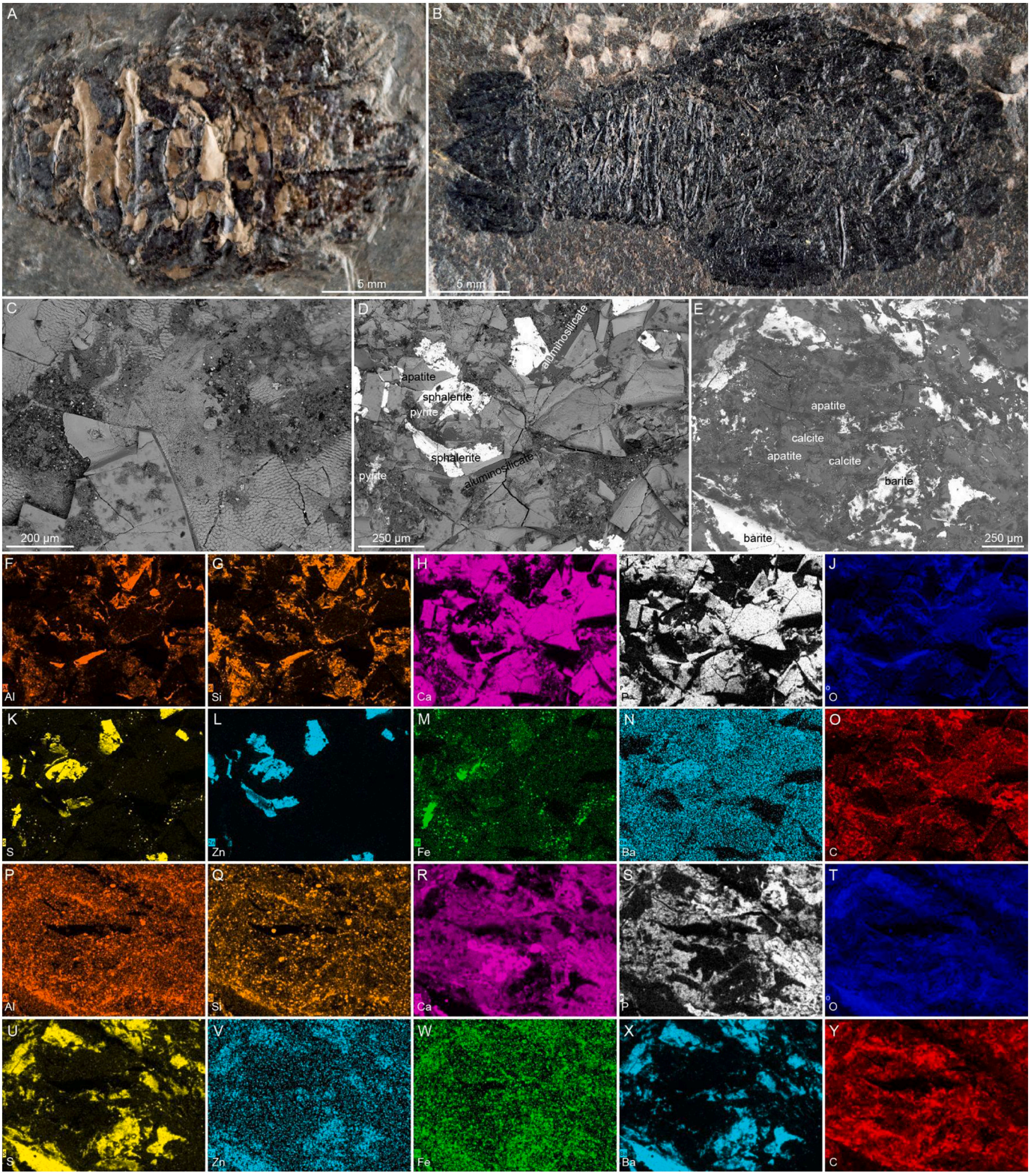

Fig. 12. Crustacean cephalothorax and pleon fossils. (A, B) Reflected light images. (A) *Proeryon* pleon and distal part of cephalothorax (NPL00096937.000) from quarry near Holzmaden (Posidonienschiefer Fm., Koblenzer). (B) *Tonneleryon* pleon and cephalothorax (NPL00096938.000) from a quarry near Holzmaden or Ohmden (Posidonienschiefer Fm.). (C-E) BSE-SEM images acquired with compositional contrast imaging mode. (C) BSE-SEM image of specimen in (A), showing fossil microstructure preserved as phosphatic material. (D) BSE-SEM image of specimen in (A) that illustrates sphalerite, pyrite, and aluminosilicate minerals coating the phosphatic material (apatite minerals) of the fossil. (E) BSE-SEM image of specimen in (B), showing barite and calcite associated with the phosphatic material of the fossil. (F-Y) EDS elemental maps with elemental labels in the lower left corners. (F-O) Maps of (D). (P-Y) Maps of (E).

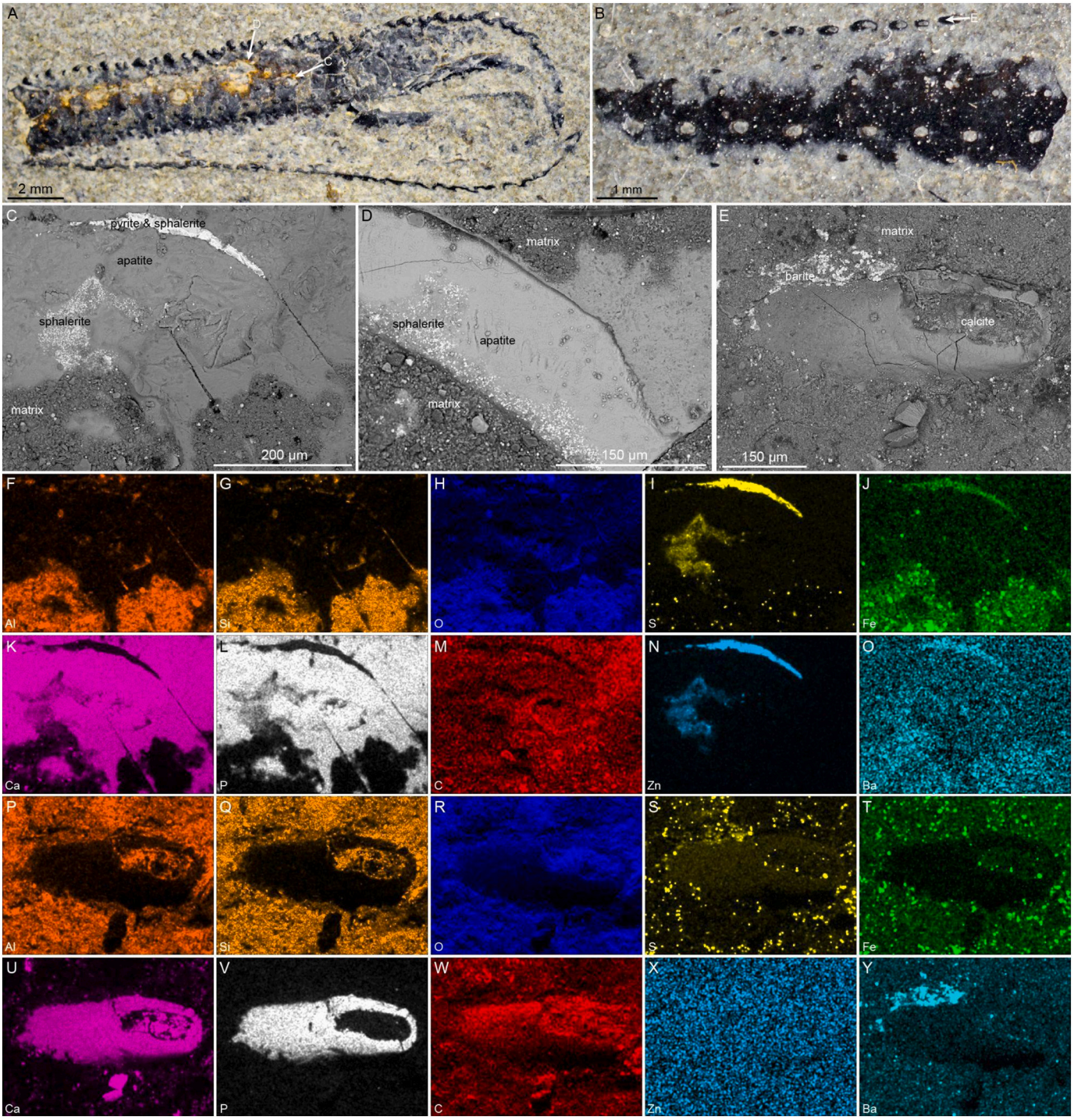

Fig. 13. Crustacean cheliped (claw) and portion of unidentified appendage. (A, B) Reflected light images. (A) *Uncina posidoniae* claw (NPL00094459.000) from the Ölschieferbruch Quarry near Dormettingen and Dotternhausen (Posidonienschiefer Fm., Unterer Schiefer). (B) Crustacean (*Uncina posidoniae*) appendage (NPL00094458.000) from the same locality and unit. (C-E) BSE-SEM images acquired with compositional contrast imaging mode. (C) Magnified image of area indicated by the arrow in (A) that pyrite and sphalerite occurring in the surface and cracks of the phosphatic fossil (composed of apatite minerals). (D) Magnified image of area indicated by the arrow in (A), showing sphalerite on the surface of the phosphatic fossil. (E) Magnified image of area indicated by the arrow in (B), showing that the phosphatic fossil is filled with blocky calcite and encrusted by barite. (F-Y) EDS elemental maps with elemental labels in the lower left corners. (F-O) Maps of (C). (P-Y) Maps of (E).

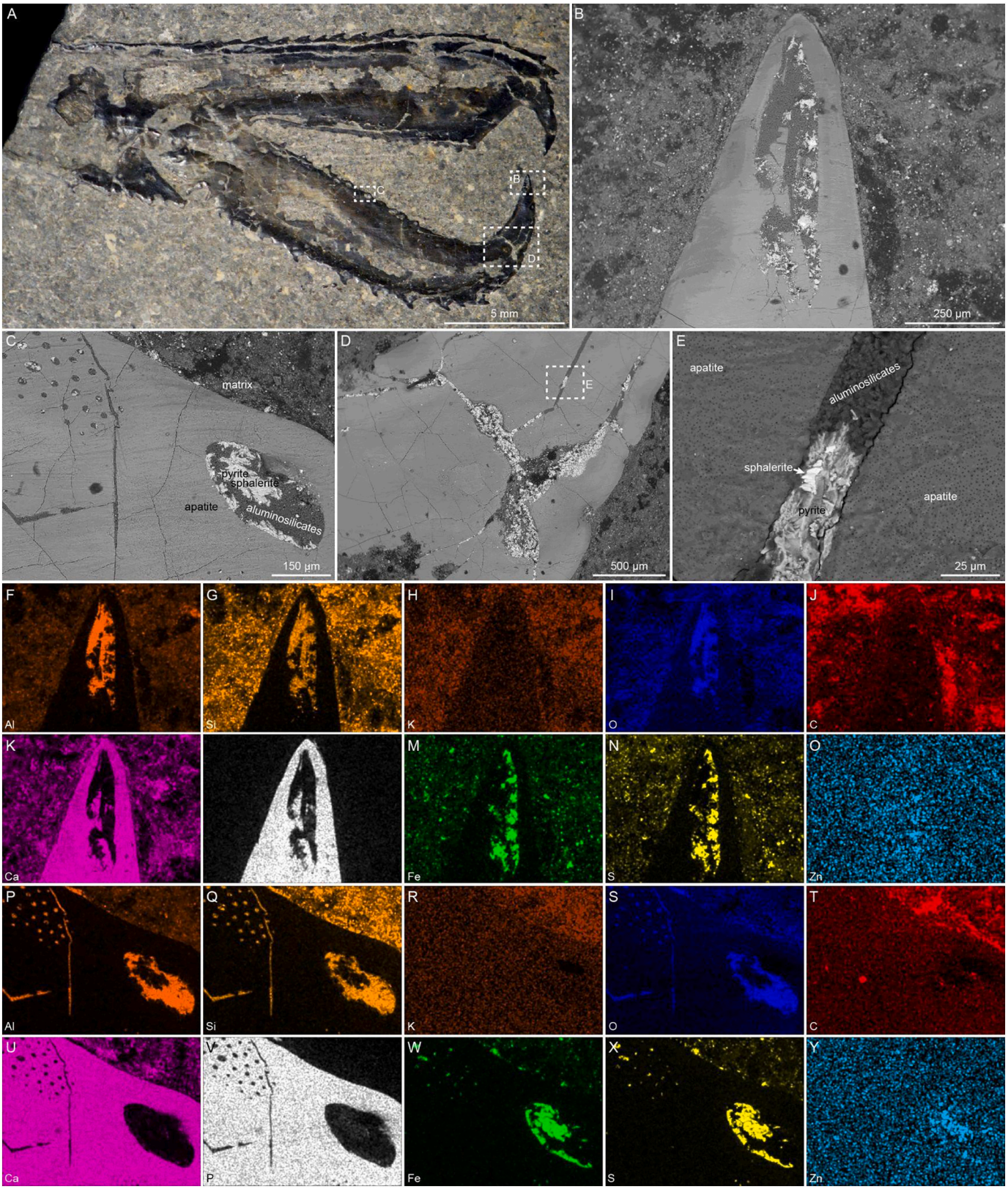

Fig. 14. Decapod, *Uncina posidoniae,* cheliped (claw). (A) Reflected light image of *Uncina posidoniae* claw (NPL00094457.000) from a quarry near Ohmden (Posidonienschiefer Fm.). (B-E) BSE-SEM images acquired with compositional contrast imaging mode. (B) Image of box in (A), showing that the phosphatic fossil is filled with pyrite, sphalerite, and aluminosilicate minerals. (C) Magnified image of box in (A) that illustrates the ultrastructure of the fossil. (D) Magnified image of area indicated by the arrow in (A). (E) Magnified image of box in (D) that illustrates the microstructure of the phosphatic fossil as well as a crack in the fossil, which is filled with pyrite, sphalerite, and aluminosilicate minerals. (F-Y) EDS elemental maps with elemental labels in the lower left corners. (F-O) Maps of (B). (P-Y) Maps of (C).

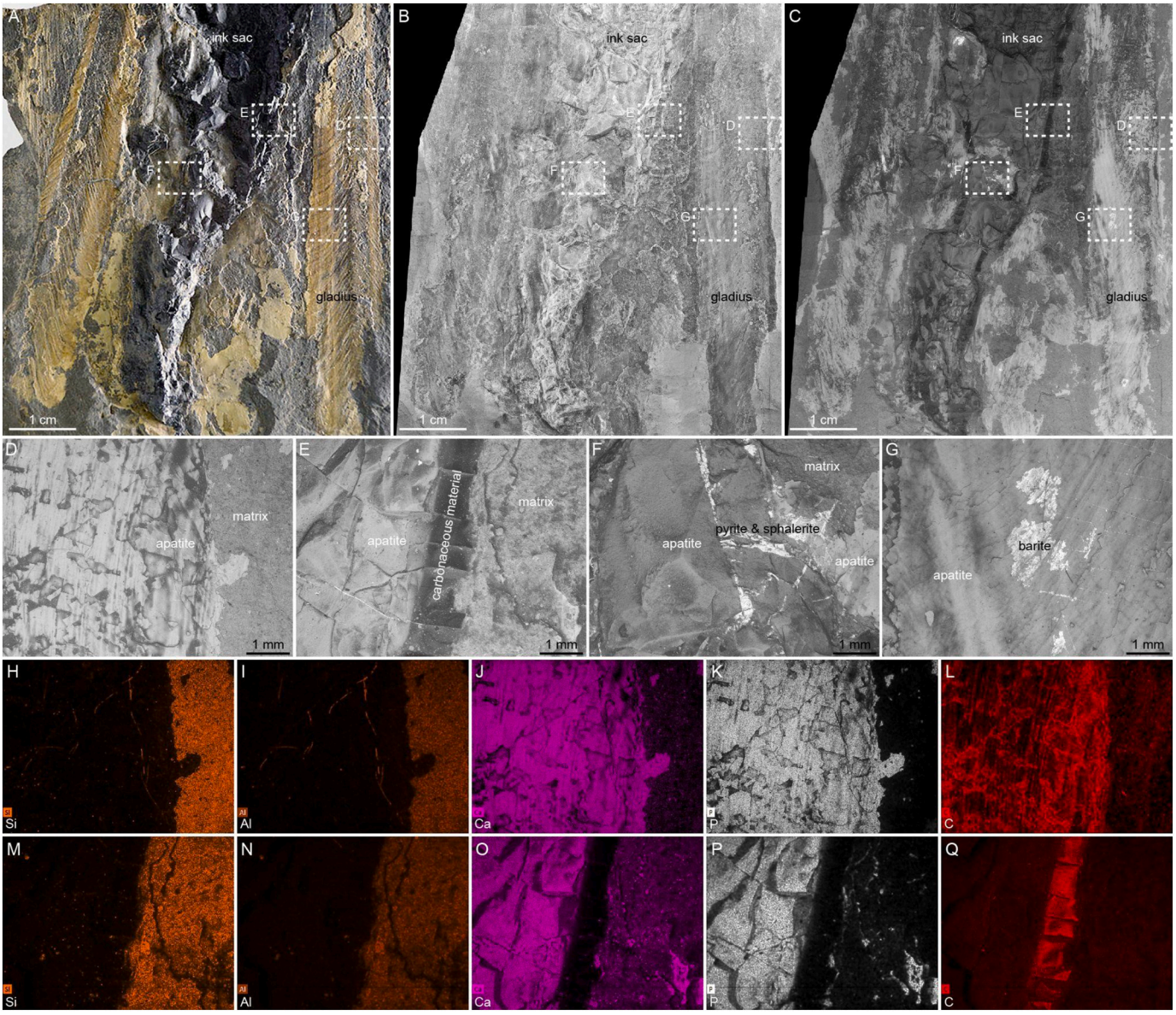

Fig. 15. Vampyropod *Loligosepia aalensis* gladius with ink sac (NPL00036037.000) from quarry in Ohmden (Posidonienschiefer Fm.). (A) Reflected light image of specimen. (B) Mosaic SE-SEM image of specimen. (C-G) BSE-SEM images acquired with compositional contrast imaging mode. (C) Mosaic BSE-SEM image of specimen. (D) Magnified image of boxes in (A-C), showing boundary between phosphatic gladius and surrounding shale matrix. (E) Magnified image of boxes in (A-C) that illustrates edge of ink sac, which consists of phosphatic material (apatite minerals) surrounded by carbonaceous material. (F) Magnified image of box in (A-C), showing cracks in phosphatic ink sac that are filled with pyrite and sphalerite (see Fig. S54). (G) Magnified image of boxes in (A-C) that shows barite on the surface of the phosphatic gladius. (H-Q) EDS elemental maps with elemental labels in the lower left corners. (H-L) Maps of (D). (M-Q) Maps of (E).

ornamental and microstructural characters, including ridges, spikes, canals, pores, and other types of surface ornamentation (Figs. 12C, 13B, 14C, E). The interior spaces within the bumps and spikes are filled with calcite cement in some places (Figs. 13E, S42B, S43B, S50B); calcite also occurs on the surfaces of some specimens (Figs. 12E). Nonetheless, the bulk of crustacean fossils consist of apatite minerals.

Crustacean fossils contain a variety of auxiliary minerals: barite, pyrite, sphalerite, and aluminosilicate minerals (Fig. 12D, E). Barite covers the surfaces of some specimens (Figs. 12E, 13E, S37, S42, S50), whereas, pyrite and sphalerite tend to occur in close association with each other (Fig. 14C-E) as (1) mineral crusts on specimen surfaces (Figs. 12D, E, 13D, S35, S36, S39–S41, S50); (2) void-filling cements in the carapace interior (Fig. 14B, C, S45, S46); and (3) crack-filling cements within fossils (Figs. 13C, 14D, E, S39, S47, S49, S51). The aluminosilicate minerals, likewise, make up void- (Figs. S14, S45, S46, S48, S49) and crack-filling cements (Figs. 12D, 14D, E, S36, S47, S49, S51); in EDS elemental maps, they appear as areas with higher concentrations of Al, O, and Si (lower concentrations of Ca and P) than the surrounding carapace (Figs. 12F-O, 14F-Y, S36, S45–S49, S51). Although the matrix and aluminosilicate minerals have similar elemental compositions, the aluminosilicate minerals appear gray in reflected light images (Fig. 14A) and have higher concentrations of Al and O (lower concentrations of Si, K, Mg, and Na) than surrounding matrix (Figs. 12F-O, 14F-Y, S36, S45–S49, S51). The crustacean fossils contain very little carbonaceous material.

4.6. Coleoids

Coleoids are mainly represented in the Posidonia Shale by eight-armed vampyropods, such as *Clarkeiteuthis* and *Loligosepia*. The best coleoid fossils include remains of gladii (internal chitinous shells), tentacles, mantle muscles, and ink sacs along with specialized tissues like

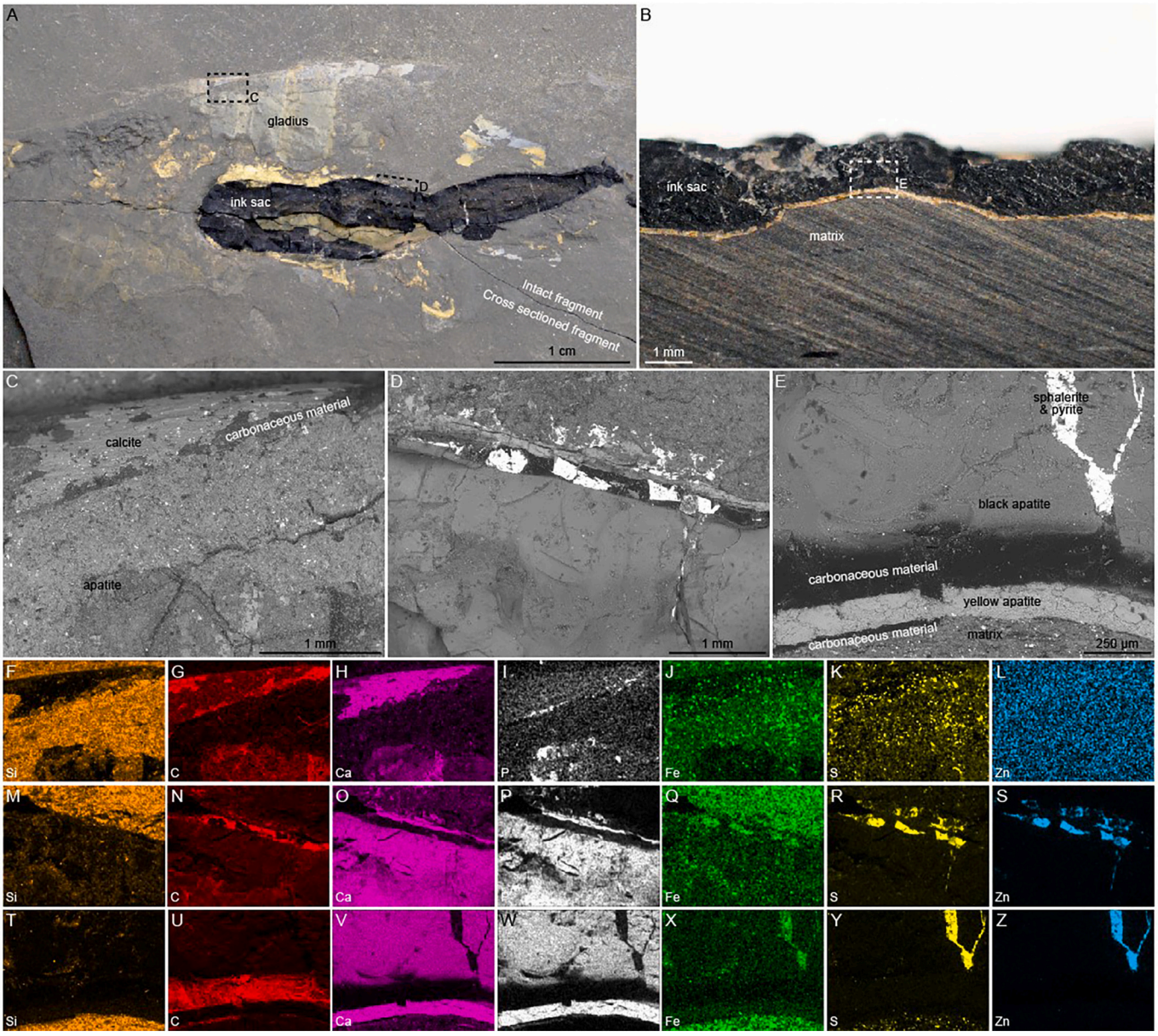

Fig. 16. Vampyropod *Clarkeiteuthis* gladius with ink sac (NPL00094460.000) from quarry in Holzmaden (Posidonienschiefer Fm.; Koblenzer or Hainzen). (A) Reflected light image of the specimen, which consists of two pieces separated by a fracture. (B) Reflected light image of a polished transverse cross section prepared from one of the two pieces shown in (A). (C-E) BSE-SEM images acquired with compositional contrast imaging mode. (C) Magnified image of box in (A), showing boundary between matrix and gladius, which consists of calcite as well as phosphatic (apatite) and carbonaceous material. (D) Magnified image of box in (A) that illustrates phosphatic ink sac with crack-filling sulfide minerals (i.e., pyrite and sphalerite) and void-filling carbonaceous material. (E) Magnified image of box in (B), showing that the phosphatic ink sac is separated from phosphatic gladius material by a layer of carbonaceous material. The phosphatic ink sac contains cracks filled with sphalerite and pyrite. (F-Z) EDS elemental maps with elemental labels in the lower left corners. (F-L) Maps of (C). (M-S) Maps of (D). (T-Z) Maps of (E).

ink ducts (Glass et al., 2012, 2013; Klug et al., 2021a; Jenny et al., 2019). In most cases, only gladii (Figs. 15A-C, 16A, S52–S66), undifferentiated mantle tissues (Figs. S67, S68), and ink sacs (Figs. 15A-C, 16A, S52–S66, S69, S70) are preserved. Reflected light microscopy (Figs. 15A, 16A, S63A) and SE-SEM (Figs. 15B, S63B) show that gladii and ink sacs have significant topographic relief and are not compressions. Integrated BSE-SEM imaging and EDS elemental mapping demonstrates these tissues largely consist of apatite minerals (Figs. 15C-Q, 16C-Z, S52–S70). Reflected light images reveal at least two distinct types of phosphatic material, which differ in mineralogy, color, and appearance. Ink sacs are composed of black apatite minerals (Figs. 15, 16), whereas gladii and mantle tissues consist of yellow-to-brown phosphatic material. Some poorly preserved gladii (Fig. 16A) also are composed of calcite and carbonaceous material (Fig. 16C), but the best specimens—ones with fine structures and definition—are preserved as phosphatic material. The apatite minerals also contribute to the three-dimensionality of the fossils.

Coleoid fossils contain notable amounts of carbonaceous material, which occurs as patches on the surfaces of gladii (Figs. 15D, 16C, S52, S56–S58) and surrounds ink sacs (Figs. 15E, 16D, E, S59–S62, S66, S69, S70). Images of a cross-sectioned specimen (i.e., Fig. 16A, B) show that spaces between the gladii (yellow apatite) and ink sacs (black apatite) are filled with carbonaceous material (Fig. 16E). This void-filling carbonaceous material creates the appearance that ink sacs are surrounded by a layer of organic matter (e.g., Fig. 15E).

Other materials in coleoid fossils include pyrite, sphalerite, and barite. The pyrite and sphalerite occur in close association as (1) void-filling cements in spaces between gladii and ink sacs (Figs. 16D,

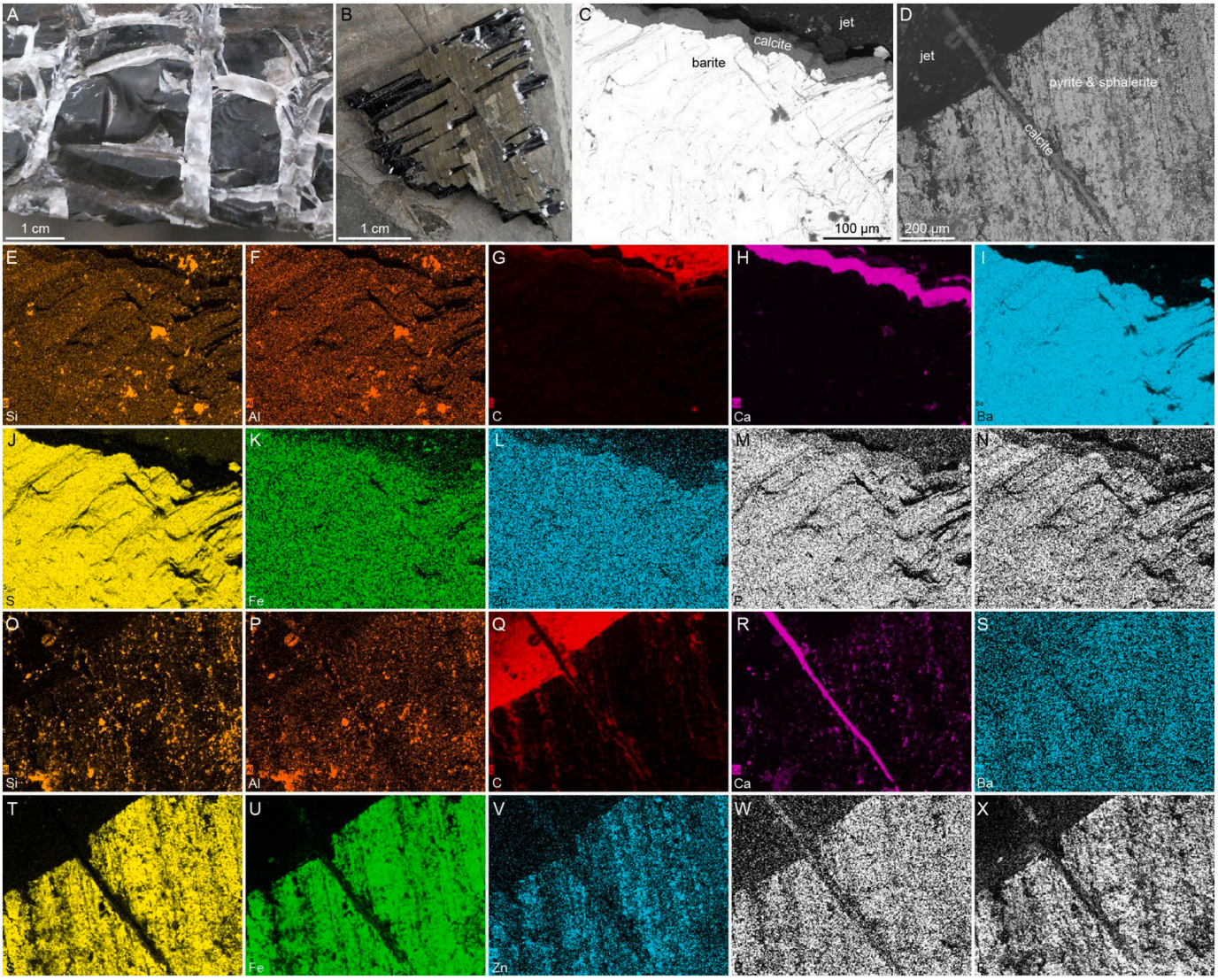

Fig. 17. Jet (wood). (A, B) Reflected light images. (A) Jet with barite veins (NPL00096939.000) from the Ölschieferbruch Quarry near Dormettingen and Dotternhausen (Posidonienschiefer Fm., upper part of Member II). (B) Jet encrusted with pyrite and sphalerite (NPL00096940.000) from the Kromer Quarry near Ohmden (Posidonienschiefer Fm., upper part of Member II above Unterer Stein). (C, D) BSE-SEM images acquired with compositional contrast imaging mode; note that the exact locations of SEM images and EDS elemental maps was not noted during collection. (C) Boundary between jet and barite veins in the specimen illustrated in (A). The jet and barite are separated by a layer of calcite in some places. (D) Pyrite framboids and sphalerite crystals on the surface of the jet piece illustrated in (B). This piece is crosscut by fractures filled with calcite. (E-X) EDS elemental maps with elemental labels in the lower left corners. (E-N) Maps of (C). (O-X) Maps of (D).

S59–S61) and (2) crack-filling cements within ink sacs (Figs. 15F, S54, S59–S62). Like the fish and crustaceans, barite only occurs as encrusting cement on the surfaces of some coleoid specimens (Figs. 15G).

4.7. Other fossils

Jet—a compact form of lignite (compressed carbonaceous mineraloid) derived from wood—occurs throughout the Posidonia Shale in the form of fossilized tree trunks (Fig. 17A, B, S71, S72). The fossils have high three-dimensionality (Fig. 17A, B), are cross-cut by conspicuous white veins (Fig. 17A, B), and in many places, coated by greenish brown material (Fig. 17B). Integrated BSE-SEM imaging and EDS elemental mapping shows that white veins variably consist of barite (Fig. 17C, E-N, S71) and calcite (Fig. 17D, O-X); barite veins have rims of calcite, which separate them from carbonaceous lignite (Fig. 17B). In contrast, BSE-SEM and elemental maps demonstrate that greenish brown material consists of pyrite and sphalerite that directly encrust lignite (Fig. 17D, O-X, S72).

Two additional fossil specimens were cross-sectioned and analyzed: a thalattosuchian crocodylomorph tooth (Fig. 18) and a coprolite (Fig. 19). In both cases, fossils consist of phosphatic material, which has a higher Z value than the surrounding matrix (Figs. 18B-D, 19C, 19D) and appear in elemental maps as areas with high concentrations of Ca, P, Fe, and Na but low concentrations of all other elements (Fig. 18D, G-N, 19D, 19H-S). In some places, the coprolite contains pyrite framboids (Fig. 19G). Likewise, the crocodylomorph tooth, which retains its external and internal ornamentation and ultrastructure (Fig. 18C,D), contains pyrite framboids along with calcite (Fig. 18E, F 18O-V), which notably occurs as a void-filling cement in the central cavity of the tooth. Pyrite is evident in elemental maps of the cavity as areas with higher concentrations of Fe and S (but lower concentrations of Ca and P) than the surrounding tooth; calcite (Figs. 18B-N) appears as high

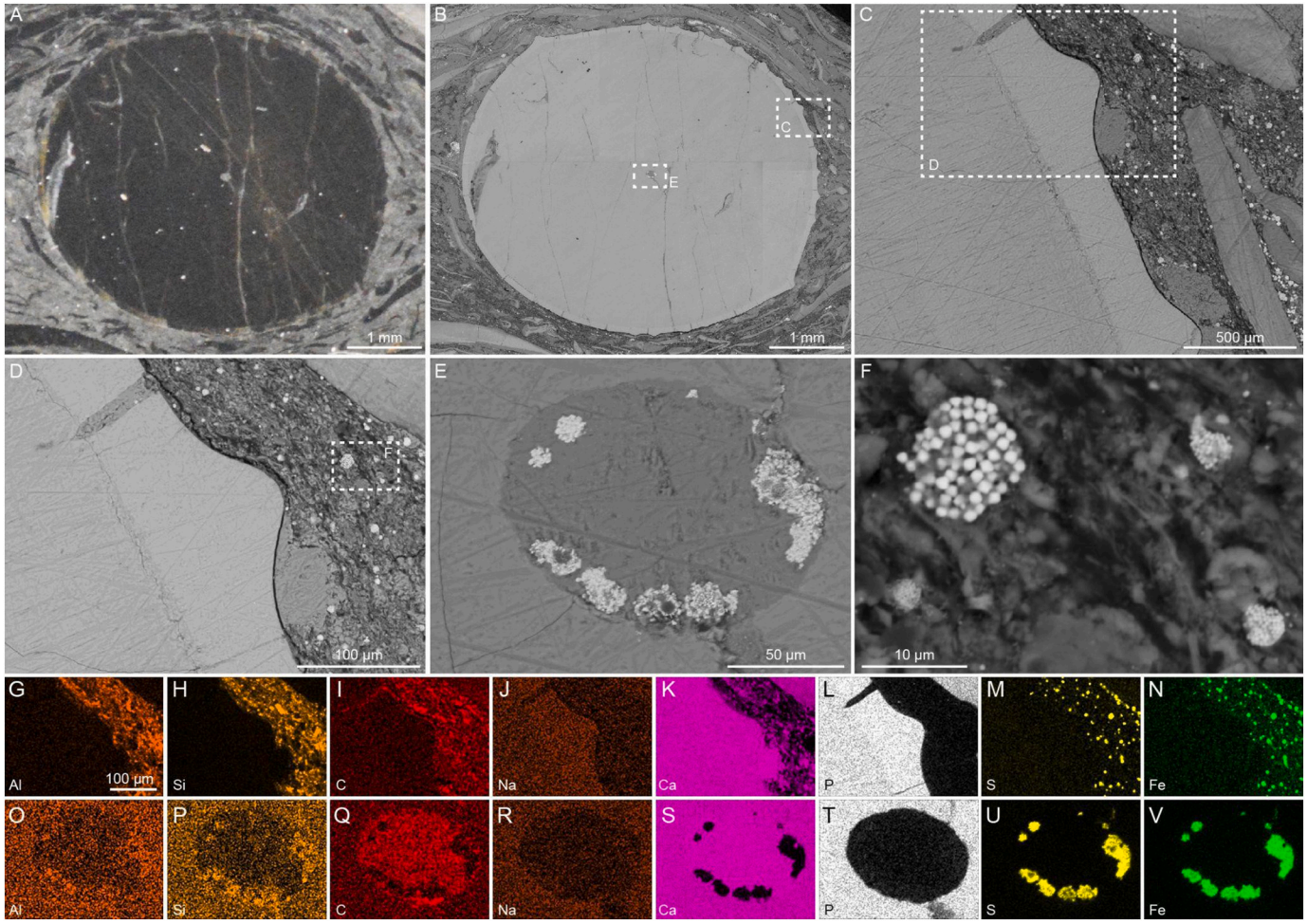

Fig. 18. Crocodylomorph tooth from one of the schlacken layers of the Posidonienschiefer Fm. exposed in the Kromer Quarry near Ohmden (NPL00094455.000). (A) Reflected-light photograph of specimen that was cross-sectioned and polished. (B-F) BSE-SEM images acquired with compositional contrast imaging mode. (C) Mosaic image of specimen. (C) Magnified view of box in (B), showing external morphology and ultrastructure of the tooth. (D) Magnified view of box in (C), showing boundary between phosphatic tooth and mudstone matrix as well as crack-filling and encrusting calcitic cements. (E) Magnified view of box in (B), showing that the central pulp cavity has been filled with calcite as well as euhedral, subhedral, and framboidal pyrite. (F) Magnified view of box in (D), showing pyrite framboids located in the mudstone matrix around the fossil. (G-V) EDS elemental maps with elemental labels in the lower left corners. (G-N) Maps of (D). (O-V) Maps of (E).

concentrations of Ca and C, but with low concentrations of all other elements, including P. Pyrite framboids also occur in abundance in the matrix around the coprolite and crocodylomorph tooth (Figs. 18F, 19E).

4.8. Pyrite framboid measurements

Micron-scale pyrite framboids occur randomly in Posidonia Shale specimens but were substantially more common in the matrix than the fossil material (Table 2). Framboid types I, II, and III (sensu Guan et al., 2014) were identified, with Type I being the most common (spherical aggregates of almost uniform-sized, closely packed microcrysts of pyrite with well-defined boundaries). Type II and III framboids were rare and typically not perfectly spherical, only displaying outer encrustation of larger euhedral crystals. Diameters of Type 1 framboids are used in the size distribution analyses (Table 2). The average framboid diameter is 6.99 µm, 9.2 µm, and 8.04 µm on the crustaceans, coprolite, and crocodylomorph tooth fossils, respectively; whereas the average framboid diameter measured on the crustacean, coprolite, and crocodylomorph tooth matrix is 6.36 µm, 8.1 µm, and 5.99 µm respectively (Table 2). Due to the lack of framboids on the fossils, statistical comparisons between matrix and fossil could not be evaluated.

5. Discussion

Posidonia Shale fossils are composed of multiple materials and minerals. The fossils chiefly consist of calcium carbonate and calcium phosphate minerals, which represent the organisms' original biomineralized skeletons and secondarily mineralized soft tissues. Fossils also contain various types of carbonaceous material, such as kerogen, bitumen, and lignite; however, these materials contribute little mass to the fossils. Some ammonite and bivalve shells consist of calcium carbonate minerals that have been partially replaced with pyrite (Figs. 6C, 8D, G), indicating that preservation of calcareous shells sometimes entailed pyritization. The remaining pyrite and other minerals (i.e., sphalerite, gypsum, barite, and aluminosilicate minerals), occur as crack-filling, void-filling, and overgrowth cements, and therefore, do not represent mineralized tissues. We did not observe differences in mineralization between fossils from the Holzmaden/Ohmden and Dotternhausen/Dormettingen areas. Altogether, these observations suggest that Posidonia Shale fossils experienced a complex taphonomic history, wherein degradation and mineralization were driven by multiple geomicrobiological processes influenced on a regional scale by paleoenvironmental conditions (Muscente et al., 2017).

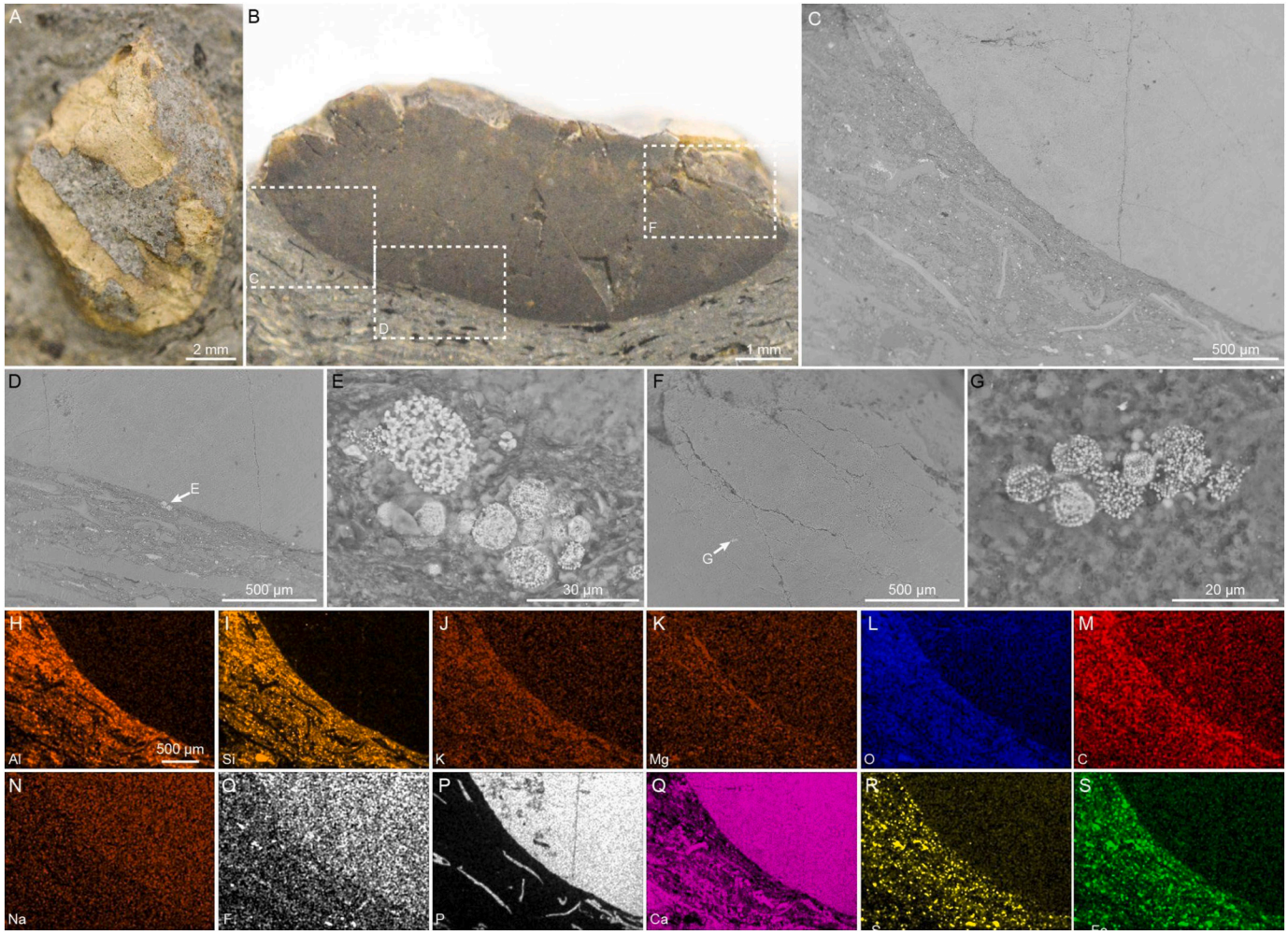

Fig. 19. Vertebrate coprolite from one of the schlacken layers of the Posidonienschiefer Fm. exposed near Ohmden (NPL00094456.000). (A) Reflected-light image of unprepared specimen. (B) Reflected-light image of cross-sectioned and polished specimen. (C-G) BSE-SEM images acquired with compositional contrast imaging mode. (C, D) Magnified views of boxes in (B), showing boundary between phosphatic coprolite and surrounding mudstone. (E) Magnified view of point in (D), showing framboidal pyrite in mudstone matrix. (F) Magnified view of box in (B), showing edge of phosphatic coprolite. (G) Magnified view of point in (F), showing framboidal pyrite within phosphatic material of coprolite. (H-S) EDS elemental maps of (C) with elemental labels in the lower left corners.

5.1. *Calcareous shells*

Calcareous shells (predominantly calcite and/or aragonite) in the Posidonia Shale represent ammonites, belemnites, bivalves, and echinoderms, as well as rare gastropods, rhynchonelliformean brachiopods, and serpulids. Some of the ammonites (aragonitic shell with an outer organic periostracum, Kulicki et al., 2015) and most of the *Parainoceramya* fossils (calcite shell; González-Casado et al., 2003) consist of calcium carbonate minerals with 'honeycomb microstructure' (Fig. 8D, G) (consistent with reports from Kulicki and Doguzhaeva, 1994; Tanabe et al., 2008; González-Casado et al., 2003). Hexagonal calcium carbonate plates in iridescent ammonites represents preservation of nacre in the Posidonia Shale. The nacre iridescence is low because the hexagonal aragonitic plates have been partially replaced with pyrite (Fig. 6C) and may also contain calcite pseudomorphs. These results suggest that at least some of the ammonite and bivalve fossils in the Posidonia Shale contain remains (or pseudomorphs) of original biominerals.

None of the ammonite fossils consist entirely of organic matter or pyrite. The fossils owe their golden-brown color to the presence of pyrite, but pervasive or complete pyritization was not observed. Instead, ammonite fossils consist of calcium carbonate and, more rarely, calcium phosphate minerals (Figs. 6, 7), even in cases where fossils contain coherent layers of carbonaceous material (e.g., Figs. 6B, F, 7B, D). These layers may be periostraca, but also resemble structures described in other studies (Muscente and Xiao, 2015a, 2015b) that formed through taphonomic demineralization of shells with significant organic matter (Muscente and Xiao, 2015a). Carbonaceous layers are preserved on top of calcite and some specimens consist of multiple varieties of calcite coating each other (e.g., Fig. 6B, F), which likely include: (1) original shell material; (2) pseudomorphs after aragonite produced through alteration; and (3) diagenetic minerals that formed due to geomicrobiological degradation of the shells (Muscente et al., 2017). Diagenetic calcite could be interpreted as periostracal mineralization, but the presence of hexagonal plates (and possibly nacre) implies the majority of the calcite comes from the actual shells; thus, Posidonia Shale ammonites are not simply periostracal films (Seilacher et al., 1976) or pyritized periostraca (Schmid-Röhl, 2021).

5.2. *Evidence of phosphatization*

Our results support the interpretation that exceptional Posidonia Shale fossils owe their preservation to phosphatization (Sinha et al., 2021; Lindgren et al., 2018), or preservation via replication of organic templates with nanometer- and micrometer-sized apatite crystals (Allison, 1988a; Martill, 1988; Wilby, 1993; Wilby and Whyte, 1995; Xiao

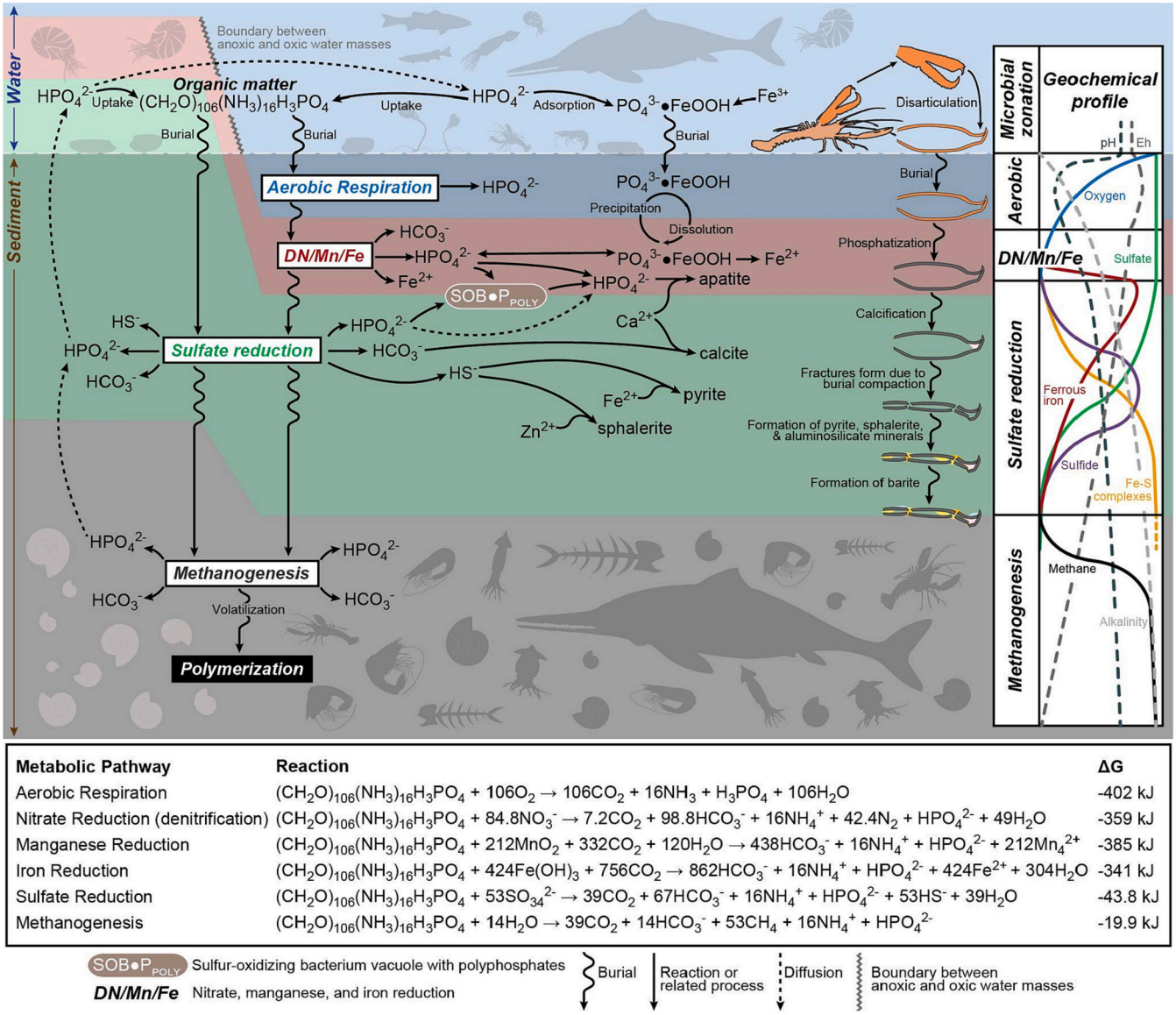

Metabolic Pathway	Reaction	ΔG
Aerobic Respiration	$(CH_2O)_{106}(NH_3)_{16}H_3PO_4 + 106O_2 \rightarrow 106CO_2 + 16NH_3 + H_3PO_4 + 106H_2O$	-402 kJ
Nitrate Reduction (denitrification)	$(CH_2O)_{106}(NH_3)_{16}H_3PO_4 + 84.8NO_3^- \rightarrow 7.2CO_2 + 98.8HCO_3^- + 16NH_4^+ + 42.4N_2 + HPO_4^{2-} + 49H_2O$	-359 kJ
Manganese Reduction	$(CH_2O)_{106}(NH_3)_{16}H_3PO_4 + 212MnO_2 + 332CO_2 + 120H_2O \rightarrow 438HCO_3^- + 16NH_4^+ + HPO_4^{2-} + 212Mn_4^{2+}$	-385 kJ
Iron Reduction	$(CH_2O)_{106}(NH_3)_{16}H_3PO_4 + 424Fe(OH)_3 + 756CO_2 \rightarrow 862HCO_3^- + 16NH_4^+ + HPO_4^{2-} + 424Fe^{2+} + 304H_2O$	-341 kJ
Sulfate Reduction	$(CH_2O)_{106}(NH_3)_{16}H_3PO_4 + 53SO_{34}^{2-} \rightarrow 39CO_2 + 67HCO_3^- + 16NH_4^+ + HPO_4^{2-} + 53HS^- + 39H_2O$	-43.8 kJ
Methanogenesis	$(CH_2O)_{106}(NH_3)_{16}H_3PO_4 + 14H_2O \rightarrow 39CO_2 + 14HCO_3^- + 53CH_4 + 16NH_4^+ + HPO_4^{2-}$	-19.9 kJ

Fig. 20. Geomicrobiological processes and fossil preservation across redox gradients. Diagram illustrates the geomicrobiological processes that occurred across the sediment-water interface (y-dimension) during deposition of the Posidonia Shale. It also illustrates variation in these processes across benthic marine environments with anoxic (left) and oxic (right) water masses (x-dimension). The processes include microorganism metabolic pathways that control organic matter (including soft tissue remains) degradation via decomposition. Such respiratory processes occur in distinct zones and depths in the water column and sediment in order of the Gibbs free energy changes (ΔG) of their reactions (Canfield and Thamdrup, 2009). The taphonomic pathway of a lobster claw, which owes its preservation to processes that occur below (sub)oxic water masses, is illustrated for reference.

Table 1
Fossil taxa/groups from the Posidonia Shale with the total number of specimens within each group analyzed using reflected light microscopy, SEM, and EDS.

Taxon/Group	Total Number Studied (Light Microscopy)	Light Microscopy, SEM, & EDS
Ammonoidea shells	24	8
Bivalvia shells	11	4
Belemnoidea rostra	7	3
Brachiopoda shells	1	1
Coleoidea gladii	6	5
Coprolite	1	1
Crocodylomorph tooth	1	1
Crustacea	12	8
Fish	2	2
Jet wood	5	3

and Knoll, 1999; Waloszek, 2003; Xiao and Schiffbauer, 2009; Schiffbauer et al., 2012; Hawkins et al., 2018; Muscente et al., 2019; Sinha et al., 2021). Although phosphatization represents one of many taphonomic processes that lead to exceptional preservation (Allison, 1988b; Briggs et al., 1993; Briggs and Wilby, 1996; Briggs, 2003; Butterfield, 2003; Xiao and Schiffbauer, 2009; Schiffbauer et al., 2014a; Muscente et al., 2015a, 2017), it receives much attention for its role in the preservation of cellular and subcellular details (Xiao and Knoll, 1999; Schiffbauer et al., 2012; Muscente et al., 2015a; Muscente et al., 2015b). Phosphatization can lead to the preservation of coleoid gladii, mantle tissues, and ink sacs (Muscente et al., 2019; Sinha et al., 2021); arthropod carapaces (Waloszek, 2003; Muscente et al., 2019; Sinha et al., 2021); coprolites and bromalites (Broce and Schiffbauer, 2017; Hawkins et al., 2018); vertebrate bones and soft tissues (Martill, 1988; Lindgren et al., 2018); and remains of mollusks (Wilby and Whyte, 1995; Mironenko, 2017), including their shells (Jurkowska and Kołodziej, 2013; Hoffmann et al., 2021). In the Posidonia Shale, apatite minerals

Table 2
Summary of pyrite framboid descriptive statistics (number of framboids measured per specimen, mean and maximum framboid diameter, standard deviation, and the percentage of ≥10 μm framboids). The crustacean specimens were collected from the Unterer Schiefer layers in the Dotternhausen quarry near Dormettingen, whereas the tooth and coprolite specimens are from one of the schlacken layers of the Posidonienschiefer Fm. exposed in the Kromer Quarry near Ohmden.

Specimen number	Type of specimen	Number of framboids measured		Mean framboid diameter (μm)		Maximum framboid diameter (μm)		Standard deviation		Skewness		Percentage of framboids diameter larger than 10 μm (%)		Percentage of framboids diameter smaller than 10 μm (%)	
		matrix	fossils	matrix	fossils	matrix	fossils	matrix	fossils	matrix	fossils	matrix	fossils	matrix	fossils
NPL94459 & NPL94458	Crustaceans	916	33	6.36	6.99	34.6	12.7	3.02	2.19	2.96	0.97	8.19	15.15	91.81	84.85
NPL94456	Coprolite	104	4	8.1	9.2	22.5	10.6	3.47	0.96	2.03	1.74	15.38	25	84.62	75
NPL94455	Crocodylomorph tooth	329	5	5.99	8.04	19.1	14.9	2.02	3.9	2.19	2.06	3.04	20	96.96	80

occur in ammonites, linguliformean brachiopods, coleoids, coprolites, crustaceans, and vertebrates, suggesting many fossils contain phosphatized remains.

Vampyropod coleoids represent the best examples of phosphatization; remains include gladii, ink sacs, and mantle tissues, which are preserved in three-dimensions as phosphatic structures with significant topography (Figs. 15, 16). Some fossils contain phosphatic remains of other labile tissues, like tentacles and ink ducts (Klug et al., 2021a; Jenny et al., 2019). None of these tissues originally contained phosphatic biominerals but consisted of biopolymers (e.g., chitin and melanin) resistant to degradation (Hunt and Nixon, 1981; Donovan and Toll, 1988; Doguzhaeva and Mutvei, 2003; Glass et al., 2012, 2013). Thus, coleoid tissues must have been transformed into apatite minerals through precipitation of phosphate derived from an environmental source.

Ammonites also provide unambiguous cases of phosphatization, with apatite minerals in a small proportion (25%) of shells. These shells have not been completely phosphatized as only parts of their walls and umbilici are preserved as apatite minerals (Fig. 7C, F-L). Phosphatization must have occurred since ammonite shells originally consisted of aragonite (Kulicki et al., 2015). Thus, phosphatization contributed to preservation of biomineralized skeletons and shells in addition to soft tissues.

The preservation of crustacean carapaces also hinged on phosphatization. A decapod carapace generally consists of a waxy outer epicuticle that acts as a barrier to diffusion and the chitinous inner procuticle that provides mechanical support. The procuticle sometimes contains biominerals (calcite, amorphous calcium carbonate, and carbonate apatite) that add rigidity (Kunkel et al., 2012; Kunkel, 2013) but is not heavily mineralized. The procuticle largely consists of chitin fibers (intermeshed with proteins), which can be preserved through transformation to more recalcitrant macromolecular carbonaceous materials (Briggs, 2003) or through secondary mineralization proecesses. Posidonia Shale crustaceans are preserved as phosphatic structures that retain evidence of biological microstructure and surface ornamentation (Figs. 12C, 13B, 14C, E). While, based on elemental analyses, carbonaceous materials were present but minimal, we suggest that the retention of finer-scale ornamentation would have been unlikely in the absence of phosphatization.

Phosphatization also contributed to preservation of both non-mineralized tissues and skeletal elements in vertebrate animals. Ichthyosaurs from the Posidonia Shale are purportedly preserved with phosphatized skin and integument (Keller, 1992; Lingham-Soliar, 2001; Lindgren et al., 2018) and fish bones (Fig. 11) and crocodylomorph teeth (Fig. 18) also consist of apatite minerals. These skeletal elements were originally composed of organic biomolecules (e.g., collagen) and bioapatite, a unique form of carbonate hydroxyapatite characterized by small (nm-sized) crystals, low OH- content, and poor crystallinity (Szpak, 2011; Combes et al., 2016). Accordingly, it is conceivable that the apatite minerals in fish bones, crocodylomorph teeth, and other vertebrate skeletal elements represent direct remains of bioapatite. While we did not directly note any change in crystal size, it is possible that some of the bones and teeth may have undergone secondary phosphate mineralization or recrystallization, much like what was observed for linguiliformean brachiopods. In either case, environments conducive to phosphatization are characterized by high concentrations of dissolved phosphate (Creveling et al., 2014; Muscente et al., 2015a), and are favorable for phosphatic skeleton preservation as the potential for bioapatite dissolution is limited.

Phosphatized fossils occur throughout Member II of the Posidonienschiefer Fm. Our review of fossil occurrence data (Fig. 3) suggests that exceptional preservation (and phosphatization) happened with the greatest frequency during deposition of the *D. semicelatum*, *H. exaratum,* and lower *H. elegans* subzones, which have the highest concentrations of coleoid, crustacean, fish, and marine reptile fossils. Our review demonstrates that phosphatized fossils occur in the Koblenzer, Hainzen (Fig. 16, S56–S62), Fleins (Figs. S51), and Unterer Schiefer (Figs. 13, S38–S44, S50) layers beneath the Unterer Stein as well as in the mudstones and condensed schlacken near the top of Member II (Figs. 7, 18, 19, S17, S18). These findings suggest that environments may have remained broadly conducive to phosphatization of ammonites and coprolites (if not also vertebrate bones, scales, and teeth) until the time of the *Hildoceras bifrons* zone.

5.3. Sources of phosphate

Fossil phosphatization typically occurs in environments conducive to phosphogenesis, or the precipitation of calcium phosphate minerals in sediment during diagenesis (Zhang et al., 1998; Muscente et al., 2015a). Phosphogenesis may produce phosphorites and other phosphatic facies as well as phosphatized fossils (Glenn et al., 1994) and can occur in any location where sediment pore water contains a high concentration of dissolved phosphate. Such pore water develops in response to physical and biogeochemical phenomena at multiple scales, including (1) large-scale processes that enhance phosphorus availability in basins; (2) meso-scale processes that facilitate phosphorus burial; and (3) local-scale processes that promote phosphorus remineralization, phosphate enrichment, and mineral precipitation in the sediment (Glenn et al., 1994). Phosphogenesis ultimately occurs in microenvironments where the phosphate concentration rises beyond supersaturation with respect to apatite, leading to precipitation in sediment.

The two major sources of phosphorus in marine sedimentary basins are oceanic upwelling of deep, nutrient-rich seawater and runoff of weathering-derived phosphate from landmasses. Although phosphogenic environments often develop in upwelling zones (Glenn et al., 1994), it is unlikely the Posidonia Shale Lagerstätte received phosphorus from upwelling. Data on the facies, stratigraphy, and palaeogeography indicate it was deposited within a silled basin (Fig. 2) that did not readily exchange water with the open Tethys Ocean (Röhl and Schmid-Röhl, 2005; Galasso et al., 2021). Therefore, the main input of phosphorus

must have been fluvial runoff, which implies phosphatized fossils of the Posidonia Shale Lagerstätte share their origin with the TOAE negative carbon isotope excursion. This excursion was purportedly caused by a climatic warming that increased delivery of nutrients to the ocean, and thereby, stimulated bioproductivity, expanded oxygen minimum zones, and increased organic matter burial (Jenkyns, 1985, 1988, 2010). Numerical models, osmium isotopes, and other detrital proxies support the inference that continental weathering rates were particularly high during the Pliensbachian-Toarcian transition (Montero-Serrano et al., 2015; Them et al., 2017b), perhaps two to five times greater than they were prior to the event (Them et al., 2017b). Such circumstances suggest the Southwestern German Basin received input of excess phosphorus, as compared to normal conditions, thus promoting phosphogenesis during the deposition of the Posidonia Shale. We posit the TOAE intensified the existing oxygen minimum zones and phosphate delivery to the Southwestern German Basin (e.g., Muscente et al., 2019), thus increasing the possibility of conditions that favored exceptional preservation during the TOAE interval.

Phosphorus enters sediment through burial of detrital apatite, phosphatic skeletal elements (e.g., linguliformean brachiopod shells, vertebrate bones, and teeth), organic matter, and iron oxide particulates (Glenn et al., 1994; Filippelli, 1997). Crustacean carapaces and vertebrate skeletons, which originally contained bioapatite, may have provided the phosphorus for their own mineralization (Martill, 1988; Briggs and Kear, 1994); however, phosphatization of coleoid gladii and ammonites must have been fueled by phosphate from other sources. Posidonia Shale TOC values indicate that the depositional environment had high organic matter burial rates, especial in the TOAE $\delta^{13}C$ excursion (Fig. 5), and the abundance of pyrite in the unit suggests that iron-(oxyhydr)oxide minerals were common in pore waters and bottom waters above the redox boundary (Riegraf et al., 1984; Röhl et al., 2001). Thus, the largest fractions of pore water phosphate probably came from (1) remineralization of phosphorus stored in organic matter, (2) desorption of phosphate from iron-(oxyhydr)oxide (FeOOH) particulates, and to a lesser degree (3) influx of phosphorus from continental weathering sources.

5.4. Origins of auxiliary minerals in the Posidonia Shale

Phosphatized and calcareous fossils largely consist of apatite minerals but also contain an array of 'auxiliary minerals' that contribute little mass to the fossils (e.g., pyrite, sphalerite, gypsum, barite, and aluminosilicate minerals). We observed one coleoid gladius (Fig. 16) that partly consists of calcite, and many partially pyritized ammonite and bivalve shells (Figs. 6, 8), but observed no other cases where labile tissues were replaced with auxiliary minerals. Auxiliary minerals occur as (1) mineral crusts on calcareous and phosphatized fossils; (2) void-filling cements in phosphatic remains; and (3) crack-filling cements within specimens. Such cross-cutting relationships imply these minerals formed after the apatite, and thus from processes following phosphatization. The occurrence of auxiliary minerals in cracks within phosphatic material suggest they also formed after phosphatized remains experienced burial compaction.

Diagenetic calcite occurs in ammonite shells (Fig. 6F), crustacean carapaces (Figs. 12E, 13E), coleoid gladii (Fig. 16C), wood (Fig. 17C), and vertebrate teeth (Fig. 18C). It forms from precipitation of bicarbonate produced by sedimentary microbial processes (Briggs and Kear, 1994; Briggs and Wilby, 1996; Schiffbauer et al., 2014b; Muscente et al., 2017), such as iron reduction, sulfate reduction, and methanogenesis (Fig. 20). In addition to increasing pore water alkalinity, these processes affect pore water pH thus influencing calcite and apatite mineral formation.

The rate of calcium phosphate precipitation is usually low under typical seawater pH (8.2). This is due to kinetic factors and the high ambient concentration of bicarbonate, which limits the availability of calcium by precipitating as calcite (Allison, 1988b; Briggs and Wilby, 1996). In low pH conditions fostered by microbial processes (e.g., aerobic respiration, iron, and sulfate reduction) around the redox boundary (Muscente et al., 2015a), existing calcium carbonate minerals are destablized and calcium phosphate precipitation is favored (Lucas and Prevot, 1991; Sagemann et al., 1999; Briggs, 2003). Below the redox gradient, microbial processes (i.e., methanogenesis) contribute to alkalinity and buffer pH reduction (Callow and Brasier, 2009). Thus, calcification tends to occur below the redox boundary after phosphatization (Schiffbauer et al., 2014b).

Pyrite and sphalerite likely formed in response to microbial sulfate reduction (MSR) (Fig. 20); sulfate-reducing microorganisms obtain energy by oxidizing organic matter and using sulfate, rather than oxygen, as an electron acceptor (Berner, 1970, 1984). This anaerobic process produces hydrogen sulfide, which can react with circumambient iron or zinc (depending on their availability) to precipitate sulfide minerals like pyrite (Briggs et al., 1996; Guan et al., 2017; Muscente et al., 2019) and sphalerite (Haymon et al., 1984; Spjeldnaes, 2002; Zabini et al., 2012; Hawkins et al., 2018; Muscente et al., 2019). Pyrite and sphalerite cements in Posidonia Shale fossils likely formed from hydrogen sulfide produced from degradation of labile tissues via MSR. When ammonite and bivalve shells provided nucleation sites and/or organic matter (Muscente and Xiao, 2015a), MSR drove partial pyritization of calcareous structures (Figs. 6, 8). The framboidal pyrite in the matrix around the fossils may have formed in the sediment (Berner, 1970, 1984) or water column during periods of bottom water euxinia (Them et al., 2018).

Pyrite framboids provide further evidence of oxygenation as framboid size distribution is a proxy for marine redox conditions in fine grained sediments (e.g., Wilkin et al., 1997; Wignall et al., 2005; Zhou and Jiang, 2009). The growth of framboids in euxinic settings is dependent on ambient buoyancy (Wilkin et al., 1996); due to hydrodynamic stability of framboids in suspension, they quickly sink through the sulfate reduction zone, and so have little time to grow (Wilkin et al., 1996; Wignall and Newton, 1998). In contrast, the duration of framboid growth in dysoxic settings is dependent on sedimentation rate; therefore, when sedimentation rate is slow, framboids have more time to grow in sediment pore waters and thus are larger than those from euxinic settings. Pyrite framboids from the three specimens (Table 2) are much more abundant in the matrix than on fossils, suggesting that dysoxia and euxinia are common background conditions during sedimentation and carcass emplacement. Moreover, framboids in the matrix are smaller than those on the fossils (both average and maximum framboid diameter, see Table 2). Framboid size data support the proposed Posidonia Shale phosphatization model, with fossilization occurring in more oxygenated intervals (e.g., Rodríguez-Tovar, 2021) even with common dysoxic/euxinic conditions.

We observed gypsum covering several fossils, which tends to occur in specimens encrusted by sphalerite and pyrite (Fig. 7). Unlike pyrite and sphalerite (Muscente et al., 2017), gypsum tends to form in shallow water environments with high rates of evaporation (Murray, 1964). Because the Posidonienschiefer Fm. was deposited below fair-weather wave base in a relatively deep marine basin, gypsum must have been produced by other processes. Because Posidonia Shale fossils contain high concentrations of pyrite and sphalerite, they may be prone to chemical weathering, which can form gypsum (Martens, 1925). Sulfide mineral (pyrite and sphalerite) oxidation produces sulfate that precipitates as gypsum through reaction with calcium ions released via dissolution of calcium carbonate and calcium phosphate minerals (Ritsema and Groenenberg, 1993). Therefore, recent chemical weathering represents the best explanation for the origin of the gypsum in Posidonienschiefer Fm. fossils.

Phosphatized crustacean fossils commonly contain white or gray aluminosilicate minerals (Figs. 12, 14); similar aluminosilicate minerals have been reported in fossils from other deposits (Orr et al., 1998, 2009; Gabbott et al., 2001; Page et al., 2008; Anderson et al., 2011; Cai et al., 2012; Muscente and Xiao, 2015b; Muscente et al., 2016; Muscente et al.,

2019), but in general, their origins remain uncertain, and causes of fossil aluminosilicification vary from one deposit to the next. Some deposits contain three dimensional fossils composed of authigenic clay minerals, suggesting they experienced aluminosilicification prior to compaction (Gabbott et al., 2001; Anderson et al., 2011; Cai et al., 2012). Other deposits, like the Burgess Shale, contain carbonaceous compressions with sheet silicate minerals that formed on the fossils due to late-stage volatilization of carbonaceous material (Orr et al., 1998; Butterfield et al., 2007; Page et al., 2008; Muscente et al., 2019); although recent work suggest some minerals formed before metamorphism (Anderson et al., 2021). Problematically, Posidonia Shale aluminosilicate minerals do not resemble any of these well-described cases of fossil-associated or fossil-related aluminosilicifcation. Instead, they have a distinct emplacement mechanism, occurring as cements within cracks of phosphatic material and thus must have followed phosphatization, burial compaction, and fracturing. Although Posidonia oil shales contain high organic matter concentrations, crustacean fossils contain little carbonaceous material. It is, therefore, unlikely that these aluminosilicate minerals represent sheet silicates produced by late-stage volatilization of organic matter. Given that aluminosilicate cements occur in cracks that also contain pyrite and sphalerite (Fig. 14E), they may have formed with those minerals in response to MSR, which lowers pH, and causes kaolinite mineralization in some environments (Gabbott et al., 2001). If so, aluminosilicate minerals in the Posidonia Shale could represent authigenic clays.

Some Posidonia Shale fossils are preserved with barite, which occurs as mineral crusts on the surfaces of specimens (Fig. 15G), veins that cross-cut lignite (Fig. 17A), and cements in the matrix around fossils (Figs. 11E, 13E). Similar occurrences of barite have been reported from other geologic deposits (Zabini et al., 2012; Broce and Schiffbauer, 2017), but their origins remain uncertain (Muscente and Xiao, 2015a; Muscente et al., 2019). In modern marine environments, there are four primary types of sedimentary barite: biogenic, hydrothermal, cold seep, and diagenetic barite (Raiswell et al., 2002; Griffith and Paytan, 2012); they differ in terms of crystal sizes and morphologies (Paytan et al., 2002; Griffith and Paytan, 2012). Biogenic barite forms within planktonic organisms and microenvironments near decaying organic matter, and typically consists of ellipsoidal crystals <5 μm in diameter, whereas hydrothermal and diagenetic barites occur as rosettes and diamond-shaped clusters of bladed, tabular crystals <20 μm in diameter (Paytan et al., 2002). In the Posidonia Shale, jet pieces are crosscut by veins of barite with tabular crystals (Fig. 17C) that resemble hydrothermal and diagenetic barites. Other fossils are preserved with barite crystals that resemble those of biogenic origin (Figs. 11E, 13E). Given the paucity of evidence for hydrothermal or volcanic influence in Southwestern Germany, barite in fossils most likely has a biogenic and/or diagenetic origin and may have precipitated due to sedimentary processing of biogenic barite near nucleation sites on the fossils. When biogenic barite becomes buried beneath the sulfate reduction zone (Fig. 20), it dissolves and releases barium to sulfate-depleted pore water. This barium-rich pore water diffuses upward into the sulfate reduction zone, where it may mix with sulfate-rich fluid and precipitate as diagenetic barite (Bolze et al., 1974; Brumsack and Gieskes, 1983; Paytan et al., 2002; Griffith and Paytan, 2012). Alternatively, barite may have formed in response to oxidative weathering of pyrite and sphalerite in the presence of Ba-rich fluid or a drop in barite solubility with diagenetic changes in fluid pressures and temperatures (Hanor, 2000; Broce and Schiffbauer, 2017). Additional studies, including sulfur isotope geochemistry of the barite, are required to test these hypotheses.

5.5. Origins of carbonaceous material

Ammonite shells (Figs. 6, 7), coleoid remains (Figs. 15, 16), and wood fossils (Fig. 17) consist, in part, of carbonaceous material (e.g., kerogen, bitumen, and lignite). Although carbonaceous material may be introduced through migration of kerogen (Muscente et al., 2018), it is more likely organic matter derived from the organisms themselves. Nevertheless, Posidonia Shale fossils do not fit within classic definitions of 'carbonaceous compression-type' fossils, as they exhibit topographic relief and contain little organic matter. Posidonia Shale wood did not collapse and coalesce into thin organic films (Rex and Chaloner, 1983; Rex, 1986; Martí Mus, 2014), but experienced burial compaction and carbonization, which transformed plant material into lignite; thus, jet represents in situ plant remains. Similarly, carbonaceous material on the surfaces of ammonite fossils may represent in situ remains of the periostraca and/or demineralized organic matrices of shells (Martí Mus, 2014; Muscente and Xiao, 2015a, 2015b). The absence of similar carbonaceous layers on bivalve and crustacean fossils implies that it did not migrate to ammonite surfaces.

Phosphatized coleoid ink sacs are separated from their gladius by a layer of carbonaceous material, but the significance of this is unclear. In some places, the layer contains sphalerite and pyrite (Fig. 16D), but we hesitate to interpret these minerals as evidence of tissue replacement, as none of the soft tissues are pyritized. Yet, the carbonaceous material does not occur within cracks of the ink sacs, which also contain pyrite and sphalerite. Given these observations, the carbonaceous layer most likely represents the muscular ink gland wall (Anadón, 2019) or some other consolidated organic matter from the animal.

5.6. Synthesis and preservational environment

Our data on fossil mineralization support a new taphonomic model for the Posidonia Shale Lagerstätte (Fig. 20). The exceptionally preserved fossils include articulated remains of marine reptiles, fishes, crinoids, and crustaceans. Given that prolonged decay and transport lead to disarticulation, it is likely the organisms did not travel far from their natural habitats, but instead, quickly reached the seafloor and were buried within 'soupy' fine-grained mud (Bandel and Knitter, 1986). Estimates suggest that this 'soupy' sediment, and the organisms' remains, decreased in thickness up to 98.5% with burial compaction (Einsele and Mosebach, 1955; Bandel and Knitter, 1986). Compaction occurred concurrently with fossil mineralization, but mineralization did not proceed rapidly or pervasively enough ensure fossils retained their original degree of three-dimensionality. Consequently, most fossils were preserved with definite but limited topographic relief.

Our data suggest phosphatization happened before other mineralization processes; many phosphatized fossils contain cracks that formed due to burial compaction of phosphatic remains. Cracks are filled with pyrite, sphalerite, and aluminosilicate minerals, implying those minerals formed long after the apatite minerals that compose the bulk of the fossils. If so, phosphatization must have occurred at relatively shallow depths within the sediment. We hypothesize that there may be a relationship between the amount of apatite in a specimen and the extent of its three dimensionality (in non-concretionary layers); the specimens with the greatest topographic relief may represent cases of particularly early or extensive phosphate mineralization, and vice versa. These observations suggest calcium phosphate and sulfide minerals formed within distinct zones of the sediment.

After the *D. tenuicostatum* chronozone, the Posidonia Shale contains little evidence of bioturbation outside of a few layers (Fig. 5) (van Acken et al., 2019; Rodríguez-Tovar, 2021), suggesting that its depositional environment developed chemically stratified sediment with microbial zonation (Callow and Brasier, 2009). Beginning at the top of the water column and proceeding down through the sediment (Fig. 20), microorganisms utilized metabolic pathways of respiration with the following oxidants as electron acceptors: oxygen, nitrate, manganese, iron, sulfate, and carbon dioxide (van Gemerden, 1993; Lyons et al., 1996). The transition between aerobic respiration (oxygen) and denitrification (nitrate reduction) zones signifies the boundary between oxic and anoxic water. It is generally thought that the conditions near this redox boundary, when below the sediment-water interface, favor phosphogenesis and fossil phosphatization (Muscente et al., 2015a), as many

physical and chemical processes that tend to promote phosphogenesis are sensitive to redox conditions (Schiffbauer et al., 2014a; Muscente et al., 2015a, 2019).

In general, there are four reasons that calcium phosphate minerals form around the redox boundary. First, phosphogenesis generally occurs in modern environments dominated by sulfate reduction (Arning et al., 2009); although all the metabolic pathways contribute to remineralization of phosphorus from organic matter, MSR is the primary source of remineralized phosphorus within sediment. Second, the cyclical iron pumping process enhances the phosphate concentration in the iron reduction zone; FeOOH particulates shuttle phosphate below the redox boundary and limit its efflux from pore water to bottom water (O'Brien et al., 1990; Glenn et al., 1994; Okubo et al., 2018). When FeOOH particulates with absorbed phosphate pass below the redox boundary, the reduction of FeOOH to ferrous iron releases phosphate to pore water. If the phosphate diffuses upward through the sediment profile, it may become re-adsorbed onto FeOOH particulates and repeat the cycle. Third, sulfur-oxidizing bacteria living just above the redox boundary store polyphosphates in their internal vacuoles. When exposed to hydrogen sulfide, these bacteria metabolize their polyphosphates and release phosphate to pore water (Brock and Schulz-Vogt, 2011). This polyphosphate metabolism can release enough phosphorus to force pore water phosphate concentrations beyond typical supersaturation levels and drive phosphorus mineralization (Schulz et al., 1999; Schulz and Schulz, 2005; Arning et al., 2008, 2009; Goldhammer et al., 2010). Lastly, anaerobic processes below the redox boundary (i.e., iron and sulfate reduction) create low pH conditions that destabilize calcium carbonate and favor calcium phosphate (Lucas and Prevot, 1991; Sagemann et al., 1999; Briggs, 2003). Altogether, these redox-sensitive processes suggest phosphatization occurred in the Southwestern German basin during times of bottom water oxygenation.

Our model (Fig. 20) supports several hypotheses concerning the redox conditions and geomicrobiological processes prevalent in the Posidonia Shale depositional environment (Röhl et al., 2001; Sinha et al., 2021). In particular, the model requires that deposition of the Posidonienschiefer Fm. (particularly Member II) was punctuated by short periods of bottom water oxygenation (Röhl et al., 2001; van Acken et al., 2019; Rodríguez-Tovar, 2021). According to our model, Konservat-Lagerstätte fossils were not preserved during prolonged periods of euxinia (Schouten et al., 2000; Röhl et al., 2001; Them et al., 2018), but rather, in environments with oxic and/or dysoxic bottom water, which have been recognized in paleoecological studies (Röhl et al., 2001; Röhl and Schmid-Röhl, 2005; Rodríguez-Tovar, 2021). Fossils may have been preserved during ephemeral pulses of oxygenation or within environments at the mobile boundaries of anoxic water bodies in oxygen minimum zones, as proposed in Muscente et al. (2019). In either case, it is likely the TOAE event enhanced exceptional preservation via phosphatization by (1) enhancing the flux of phosphate from the continent to the ocean and (2) promoting the release of phosphorus from sediment in environments with anoxic bottom water (Fig. 20), thereby trapping phosphate in the water column and making it available for phosphogenesis at places and times with bottom water oxygenation (Muscente et al., 2019; Sinha et al., 2021). Anoxic conditions likely delayed carcass disarticulation and inhibited soft-tissue decay prior to mineralization (Muscente et al., 2019; Sinha et al., 2021). Thus, the model corroborates the hypotheses that Oceanic Anoxic Events (Muscente et al., 2017; Martindale et al., 2017), and specifically the TOAE (Muscente et al., 2019; Sinha et al., 2021), amplify exceptional fossil preservation via phosphatization.

Posidonia Shale taphonomic pathways did not end with phosphatization; ammonite shells experienced a combination of geological and geomicrobiological processes during diagenesis. The traditional model for the preservation of ammonites relates their origin to four concurrent and interrelated processes in sediment: (1) microbial degradation, (2) secondary mineralization, (3) shell dissolution, and (4) burial compaction (Seilacher et al., 1976). Microorganisms broke down the labile tissues of the ammonite animal as well as the periostracum and organic matrix of its shell, producing chemical by-products (e.g., H_2S, HCO_3^-, HPO_4^{2-}, and H^+ among others, Fig. 20) that precipitated as secondary replacement minerals and cements (Briggs, 2003; Muscente et al., 2017). These metabolic pathways led to secondary mineralization of many shells with calcium carbonate, calcium phosphate, and pyrite. Concurrently, they caused a net production of H^+ (decline in pH) causing the dissolution of aragonite (Dullo and Bandel, 1988), and the compaction and preservation of the remaining organic matter (Seilacher et al., 1976). Our observations of ammonite shells with carbonaceous layers on calcite suggest aragonite dissolution did not always proceed to completion; specimens may, instead, represent degrees of taphonomic demineralization (Muscente and Xiao, 2015a, 2015b).

6. Implications for other Konservat-Lagerstätten: synthesis of new and existing data

Various workers have attempted to sort Konservat-Lagerstätten into functional categories (Seilacher, 1970; Seilacher and Westphal, 1971; Seilacher et al., 1985). Notably, Seilacher et al. (1985) proposed a conceptual framework for classifying Konservat-Lagerstätten with respect to three factors responsible for their formation: stagnation, obrution, and diagenesis (e.g., "bacterial sealing"). According to this classification, these factors do not represent distinct categories, but exemplify end-members of a continuous spectrum of environmental regimes that allow exceptional preservation, with Konservat-Lagerstätten distributed across this spectrum based on the relative degrees to which their preservation depended on the three processes. The classification does not consider other factors that affect fossilization (e.g., sea level, geochemical conditions, and environmental setting), and is based on qualitative assessments of the fossil record. Nevertheless, the classification has been widely cited in discussions of Konservat-Lagerstätten due its practicality and wide applicability.

The Posidonia Shale represents the archetype Konservat-Lagerstätten preserved in stagnant basins (Seilacher, 1970; Seilacher and Westphal, 1971; Seilacher et al., 1985). Other 'stagnation deposits' include the Solnhofen (Keupp et al., 2007), Nusplingen (Dietl and Schweigert, 2004), Crato (Heimhofer et al., 2010), Osteno (Pinna, 1985), Monte Solane (Giusberti et al., 2014), Pesciara di Bolca (Papazzoni and Trevisani, 2006), Las Hoyas (Buscalioni and Fregenal-Martínez, 2010), Vallecillo (Ifrim et al., 2007), El Rosario (Ifrim et al., 2007), and Ya Ha Tinda (Martindale et al., 2017; Muscente et al., 2019) deposits, among others. Many, if not most, stagnation deposits contain phosphatized fossils (Pinna, 1985; Briggs et al., 2005; Ifrim et al., 2007; Muscente et al., 2019), which occur in thinly-laminated fine-grained rocks with minimal, varying evidence of bottom water currents, bioturbation, and infaunal life. Most workers have argued that fossils were preserved in anoxic depositional environments (Dietl and Schweigert, 2004; Papazzoni and Trevisani, 2006; Ifrim et al., 2007; Heimhofer et al., 2010), but these interpretations remain open to debate; few deposits have received the same level of attention from fossil collectors, professional geologists, geochemists, and other academics as the Posidonia Shale. In this context, the taphonomy of the Posidonia Shale may shed light on the origins of these other deposits. Our findings indicate that exceptional fossils were preserved via phosphatization beneath (sub)oxic rather than anoxic bottom water (Fig. 20) and similar preservational models likely apply to other stagnation deposits with phosphatized fossils (Pinna, 1985; Briggs et al., 2005; Ifrim et al., 2007; Muscente et al., 2019).

Our Posidonia Shale taphonomic and paleoenvironmental model clarifies the role anoxia plays in exceptional preservation. Historically, it has been debated whether exceptional preservation occurred in depositional environments where anoxic conditions were limited to sediment or occurred in the water column (Seilacher et al., 1985; Kauffman, 1981; Röhl et al., 2001); our model implies the former. Although stagnation leads to development of low oxygen conditions, thus limiting predators, scavengers, and aerobic microbes that degrade soft tissues, bottom

water anoxia does not guarantee survival of soft tissues—anaerobic microorganisms break down organic matter as rapidly as aerobic bacteria (Allison, 1988b). Constructive processes, therefore, are necessary to ensure their preservation. Posidonia Shale phosphatized fossils, as well as those in other stagnation deposits (Pinna, 1985; Briggs et al., 2005; Ifrim et al., 2007; Muscente et al., 2019), support the hypothesis that stagnation leads to exceptional preservation by promoting fossil mineralization (Muscente et al., 2019; Sinha et al., 2021).

Our model implies that stagnation affects fossil mineralization in two ways. First, stagnation leads to the origination and expansion of anoxic water masses that trap nutrients in basins (Muscente et al., 2019; Sinha et al., 2021). These anoxic water masses do not guarantee survival of soft tissues, but their nutrients represent potential fuel for phosphatization in nearby environments with (sub)oxic bottom water (Fig. 20). Second, stagnation contributes to the formation of environments where the oxic/anoxic boundary is located just below the sediment-water interface. These environments variably develop (1) along the boundaries of anoxic water masses and (2) during ephemeral pulses of seafloor oxygenation in otherwise anoxic settings (Fig. 20). Such environments are conducive to fossil mineralization because they have steep redox gradients, which cause geomicrobiological processes (e.g., MSR and iron-pumping) to become localized to distinct sedimentary zones and microenvironments (Schiffbauer et al., 2014b; Muscente et al., 2015a, 2017); the focused geomicrobiological processes in these microenvironments produce chemical by-products that drive mineralization of soft tissues via phosphatization, silicification, pyritization, and other processes (Briggs et al., 1991, 1996; Muscente et al., 2015a, 2019; Guan et al., 2017). Although the same processes occur below anoxic bottom water, they are not localized to the sediment; as a result, chemical by-products of the processes may less frequently become sufficiently concentrated for soft tissue mineralization. If so, anoxic bottom water may actually hinder exceptional preservation by impeding preservational processes like phosphatization, silicification, and pyritization. This conclusion implies that exceptional preservation in stagnation deposits occurs in intermediate environments between fully oxic and anoxic conditions, unless there are high sedimentation rates that facilitate rapid burial, thereby ensuring organisms reach anaerobic zones of mineralization or bypass them (Seilacher et al., 1985; Brett et al., 2012; Schiffbauer et al., 2014b).

The model helps explain the geospatial distribution of Konservat-Lagerstätten. Exceptionally preserved fossil assemblages occur in clusters but are not homogeneously distributed across geographic and stratigraphic space (Muscente et al., 2017); the frequencies and characteristics of fossils vary across regions, even those representing seemingly uniform paleoenvironments. Konservat-Lagerstätten occur in Early Jurassic bituminous rocks at various locations in Europe (Doyle, 1990; Röhl et al., 2001; Ansorge, 2003), most of which were deposited beneath the European Epicontinental Sea during the TOAE (Fig. 2). Yet, some deposits yield far greater numbers of fossils than others (Ansorge, 2003), and some yield no fossils. In some basins, exceptionally preserved fossils seemingly occur at discrete locations; our model suggests these patterns reflect the complex relationship between anoxia and exceptional preservation. If stagnation deposits like the Posidonia Shale tend to form in environments with steep sediment-water interface redox gradients rather than locations where anoxic bottom water is present, exceptional preservation must have principally occurred along the boundaries of anoxic water masses during the TOAE. This interpretation accounts for the limited number of marine Lagerstätten of Toarcian age in Europe. Assuming anoxia dominated in the various basins of Europe during the TOAE, Lagerstätten may have only been preserved at intervals where the oxic/anoxic boundary intersected the seafloor.

7. Conclusions

Despite its long history of study, the Posidonienschiefer Fm. continues to provide new insights into the taphonomy of exceptionally preserved fossils. The Posidonia Shale is considered the best example of a stagnation deposit; our review and new data affirm that exceptional fossils were preserved via phosphatization during the TOAE, when widespread anoxic conditions existed in the Southwestern German Basin. Anoxic conditions promoted preservation of articulated multi-element skeletons and soft tissues by not simply limiting the activities of aerobic predators, scavengers, and microorganisms, but promoting the release of phosphorus from sediment, trapping the phosphate in the water column of the basin, and creating environments with steep redox gradients that were conducive to phosphatization. Contrary to traditional notions, the fossils were not preserved beneath anoxic bottom water; phosphatization occurred around the oxic/anoxic boundary, which was located *within* the sediment. Therefore, exceptional preservation happened in environments with at least partly oxygenated bottom water; oxygenation was not only necessary for benthic colonization, but it is also required for exceptional fossilization in the Posidonia Shale Lagerstätten. These environments were probably located along the boundaries of anoxic water masses or developed during ephemeral pulses of seafloor oxygenation. This new model provides an explanation for the heterogenous distribution of Toarcian-aged marine Lagerstätten across Europe and accounts for the origins of comparable stagnation deposits. Anoxia is crucial for exceptional preservation, but its role is indirect; the best environments for exceptional preservation do not have anoxic bottom water, but rather, steep redox gradients across the sediment-water interface, high sedimentation rates, and other factors (e.g., microbial mats) that enhance the likelihood organisms experience diagenetic mineralization and/or bypass major pathways of anaerobic decay.

Declaration of Competing Interest

The authors declare none.

Data availability

All data are provided in the supplemental material.

Acknowledgements

L. Boucher and L. Appleton are thanked for curatorial assistance. A. Schmidt-Röhl and A. Matzke are thanked for specimen access and E. Salgado Jaureguí is thanks for help with fieldwork. K. Horkley is thanked for assistance with the SEM at the MATfab facility and P. Orlandini is thanked for help with data collection at UT Austin. This work is supported by the Cornell Summer Research Institute at Cornell College to ADM, and by the National Science Foundation Division of Earth Sciences (NSF EAR) under awards #1660005 and #1848393 to RCM and awards #1652351 and #1636643 to JDS.

Appendix A. Supplementary data

Supplementary data to this article can be found online at https://doi.org/10.1016/j.earscirev.2023.104323.

References

Al-Suwaidi, A.H., Jenkyns, H.C., Hesselbo, S.P., Angelozzi, G.N., Baudin, F., Riccardi, A. C., Manceñido, M.O., Damborenea, S.E., 2010. First record of the early Toarcian Oceanic Anoxic Event from the Southern Hemisphere, Neuquén Basin, Argentina. J. Geol. Soc. 167, 633–636. https://doi.org/10.1144/0016-76492010-025.

Ajuaba, S., Sachsenhofer, R.F., Bechtel, A., Galasso, F., Gross, D., Misch, D., Schneebeli-Hermann, E., 2022. Biomarker and compound-specific isotope records across the Toarcian CIE at the Dormettingen section in SW Germany. Int. J. Earth Sci.(Geol Rundsch) 111, 1631–1661. https://doi.org/10.1007/s00531-022-02196-z.

Allison, P.A., 1988a. Konservat-Lagerstätten: causes and classifications. Paleobiology 14 (4), 331–344. https://doi.org/10.1017/S0094837300012082.

Allison, P.A., 1988b. The role of anoxia in the decay and mineralization of proteinaceous macro-fossils. Paleobiology 14, 139–154. https://doi.org/10.1017/S009483730001188X.

Allison, P.A., Briggs, D.E.G., 1991. Taphonomy of non-mineralized tissues. In: Allison, P. A., Briggs, D.E.G. (Eds.), Taphonomy: Releasing the Data Locked in the Fossil Record. Plenum Press, New York, pp. 25–70.
Allison, P.A., Briggs, D.E.G., 1993. Exceptional fossil record: distribution of exceptional preservation through the Phanerozoic. Geology 21, 527–530. https://doi.org/10.1130/0091-7613(1993)021<0527:EFRDOS>2.3.CO;2.
Anadón, R., 2019. Functional histology: The tissues of common coleoid cephalopods. In: Gestal, C., Pascual, S., Guerra, Á., Fiorito, G., Vieites, J. (Eds.), Handbook of Pathogens and Diseases in Cephalopods. Springer, Switzerland, pp. 39–84. https://doi.org/10.1007/978-3-030-11330-8_4.
Anderson, E., Schiffbauer, J.D., Xiao, S., 2011. Taphonomic study of Ediacaran organic-walled fossils confirms the importance of clay minerals and pyrite in Burgess Shale-type preservation. Geology 39, 643–646. https://doi.org/10.1130/G31969.1.
Anderson, R.P., Tosca, N.J., Gaines, R.R., Mongiardino Koch, N., Briggs, D.E.G., 2018. A mineralogical signature for Burgess Shale-type fossilization. Geology 46, 347–350. https://doi.org/10.1130/g39941.1.
Anderson, R.P., Tosca, N.J., Saupe, E.E., Wade, J., Briggs, D.E.G., 2021. Early formation and taphonomic significance of kaolinite associated with Burgess Shale fossils. Geology 49, 355–359. https://doi.org/10.1130/G48067.1.
Ansorge, J., 2003. Insects from the lower Toarcian of Middle Europe and England. Acta Zool. Cracov. 46, 291–310.
Arning, E.T., Birgel, D., Brunner, B., Peckmann, J., 2009. Bacterial formation of phosphatic laminites off Peru. Geobiology 7, 295–307. https://doi.org/10.1111/j.1472-4669.2009.00197.x.
Arning, E.T., Birgel, D., Schulz-Vogt, H.N., Holmkvist, L., Jørgensen, B.B., Larson, A., Peckmann, J., 2008. Lipid biomarker patterns of phosphogenic sediments from upwelling regions. Geomicrobiol J. 25, 69–82. https://doi.org/10.1080/01490450801934854.
Bandel, K., Knitter, H., 1986. On the origin and diagenesis of the bituminous Posidonia Shale (Toarcian) of Southern Germany. In: , 60. Mitteilungen aus dem Geologisch-Paläontologischen Institut (GPI) der Universität Hamburg, pp. 151–177.
Berner, R.A., 1970. Sedimentary pyrite formation. Am. J. Sci. 268, 1–23. https://doi.org/10.2475/ajs.268.1.1.
Berner, R.A., 1984. Sedimentary pyrite formation: an update. Geochim. Cosmochim. Acta 48, 605–615. https://doi.org/10.1016/0016-7037(84)90089-9.
Bolze, C.E., Malone, P.G., Smith, M.J., 1974. Microbial mobilization of barite. Chem. Geol. 13, 141–143. https://doi.org/10.1016/0009-2541(74)90006-0.
Brenner, K., 1976. Biostratinomische Untersuchungen im Posidonienschiefer (Lias epsilon, Unteres Toarcium) von Holzmaden (Württemberg, Süd-Deutschland). Zbl. Geol. Paläontol. 1976 (2), 223–226.
Brenner, K., Seilacher, A., 1978. New aspects about the origin of the Toarcian Posidonia Shales. Neues Jahrb. Geol. Palaontol. Abh. 157, 11–18.
Brett, C.E., Zambito, J.J., Hunda, B.R., Schindler, E., 2012. Mid-Paleozoic trilobite Lagerstätten: Models of diagenetically enhanced obrution deposits. Palaios 27, 326–345. https://doi.org/10.2110/palo.2011.p11-040r.
Briggs, D.E.G., 1991. Extraordinary fossils. Am. Sci. 79, 130–141.
Briggs, D.E.G., 2003. The role of decay and mineralization in the preservation of soft-bodied fossils. Annu. Rev. Earth Planet. Sci. 31, 275–301. https://doi.org/10.1146/annurev.earth.31.100901.144746.
Briggs, D.E.G., Bottrell, S.H., Raiswell, R., 1991. Pyritization of soft-bodied fossils: Beecher's Trilobite Bed, Upper Ordovician, New York State. Geology 19, 1221–1224. https://doi.org/10.1130/0091-7613(1991)019<1221:POSBFB>2.3.CO;2.
Briggs, D.E.G., Kear, A.J., 1994. Decay and mineralization of shrimps. Palaios 9, 431–456. https://doi.org/10.2307/3515135.
Briggs, D.E.G., Kear, A.J., Martill, D.M., Wilby, P.R., 1993. Phosphatization of soft-tissue in experiments and fossils. J. Geol. Soc. 150, 1035–1038. https://doi.org/10.1144/gsjgs.150.6.1035.
Briggs, D.E.G., Moore, R.A., Shultz, J.W., Schweigert, G., 2005. Mineralization of soft-part anatomy and invading microbes in the horseshoe crab Mesolimulus from the Upper Jurassic Lagerstätte of Nusplingen, Germany. Proc. R. Soc. B 272, 627–632. https://doi.org/10.1098/rspb.2004.3006.
Briggs, D.E.G., Raiswell, R., Bottrell, S.H., Hatfield, D., Bartels, C., 1996. Controls on the pyritization of exceptionally preserved fossils: an analysis of the lower Devonian Hunsrück Slate of Germany. Am. J. Sci. 296, 633–663.
Briggs, D.E.G., Wilby, P.R., 1996. The role of calcium carbonate-calcium phosphate switch in the mineralization of soft-bodied fossils. J. Geol. Soc. 153, 665–668. https://doi.org/10.1144/gsjgs.153.5.0665.
Broce, J.S., Schiffbauer, J.D., 2017. Taphonomic analysis of Cambrian vermiform fossils of Utah and Nevada, and implications for the chemistry of Burgess Shale-type preservation. Palaios 32, 600–619. https://doi.org/10.2110/palo.2017.011.
Brock, J., Schulz-Vogt, H.N., 2011. Sulfide induces phosphate release from polyphosphate in cultures of a marine Beggiatoa strain. ISME J. 5, 497–506.
Brumsack, H.J., Gieskes, J.M., 1983. Interstitial water trace-metal chemistry of laminated sediments from the Gulf of California, Mexico. Mar. Chem. 14, 89–106. https://doi.org/10.1016/0304-4203(83)90072-5.
Buch, L.von, 1839. In: Über den Jura von Deutschland, 1837. Abhandlungen der Königlich Preussischen Akademie der Wissenschaften, Berlin, pp. 49–135.
Buscalioni, A.D., Fregenal-Martínez, M.A., 2010. A holistic approach to the palaeoecology of the Las Hoyas Konservat-Lagerstätte (La Huérguina Formation, lower cretaceous, Iberian Ranges, Spain). J. Iber. Geol. 36 (2), 297–326. https://doi.org/10.5209/rev_JIGE.2010.v36.n2.13.
Butler, I.B., Rickard, D., 2000. Framboidal pyrite formation via the oxidation of iron (II) monosulfide by hydrogen sulphide. Geochim. Cosmochim. Acta 64 (15), 2665–2672. https://doi.org/10.1016/S0016-7037(00)00387-2.
Butterfield, N.J., 1990. Organic preservation of non-mineralizing organisms and the taphonomy of the Burgess Shale. Paleobiology 16, 272–286. https://doi.org/10.1017/S0094837300009994.
Butterfield, N.J., 2003. Exceptional fossil preservation and the Cambrian Explosion. Integr. Comp. Biol. 43, 166–177. https://doi.org/10.1093/icb/43.1.166.
Butterfield, N.J., Balthasar, U., Wilson, L.A., 2007. Fossil diagenesis in the Burgess Shale. Palaeontology 50, 537–543. https://doi.org/10.1111/j.1475-4983.2007.00656.x.
Cai, Y., Schiffbauer, J.D., Hua, H., Xiao, S., 2012. Preservational modes in the Ediacaran Gaojiashan Lagerstätte: pyritization, aluminosilicification, and carbonaceous compression. Palaeogeogr. Palaeoclimatol. Palaeoecol. 326–328, 109–117.
Callow, R.H.T., Brasier, M.D., 2009. Remarkable preservation of microbial mats in Neoproterozoic siliciclastic settings: Implications for Ediacaran taphonomic models. Earth Sci. Rev. 96, 207–219. https://doi.org/10.1016/j.earscirev.2009.07.002.
Canfield, D.E., Thamdrup, B., 2009. Towards a consistent classification scheme for geochemical environments, or, why we wish the term 'suboxic' would go away. Geobiology 7, 385–392. https://doi.org/10.1111/j.1472-4669.2009.00214.x.
Caruthers, A.H., Gröcke, D.R., Smith, P.L., 2011. The significance of an early Jurassic (Toarcian) carbon-isotope excursion in Haida Gwaii (Queen Charlotte Islands), British Columbia, Canada. Earth Planet. Sci. Lett. 307, 19–26. https://doi.org/10.1016/j.epsl.2011.04.013.
Caswell, B.A., Coe, A.L., Cohen, A.S., 2009. New range data for marine invertebrate species across the early Toarcian (Early Jurassic) mass extinction. J. Geol. Soc. 166, 859–872. https://doi.org/10.1144/0016-76492008-0831.
Combes, C., Cazalabou, S., Rey, C., 2016. Apatite biominerals. Minerals 6, 1–25. https://doi.org/10.3390/min6020034.
Creveling, J.R., Johnston, D.T., Poulton, S.W., Kotrc, B., März, C., Schrag, D.P., Knoll, A. H., 2014. Phosphorus sources for phosphatic Cambrian carbonates. Geol. Soc. Am. Bull. 126, 145–163. https://doi.org/10.1130/b30819.1.
Dahl, T.W., Hammarlund, E.U., Anbar, A.D., Bond, D.P.G., Gill, B.C., Gordon, G.W., Knoll, A.H., Nielsen, A.T., Schovsbo, N.H., Canfield, D.E., 2010. Devonian rise in atmospheric oxygen correlated to the radiation of terrestrial plants and large predatory fish. Proc. Natl. Acad. Sci. 107, 17911–17915. https://doi.org/10.1073/pnas.1011287107.
Dick, D.G., 2015. An ichthyosaur carcass-fall community from the Posidonia Shale (Toarcian) of Germany. Palaios 30, 353–361. https://doi.org/10.2110/palo.2014.095.
Dickson, A.J., Gill, B.C., Ruhl, M., Jenkyns, H.C., Porcelli, D., Idiz, E., Lyons, T.W., van den Boorn, S.H.J.M., 2017. Molybdenum-isotope chemostratigraphy and paleoceanography of the Toarcian Oceanic Anoxic Event (Early Jurassic). Paleoceanography 32, 813–829. https://doi.org/10.1002/2016PA003048.
Dietl, G., Schweigert, G., 2004. The Nusplingen Lithographic Limestone—A "fossil lagerstätte" of late Kimmeridgian age from the Swabian Alb (Germany). Riv. Ital. Paleontol. Stratigr. 110 (1), 303–309.
Doguzhaeva, L.A., Mutvei, H., 2003. Gladius composition and ultrastructure in extinct squid-like coleoids: Loligosepia, Trachyteuthis and Teudopsis. Rev. Paléobiol. 22, 877–894.
Donovan, D.T., Toll, R.B., 1988. The gladius in coleoid (Cephalopoda) evolution. In: Clarke, M.R., Trueman, E.R. (Eds.), Paleontology and Neontology of Cephalopods. Academic Press, London, pp. 89–101.
Doyle, P., 1990. Teuthid cephalopods from the lower Jurassic of Yorkshire. Palaeontology 33 (1), 193–207.
Dullo, W.C., Bandel, K., 1988. Diagenesis of molluscan shells: a case study. In: Wiedmann, J., Kullmann, J. (Eds.), Cephalopods-Present and Past. Schweizerbart, Stuttgart, pp. 719–729.
Edwards, C.T., Saltzman, M.R., Royer, D.L., Fike, D.A., 2017. Oxygenation as a driver of the Great Ordovician Biodiversification Event. Nat. Geosci. 10, 925–929. https://doi.org/10.1038/s41561-017-0006-3.
Einsele, G., Mosebach, R., 1955. Zur Petrographie, Fossilerhaltung und Entstehung der Gesteine des Posidonienschiefer im Schwäbischen Jura. Neues Jahrb. Geol. Palaontol. Abh. 101, 319–430.
Eriksson, M.E., De La Garza, R., Horn, E., Lindgren, J., 2022. A review of ichthyosaur (Reptilia, Ichthyopterygia) soft tissues with implications for life reconstructions. Earth Sci. Rev. 226, 103965 https://doi.org/10.1016/j.earscirev.2022.103965.
Feldmann, R.M., Villamil, T., Kauffman, E.G., 1999. Decapod and stomatopod crustaceans from mass mortality Lagerstatten: Turonian (Cretaceous) of Colombia. J. Paleontol. 73, 91–101. https://doi.org/10.1017/S0022336000027578.
Filippelli, G.M., 1997. Controls on phosphorus concentration and accumulation in oceanic sediments. Mar. Geol. 139, 231–240. https://doi.org/10.1016/S0025-3227(96)00113-2.
Gabbott, S.E., Norry, M.J., Aldridge, R.J., Theron, J.N., 2001. Preservation of fossils in clay minerals; a unique example from the Upper Ordovician Soom Shale, South Africa. Proc. Yorks. Geol. Soc. 53, 237–244. https://doi.org/10.1144/pygs.53.3.237.
Galasso, F., Schmid-Röhl, A., Feist-Burkhardt, S., Bernasconi, S.M., Schneebeli-Hermann, E., 2021. Changes in organic matter composition during the Toarcian Oceanic Anoxic Event (T-OAE) in the Posidonia Shale Formation from Dormettingen (SW-Germany). Palaeogeogr. Palaeoclimatol. Palaeoecol. 569, 110327 https://doi.org/10.1016/j.palaeo.2021.110327.
Gill, B.C., Lyons, T.W., Young, S.A., Kump, L.R., Knoll, A.H., Saltzman, M.R., 2011. Geochemical evidence for widespread euxinia in the later Cambrian Ocean. Nature 469, 80–83. https://doi.org/10.1038/nature09700.
Giusberti, L., Bannikov, A.F., Boscolo Galazzo, F., Fornaciari, E., Frieling, J., Luciani, V., Papazzoni, C.A., Roghi, G., Schouten, S., Sluijs, A., Bosellini, F.R., Zorzin, R., 2014. A new Fossil-Lagerstätte from the lower Eocene of Lessini Mountains (northern Italy): a multidisciplinary approach. Palaeogeogr. Palaeoclimatol. Palaeoecol. 403, 1–15. https://doi.org/10.1016/j.palaeo.2014.03.012.

Glass, K., Ito, S., Wilby, P.R., Sota, T., Nakamura, A., Bowers, C.R., Vinther, J., Dutta, S., Summons, R., Briggs, D.E.G., Wakamatsu, K., Simon, J.D., 2012. Direct chemical evidence for eumelanin pigment from the Jurassic period. Proc. Natl. Acad. Sci. 109, 10218–10223. https://doi.org/10.1073/pnas.1118448109.

Glass, K., Ito, S., Wilby, P.R., Sota, T., Nakamura, A., Bowers, C.R., Miller, K.E., Dutta, S., Summons, R.E., Briggs, D.E., Wakamatsu, K., 2013. Impact of diagenesis and maturation on the survival of eumelanin in the fossil record. Org. Geochem. 64, 29–37. https://doi.org/10.1016/j.orggeochem.2013.09.002.

Glenn, C.R., Föllmi, K.B., Riggs, S.R., Baturin, G.N., Grimm, K.A., Trappe, J., Abed, A.M., Galli-Olivier, C., Garrison, R.E., Ilyin, A.V., Jehl, C., Rohrlich, V., Sadaqah, R.M.Y., Schidlowski, M., Sheldon, R.E., Siegmund, H., 1994. Phosphorus and phosphorites: Sedimentology and environments of formation. Eclogae Geol. Helv. 87, 747–788.

Goldhammer, T., Bruchert, V., Ferdelman, T.G., Zabel, M., 2010. Microbial sequestration of phosphorus in anoxic upwelling sediments. Nat. Geosci. 3, 557–561. https://doi.org/10.1038/ngeo913.

González-Casado, J.M., Jiménez-Berrocoso, A., Cuevasm, C., Elorza, J., 2003. Strain determinations using inoceramid shells as strain markers: A comparison of the calcite strain gauge technique and the Fry method. J. Struct. Geol. 25, 1773–1778. https://doi.org/10.1016/S0191-8141(03)00040-3.

Griffith, E.M., Paytan, A., 2012. Barite in the ocean—occurrence, geochemistry and palaeoceanographic applications. Sedimentology 59, 1817–1835. https://doi.org/10.1111/j.1365-3091.2012.01327.x.

Gröcke, D.R., Hori, R.S., Trabucho-Alexandre, J., Kemp, D.B., Schwark, L., 2011. An open ocean record of the Toarcian Oceanic Anoxic Event. Solid Earth 2, 245–257. https://doi.org/10.5194/se-2-245-2011.

Guan, C., Zhou, C., Wang, W., Wan, B., Yuan, X., Chen, Z., 2014. Fluctuation of shelf basin redox conditions in the early Ediacaran: evidence from Lantian Formation black shales in South China. Precambrian Res. 245, 1–12. https://doi.org/10.1016/j.precamres.2014.01.003.

Guan, C., Wang, W., Zhou, C., Muscente, A.D., Wan, B., Chen, X., Yuan, X., Chen, Z., Ouyang, Q., 2017. Controls on the fossil pyritization: Redox conditions, sedimentary organic matter content and Chuaria preservation in the Ediacaran Lantian Biota. Palaeogeogr. Palaeoclimatol. Palaeoecol. 474, 26–35. https://doi.org/10.1016/j.palaeo.2016.05.013.

Hanor, J.S., 2000. Barite–celestine geochemistry and environments of formation. Rev. Mineral. Geochem. 40, 193–275. https://doi.org/10.2138/rmg.2000.40.4.

Haq, B.U., 2017. Jurassic Sea-level variations: a reappraisal. GSA Today 4–10. https://doi.org/10.1130/GSATG359A.1.

Haq, B.U., Hardenbol, J.A.N., Vail, P.R., 1988. Chronology of fluctuating sea levels since the Triassic. Science 235 (4793), 1156–1167. https://doi.org/10.1126/science.235.4793.1156.

Haq, B.U., Al-Qahtani, A.M., 2005. Phanerozoic cycles of sea-level change on the Arabian Platform. GeoArabia 10 (2), 127–160. https://doi.org/10.2113/geoarabia1002127.

Hardenbol, J., Thierry, J., Farley, M.B., Jacquin, T., Graciansky, P.-C.D., Vail, P.R., 1999. Mesozoic and Cenozoic sequence chronostratigraphic framework of european basins. In: de Graciansky, P.-C., Hardenbol, J., Jacquin, T., Vail, P.R. (Eds.), Mesozoic and Cenozoic Sequence Stratigraphy of European Basins. SEPM Society for Sedimentary Geology, pp. 3–13. https://doi.org/10.2110/pec.98.02.0003.

Hauff, B., 1921. Untersuchungen der Fossilfundstätten von Holzmaden in Posidonienschiefer des Oberen Lias Württembergs. Palaeontographica 64, 1–42.

Hauff, B., Hauff, R., 1981. Das Holzmadenbuch, 2nd ed. Published by the authors, Holzmaden.

Hawkins, A.D., Liu, H.P., Briggs, D.E.G., Muscente, A.D., Mckay, R.M., Witzke, B.J., Xiao, S., 2018. Taphonomy and biological affinitiy of three-dimensionally phosphatized bromalites from the middle Ordovician Winneshiek Lagerstätte, northeastern Iowa, USA. PALAIOS 33, 1–15. https://doi.org/10.2110/palo.2017.053.

Haymon, R.M., Koski, R.A., Sinclair, C., 1984. Fossils of hydrothermal vent worms from cretaceous sulfide ores of the Samail Ophiolite, Oman. Science 223, 1407–1409. https://doi.org/10.1126/science.223.4643.1407.

Heibert, K.F., 1988. The role of bacteria in the deposition and early diagenesis of the Posidonienschiefer, a Jurassic oil Shale in Southern Germany. In: University of Texas at Austin, p. 125 pp.. Masters Thesis (advisor: Folk, L).

Heimhofer, U., Ariztegui, D., Lenniger, M., Hesselbo, S.P., Martill, D.M., Rios-Netto, A.M., 2010. Deciphering the depositional environment of the laminated Crato fossil beds (Early cretaceous, Araripe Basin, North-eastern Brazil). Sedimentology 57, 677–694. https://doi.org/10.1111/j.1365-3091.2009.01114.x.

Heller, W., 1966. Untersuchungen zur sogenannten Hauterhaltung bei Ichthyosauriern aus dem Lias epsilon Holzmadens (Schwaben). Neues Jb. Mineral. Monat. 5, 304–317.

Hess, H., 1999. Lower Jurassic Posidonia Shale of Southern Germany. In: Hess, H., Ausich, W.I., Brett, C.E., Simms, M.J. (Eds.), Fossil Crinoids. Cambridge University Press, pp. 183–196.

Hoffmann, R., Morón-Alfonso, D., Klug, C., Tanabe, K., 2021. Report on ammonoid soft tissue remains revealed by computed tomography. Swiss J. Palaeontol. 140, 1–11. https://doi.org/10.1186/s13358-021-00226-y.

Hunt, S., Nixon, M., 1981. A comparative study of protein composition in the chitin-protein complexes of the beak, pen, sucker disc, radula and oesophageal cuticle of cephalopods. Comp. Biochem. Physiol. B 68, 535–546. https://doi.org/10.1016/0305-0491(81)90071-7.

Ifrim, C., Stinnesbeck, W., Frey, E., 2007. Upper cretaceous (Cenomanian-Turonian and Turonian-Coniacian) open marine plattenkalk deposits in NE Mexico. Neues Jahrb. Geol. Palaontol. Abh. 245, 71–81. https://doi.org/10.1127/0077-7749/2007/0245-0071.

Izumi, K., 2012. Formation process of the trace fossil Phymatoderma granulata in the lower Jurassic black shale (Posidonia Shale, southern Germany) and its paleoecological implication. Palaeogeogr. Palaeoclimatol. Palaeoecol. 353–355, 116–122. https://doi.org/10.1016/j.palaeo.2012.07.021.

Izumi, K., Rodríguez-Tovar, F.J., Piñuela, L., García-Ramos, J.C., 2014. Substrate-independent feeding mode of the ichnogenus Phymatoderma from the lower Jurassic self-sea deposits of central and western Europe. Sediment. Geol. 312, 19–30.

Jenkyns, H.C., 1985. The early Toarcian and Cenomanian-Turonian anoxic event in Europe: Comparisons and contrast. Geol. Rundsch. 74, 505–518. https://doi.org/10.1007/BF01821208.

Jenkyns, H.C., 1988. The early Toarcian (Jurassic) event: Stratigraphy, sedimentary and geochemistry evidence. Am. J. Sci. 288, 101–151. https://doi.org/10.2475/ajs.288.2.101.

Jenkyns, H.C., 2010. Geochemistry of oceanic anoxic events. Geochem. Geophys. Geosyst. 11 (3), 1–30. https://doi.org/10.1029/2009GC002788.

Jenny, D., Fuchs, D., Arkhipkin, A.I., Hauff, R.B., Fritschi, B., Klug, C., 2019. Predatory behavior and taphonomy of a Jurassic belemnoid coleoid (Diplobelida, Cephalopoda). Sci. Rep. 9, 7944. https://doi.org/10.1038/s41598-019-44260-w.

Jurkowska, A., Kołodziej, B., 2013. Taphonomic differentiation of Oxfordian ammonites from the Cracow Upland, Poland. Paläontol. Z. 87, 67–82. https://doi.org/10.1007/s12542-012-0149-x.

Kauffman, E.G., 1978. Benthic environments and paleoecology of the Posidonienschiefer (Toarcian). Neues Jahrb. Geol. Palaontol. Abh. 157, 18–36.

Kauffman, E.G., 1981. Ecological reappraisal of the German Posidonienschiefer (Toarcian) and the stagnant basin model. In: Gray, J., Boucot, A.J., Berry, W.B.N. (Eds.), Communities of the Past. Hutchinson Ross, Stroundsburg, pp. 311–381.

Keller, T., 1992. In: "Weichteil-Erhaltung" bei großen Vertebraten (Ichthyosauriern) des Posidonienschiefers Holzmadens (Oberer Lias, Mesozoikum Süddeutschlands)., 1. Darmstädter Beiträge zur Naturgeschichte, Kaupia, pp. 23–62.

Kemp, D.B., Izumi, K., 2014. Multiproxy geochemical analysis of a Panthalassic margin record of the early Toarcian oceanic anoxic event (Toyora area, Japan). Palaeogeogr. Palaeoclimatol. Palaeoecol. 414, 332–341. https://doi.org/10.1016/j.palaeo.2014.09.019.

Keupp, H., Koch, R., Schweigert, T., Viohl, G., 2007. Geological history of the Southern Franconian Alb – the area of the Solnhofen Lithographic Limestone. Neues Jahrb. Geol. Palaontol. Abh. 245, 3–21. https://doi.org/10.1127/0077-7749/2007/0245-0003.

Klug, C., Riegraf, W., Lehmann, J., 2012. Soft-part preservation in heteromorph ammonites from the Cenomanian-Turonian Boundary Event (OAE 2) in north-West Germany. Palaeontology 55, 1307–1331. https://doi.org/10.1111/j.1475-4983.2012.01196.x.

Klug, C., Schweigert, G., Fuchs, D., De Baets, K., 2021a. Distraction sinking and fossilized Coleoid predatory behavior from the German early Jurassic. Swiss J. Palaeontol. 140, 7. https://doi.org/10.1186/s13358-021-00218-y.

Klug, C., Schweigert, G., Hoffmann, R., Weis, R., De Baets, K., 2021b. Fossilized leftover falls as sources of palaeoecological data: a 'pabulite' comprising a crustacean, a belemnite and vertebrate from the early Jurassic Posidonia Shale. Swiss J. Palaeontol. 140, 10. https://doi.org/10.1186/s13358-021-00225-z.

Kulicki, C., Doguzhaeva, L.A., 1994. Development and calcification of the ammonitella shell. Acta Palaeontol. Polon. 39 (1), 17–44.

Kulicki, C., Tanabe, K., Landman, N.H., Kaim, A., 2015. Ammonoid shell microstructure. In: Klug, C., Korn, D., De Baets, K., Kruta, I., Mapes, R.H. (Eds.), Ammonoid Paleobiology: From Anatomy to Ecology. Springer, Dordrecht, pp. 321–357.

Krencker, F.N., Lindström, S., Bodin, S., 2019. A major sea-level drop briefly precedes the Toarcian oceanic anoxic event: Implication for early Jurassic climate and carbon cycle. Sci. Rep. 9, 12518. https://doi.org/10.1038/s41598-019-48956-x.

Kunkel, J.G., 2013. Modeling the calcium and phosphate mineralization of American lobster cuticle. Can. J. Fish. Aquat. Sci. 70, 1601–1611. https://doi.org/10.1139/cjfas-2013-0034.

Kunkel, J.G., Nagel, W., Jercinovic, M.J., 2012. Mineral fine structure of the American lobster cuticle. J. Shellfish Res. 31, 515–526. https://doi.org/10.2983/035.031.0211.

Küspert, W., 1982. Environmental changes during oil shale deposition as deduced from stable isotope ratios. In: Einsele, G., Seilacher, A. (Eds.), Cyclic and Event Stratification. Springer, Heidelberg, pp. 482–501.

Leventhal, J.S., 1983. An interpretation of carbon and sulfur relationships in Black Sea sediments as indicators of environments of deposition. Geochim. Cosmochim. Acta 47, 133–137. https://doi.org/10.1016/0016-7037(83)90097-2.

Levin, A., 2003. Oxygen minimum zone benthos: Adaptation and community response to hypoxia. In: Gibson, R.N., Atkinson, R.J.A. (Eds.), Oceanography and Marine Biology: An Annual Review, Volume 41. CRC Press, London, pp. 1–45. https://doi.org/10.1201/9780203180570.

Li, Y.-X., Bralower, T.J., Montañez, I.P., Osleger, D.A., Arthur, M.A., Bice, D.M., Herbert, T.D., Erba, E., Premoli Silva, I., 2008. Toward an orbital chronology for the early Aptian Oceanic Anoxic Event (OAE1a, ~120 Ma). Earth Planet. Sci. Lett. 271, 88–100. https://doi.org/10.1016/j.epsl.2008.03.055.

Lindgren, J., Sjövall, P., Thiel, V., Zheng, W., Ito, S., Wakamatsu, K., Hauff, R., Kear, B.P., Engdahl, A., Alwmark, C., Eriksson, M.E., Jarenmark, M., Sachs, S., Ahlberg, P.E., Marone, F., Kuriyama, T., Gustafsson, O., Malmberg, P., Thomen, A., Rodríguez-Meizoso, I., Uvdal, P., Ojika, M., Schweitzer, M.H., 2018. Soft-tissue evidence for homeothermy and crypsis in a Jurassic ichthyosaur. Nature 564, 359–365. https://doi.org/10.1038/s41586-018-0775-x.

Lingham-Soliar, T., 2001. The ichthyosaur integument: skin fibers, a means for a strong, flexible and smooth skin. Lethaia 34, 287–302. https://doi.org/10.1111/j.1502-3931.2001.tb00058.x.

Lucas, J., Prevot, L.E., 1991. Phosphates and fossil preservation. In: Allison, P.A., Briggs, D.E.G. (Eds.), Taphonomy: Releasing the Data Locked in the Fossil Record. Plenum Press, New York, pp. 389–409.

Lyons, W.B., Lent, R.M., Burnett, W.C., Chin, P., Landing, W.M., Orem, W.H., McArthur, J.M., 1996. Jellyfish Lake, Palau: regeneration of C, N, Si, and P in anoxic marine lake sediments. Limnol. Oceanogr. 41, 1394–1403.
Maisch, M.W., 2018. Neue Dactylioceratiden (Cephalopoda, Ammonitina) aus dem untersten Toarcium (Tenuicostatum-Zone) von Baden-Württemberg, Südwestdeutschland und ihre biochronologische Bedeutung. Jahreshefte Gesellschaft Naturkunde Württemberg 174, 143–172. https://doi.org/10.26251/jhgfn.174.2018.143-172.
Maisch, M.W., 2021. Neubewertung der Ammonitenfauna der Posidonienschiefer-Formation (Unterjura, Toarcium) von Baden-Württemberg, Südwestdeutschland. Jahreshefte Gesellschaft Naturkunde Württemberg 177, 265–347. https://doi.org/10.26251/jhgfn.177.2021.265-347.
Maisch, M.W., Matzke, A.T., 2017. Schichtenfolge und Ammonitenfauna des Grenzbereichs Unter-/Obertoarcium (Unterer Jura) von Dormettingen, Baden-Württemberg. Jahreshefte Gesellschaft Naturkunde Württemberg 173, 85–114. https://doi.org/10.26251/jhgfn.173.2017.085-114.
Martens, J.H.C., 1925. Sulphate minerals from weathering of shale near Ithaca, New York. J. Mineral. Soc. Am. 10, 175–176.
Martin, J.E., Suan, G., Suchéras-Marx, B., Rulleau, L., Schlögl, J., Janneau, K., Williams, M., Léna, A., Grosjean, A.S., Sarroca, E., Perrier, V., Fernandez, V., Cherruault, A.-L., Maxwell, E.E., Vincent, P., 2021. Stenopterygiids from the lower Toarcian of Beaujolais and a chemostratigraphic context for ichthyosaur preservation during the Toarcian Oceanic Anoxic Event. Geol. Soc. Lond., Spec. Publ. 514 https://doi.org/10.1144/SP514-2020-232.
Martí Mus, M., 2014. Interpreting 'shelly' fossils preserved as organic films: the case of hyolithids. Lethaia 47, 397–404. https://doi.org/10.1111/let.12066.
Martill, D.M., 1988. Preservation of fish in the cretaceous Santana Formation of Brazil. Palaeontology 31, 1–18.
Martill, D.M., Ibrahim, N., Brito, P.M., Baider, L., Zhouri, S., Loveridge, R., Naish, D., Hing, R., 2011. A new Plattenkalk Konservat Lagerstätte in the Upper cretaceous of Gara Sbaa, South-Eastern Morocco. Cretac. Res. 32, 433–446. https://doi.org/10.1016/j.cretres.2011.01.005.
Martindale, R.C., Aberhan, M., 2017. Response of macrobenthic communities to the Toarcian Oceanic Anoxic Event in northeastern Panthalassa (Ya Ha Tinda, Alberta, Canada). Palaeogeogr. Palaeoclimatol. Palaeoecol. 478, 103–120. https://doi.org/10.1016/j.palaeo.2017.01.009.
Martindale, R.C., Them, T.R., Gill, B.C., Marroquín, S.M., Knoll, A.H., 2017. A new early Jurassic (ca. 183 Ma) fossil Lagerstätte from Ya Ha Tinda, Alberta. Canada. Geology 45, 255–258. https://doi.org/10.1130/G38808.1.
Matzke, A.T., Maisch, M.W., 2019. Palaeoecology and taphonomy of a Seirocrinus (Echinodermata: Crinoidea) colony from the early Jurassic Posidonienschiefer Formation (Early Toarcian) of Dotternhausen (SW Germany). Neues Jahrb. Geol. Palaontol. Abh. 291 (1), 89–107. https://doi.org/10.1127/njgpa/2019/0791.
Maxwell, E.E., Vincent, P., 2016. Effects of the early Toarcian Anoxic Event on ichthyosaur body size and faunal composition in the southwest German Basin. Paleobiology 42, 117–126. https://doi.org/10.1017/pab.2015.34.
Maxwell, E.E., Cooper, S.L.A., Mujal, E., Miedema, F., Serafini, G., Schweigert, G., 2022. Evaluating the Existence of Vertebrate Deadfall Communities from the early Jurassic Posidonienschiefer Formation. Geosciences 2022 (12), 158. https://doi.org/10.3390/geosciences12040158.
Merdith, A.S., Williams, S.E., Collins, A.S., Tetley, M.G., Mulder, J.A., Blades, M.L., Young, A., Armistead, S.E., Cannon, J., Zahirovic, S., Müller, R.D., 2021. Extending full-plate tectonic models into deep time: linking the Neoproterozoic and the Phanerozoic. Earth-Sci. Rev. 214, 103477 https://doi.org/10.1016/j.earscirev.2020.103477.
McCann, T., 2008. The Geology of Central Europe, Vol. 2: Mesozoic and Cenozoic. The Geological Society, London.
Miller, K.G., Kominz, M.A., Browning, J.V., Wright, J.D., Mountain, G.S., Katz, M.E., Sugarman, P.J., Cramer, B.S., Christie-Blick, N., Pekar, S.F., 2005. The Phanerozoic record of global sea-level change. Science 310, 1293–1298. https://doi.org/10.1126/science.1116412.
Mironenko, A.A., 2017. Siphuncle soft-parts in the Upper Jurassic ammonite Kachpurites fulgens. Palaios 32, 153–157. https://doi.org/10.2110/palo.2016.068.
Mönnig, E., Franz, M., Schweigert, G., 2018. Der Jura in der Stratigraphischen Tabelle von Deutschland (STD 2016). Z. Dtsch. Ges. Geowiss. 169 (2), 225–246. https://doi.org/10.1127/zdgg/2018/0148.
Montero-Serrano, J.-C., Föllmi, K.B., Adatte, T., Spangenberg, J.E., Tribovillard, N., Fantasia, A., Suan, G., 2015. Continental weathering and redox conditions during the early Toarcian Oceanic Anoxic Event in the northwestern Tethys: insight from the Posidonia Shale section in the Swiss Jura Mountains. Palaeogeogr. Palaeoclimatol. Palaeoecol. 429, 83–99. https://doi.org/10.1016/j.palaeo.2015.03.043.
Müller, R.D., Cannon, J., Qin, X., Watson, R.J., Gurnis, M., Williams, S., Pfaffelmoser, T., Seton, M., Russell, S.H.J., Zahirovic, S., 2018. GPlates: building a virtual Earth through deep time. Geochem. Geophys. Geosyst. 19, 2243–2261. https://doi.org/10.1029/2018GC007584.
Müller, T., Karancz, S., Mattioli, E., Milovský, R., Pálfy, J., Schlögl, J., Segit, T., Šimo, V., Tomašových, A., 2020. Assessing anoxia, recovery and carbonate production setback in a hemipelagic Tethyan basin during the Toarcian Oceanic Anoxic Event (Western Carpathians). Glob. Planet. Chang. 195, 103366 https://doi.org/10.1016/j.gloplacha.2020.103366.
Murray, R.C., 1964. Origin and diagenesis of gypsum and anhydrite. Journal of Sedimentary Research 34, 512–523. https://doi.org/10.1306/74d710d2-2b21-11d7-8648000102c1865d.
Muscente, A.D., Allmon, W.D., Xiao, S., 2016. The hydroid fossil record and analytical techniques for assessing the affinities of putative hydrozoans and possible hemichordates. Palaeontology 59, 71–87. https://doi.org/10.1111/pala.12209.
Muscente, A.D., Czaja, A.D., Riedman, L.A., Colleary, C., 2018. Organic matter in fossils. In: White, W.M. (Ed.), Earth Science Series, Encyclopedia of Geochemistry. Springer, Switzerland, pp. 1–5. https://doi.org/10.1007/978-3-319-39193-9.
Muscente, A.D., Hawkins, A.D., Xiao, S., 2015a. Fossil preservation through phosphatization and silicification in the Ediacaran Doushantuo Formation (South China): a comparative synthesis. Palaeogeogr. Palaeoclimatol. Palaeoecol. 434, 46–62. https://doi.org/10.1016/j.palaeo.2014.10.013.
Muscente, A.D., Martindale, R.C., Schiffbauer, J.D., Creighton, A.L., Bogan, B.A., 2019. Taphonomy of the lower Jurassic Konservat-Lagerstätte at Ya Ha Tinda (Alberta, Canada) and its significance for exceptional fossil preservation during oceanic anoxic events. Palaios 34, 515–541. https://doi.org/10.2110/palo.2019.050.
Muscente, A.D., Michel, F.M., Dale, J.G., Xiao, S., 2015b. Assessing the veracity of Precambrian 'sponge' fossils using in situ nanoscale analytical techniques. Precambrian Res. 263, 142–156. https://doi.org/10.1016/j.precamres.2015.03.010.
Muscente, A.D., Schiffbauer, J.D., Broce, J., Laflamme, M., O'Donnell, K., Boag, T.H., Meyer, M., Hawkins, A.D., Huntley, J.W., McNamara, M., MacKenzie, L.A., Stanley, G.D., Hinman, N.W., Hofmann, M.H., Xiao, S., 2017. Exceptionally preserved fossil assemblage through geologic time. Gondwana Res. 48, 164–188. https://doi.org/10.1016/j.gr.2017.04.020.
Muscente, A.D., Xiao, S., 2015a. New occurrences of Sphenothallus in the lower Cambrian of South China: implications for its affinities and taphonomic demineralization of shelly fossils. Palaeogeogr. Palaeoclimatol. Palaeoecol. 437, 141–146. https://doi.org/10.1016/j.palaeo.2015.07.041.
Muscente, A.D., Xiao, S., 2015b. Resolving three-dimensional and subsurficial features of carbonaceous compressions and shelly fossils using backscattered electron scanning electron microscopy (BSE-SEM). Palaios 30, 462–481. https://doi.org/10.2110/palo.2014.094.
Nakagawa, Y., Takano, S., Firdaus, M.L., Norisuye, K., Hirata, T., Vance, D., Sohrin, Y., 2012. The molybdenum isotopic composition of the modern ocean. Geochem. J. 46, 131–141. https://doi.org/10.2343/geochemj.1.0158.
Nielsen, S.G., Rehkämper, M., Prytulak, J., 2017. Investigation and application of thallium isotope fractionation. Rev. Mineral. Geochem. 82, 759–798. https://doi.org/10.2138/rmg.2017.82.18.
O'Brien, G.W., Milnes, A.R., Weeh, H.H., Heggie, D.T., Riggs, S.R., Cullen, D.J., Marshall, J.F., Cook, P.J., 1990. Sedimentation dynamics and redox iron-cycling: Controlling factors for the apatite-glauconite association on the east Australian continental margin. In: Notholt, A.J.G., Jarvis, I. (Eds.), Phosphorite Research and Development, 52. Geological Society, London, pp. 61–86. https://doi.org/10.1144/GSL.SP.1990.052.01.06. Special Publication.
Okubo, J., Muscente, A.D., Luvizotto, G.L., Uhlein, G.J., Warren, L.V., 2018. Phosphogenesis, aragonite fan formation and seafloor environments following the Marinoan glaciation. Precambrian Res. 311, 24–36. https://doi.org/10.1016/j.precamres.2018.04.002.
Orr, P.J., Briggs, D.E.G., Kearns, S.L., 1998. Cambrian Burgess Shale animals replicated in clay minerals. Science 281, 1173–1175. https://doi.org/10.1126/science.281.5380.1173.
Orr, P.J., Kearns, S.L., Briggs, D.E.G., 2002. Backscattered electron imaging of fossils exceptionally-preserved as organic compressions. Palaios 17, 110–117. https://doi.org/10.1669/0883-1351(2002)017<0110:BEIOFE>2.0.CO;2.
Orr, P.J., Kearns, S.L., Briggs, D.E.G., 2009. Elemental mapping of exceptionally preserved "carbonaceous compression" fossils. Palaeogeogr. Palaeoclimatol. Palaeoecol. 277, 1–8. https://doi.org/10.1016/j.palaeo.2009.02.009.
Owens, J.D., Nielsen, S.G., Horner, T.J., Ostrander, C.M., Peterson, L.C., 2017. Thallium-isotopic compositions of euxinic sediments as a proxy for global manganese-oxide burial. Geochim. Cosmochim. Acta 213, 291–307. https://doi.org/10.1016/j.gca.2017.06.04.
Page, A., Gabbott, S.E., Wilby, P.R., Zalasiewicz, J.A., 2008. Ubiquitous Burgess Shale-style "clay templates" in low-grade metamorphic mudrocks. Geology 36, 855–858. https://doi.org/10.1130/G24991A.
Page, K.N., 2003. The lower Jurassic of Europe: its subdivision and correlation. GEUS Bull. 1, 23–59. https://doi.org/10.34194/geusb.v1.464.
Pannkoke, E., 1965. Die Ammonitenfauna des Posidonienschiefers von Holzmaden (Württemberg). Dissertation Universität Tübingen.
Papazzoni, C.A., Trevisani, E., 2006. Facies analysis, palaeoenvironmental reconstruction, and biostratigraphy of the "Pesciara di Bolca" (Verona, northern Italy): an early Eocene Fossil-Lagerstätte. Palaeogeogr. Palaeoclimatol. Palaeoecol. 242, 21–35. https://doi.org/10.1016/j.palaeo.2006.05.01.
Paytan, A., Mearon, S., Cobb, K., Kastner, M., 2002. Origin of marine barite deposits: Sr and S isotope characterization. Geology 30, 747–750. https://doi.org/10.1130/0091-7613(2002)030<0747:OOMBDS>2.0.CO.
Pinna, G., 1985. Exceptional preservation in the Jurassic of Osteno. Philos. Trans. R. Soc. Lond. B 311, 171–180. https://doi.org/10.1098/rstb.1985.014.
Prauss, M., Ligouis, B., Luterbacher, H., 1991. Organic matter and palynomorphs in the 'Posidonienschiefer' (Toarcian, Lower Jurassic) of southern Germany. In: Tyson, R. V., Pearson, T.H. (Eds.), Modern and Ancient Continental Shelf Anoxia, 58. Geological Society, London, pp. 335–351. https://doi.org/10.1144/GSL.SP.1991.058.01.2. Special Publications.
Poulton, S.W., Canfield, D.E., 2011. Ferruginous conditions: a dominant feature of the ocean through Earth's history. Elements 7 (2), 107–112. https://doi.org/10.2113/gselements.7.2.107.
Poulton, S.W., Raiswell, R., 2002. The low-temperature geochemical cycle of iron: from continental fluxes to marine sedi-ment deposition. Am. J. Sci. 302, 774–805. https://doi.org/10.2475/ajs.302.9.774.
Přikryl, T., Košták, M., Mazuch, M., Mikuláš, R., 2012. Evidence for fish predation on a coleoid cephalopod from the lower Jurassic Posidonia Shale of Germany. Neues

Jahrb. Geol. Palaontol. Abh. 263, 25–33. https://doi.org/10.1127/0077-7749/2012/0206.
Quenstedt, F.A., 1843. Das Flözgebirge Würtembergs mit besonderer Rücksicht auf den Jura. In: 1st ed. Tübingen (Laupp), p. 558 pp..
Quenstedt, F.A., 1858. Der Jura, Tübingen (Laupp), 842 pp.
Raiswell, R., Berner, R.A., 1985. Pyrite formation in euxinic and semi-euxinic sediments. Am. J. Sci. 285, 710–724. https://doi.org/10.2475/ajs.285.8.710.
Raiswell, R., Bottrell, S.H., Dean, S.P., Marshall, J.D., Carr, A., Hatfield, D., 2002. Isotopic constraints on growth conditions of multiphase calcite-pyrite-barite concretions in Carboniferous mudstones. Sedimentology 49, 237–254. https://doi.org/10.1046/j.1365-3091.2002.00439.x.
Raiswell, R., Canfield, D.E., 1998. Sources of iron for pyrite formation in marine sediments. Am. J. Sci. 298, 219–245. https://doi.org/10.2475/ajs.298.3.219.
Raiswell, R., Hardisty, D.S., Lyons, T.W., Canfield, D.E., Owens, J.D., Planavsky, N.J., Poulton, S.W., Reinhard, C.T., 2018. The iron paleoredox proxies: a guide to the pitfalls, problems and proper practice. Am. J. Sci. 318 (5), 491–526.
Reisdorf, A.G., Wetzel, A., Schlatter, R., Jordan, P., 2011. The Staffelegg Formation: a new stratigraphic scheme for the early Jurassic of northern Switzerland. Swiss J. Geosci. 104, 97–146. https://doi.org/10.1007/s00015-011-0057-1.
Reolid, M., Mattioli, E., Duarte, E.V., Ruebsam, W., 2021. The Toarcian Oceanic Anoxia Event: where do we stand? Geol. Soc. Lond., Spec. Publ. 514, 1–11. https://doi.org/10.1144/SP514-2021-74.
Rex, G.M., 1986. Further experimental investigations on the formation of plant compression fossils. Lethaia 19, 143–159. https://doi.org/10.1111/j.1502-3931.1986.tb00725.x.
Rex, G.M., Chaloner, W.G., 1983. The experimental formation of plant compression fossils. Palaeontology 26, 231–252.
Rhoads, D.C., Morse, J.W., 1971. Evolutionary and ecologic significance of oxygen-deficient marine basins. Lethaia 4, 413–428. https://doi.org/10.1111/j.1502-3931.1971.tb01864.x.
Riccardi, A.C., 2005. First teuthid cephalopod from the lower Jurassic of South America (Neuquén Basin, Argentina). Geol. Acta 3 (2), 179–184.
Riegraf, W., 1985. Mikrofauna, Biostratigraphie und Fazies im Unteren Toarcium Südwestdeutschlands und Vergleiche mit benachbarten Gebieten. Tübinger Mikropaläontologische Mitteilungen 3, 1–232.
Riegraf, W., Werner, G., Lörcher, F., 1984. In: Der Posidonienschiefer: Biostratigraphie, Fauna Und Fazies Des südwestdeutschen Untertoarciums (Lias ε). Ferdinand Enke Verlag, Stuttgart, p. 195.
Ritsema, C.J., Groenenberg, J.E., 1993. Pyrite oxidation, carbonate weathering, and gypsum formation in a drained potential acid sulfate soil. Soil Sci. Soc. Am. J. 57, 968–976. https://doi.org/10.2136/sssaj1993.03615995005700040015x.
Rodríguez-Tovar, F.J., 2021. Ichnology of the Toarcian Oceanic Anoxic Event: an understimated tool to assess palaeoenvironmental interpretations. Earth Sci. Rev. 216, 103579 https://doi.org/10.1016/j.earscirev.2021.103579.
Röhl, H.-J., Schmid-Röhl, A., Oschmann, W., Frimmel, A., Schwark, L., 2001. The Posidonia Shale (Lower Toarcian) of SW-Germany: an oxygen-depleted ecosystem controlled by sea level and palaeoclimate. Palaeogeogr. Palaeoclimatol. Palaeoecol. 165, 27–52. https://doi.org/10.1016/S0031-0182(00)00152-8.
Röhl, H.-J., Schmid-Röhl, A., 2005. Lower Toarcian (Upper Liassic) black shales of the central european epicontinental basin: a sequence stratigraphic case study from the SW German Posidonia Shale. The Deposition of Organic-Carbon-Rich Sediments: Models, Mechanisms, and Consequences. SEPM Spec. Publ. 82, 165–189. https://doi.org/10.2110/pec.05.82.0165.
Ruebsam, W., Al-Husseini, M., 2020. Calibrating the early Toarcian (Early Jurassic) with stratigraphic black holes (SBH). Gondwana Res. 82, 317–336. https://doi.org/10.1016/j.gr.2020.01.011.
Sagemann, J., Bale, S.J., Briggs, D.E.G., Parkes, J.R., 1999. Controls on the formation of authigenic minerals in association with decaying organic matter: an experimental approach. Geochim. Cosmochim. Acta 63, 1083–1095. https://doi.org/10.1016/S0016-7037(99)00087-3.
Savrda, C.E., Bottjer, D.J., 1989. Anatomy and implications of bioturbated beds in "black shale" sequences: examples from the Jurassic Posidonienschiefer (southern Germany). Palaios 4, 330–342. https://doi.org/10.2307/3514557.
Schiffbauer, J.D., Wallace, A.F., Broce, J., Xiao, S., 2014. Exceptional fossil conservation through phosphatization. In: Laflamme, M., Schiffbauer, J.D., Darroch, S.A.F. (Eds.), The Paleontological Society Papers, pp. 59–82.
Schiffbauer, J.D., Xiao, S., Cai, Y., Wallace, A.F., Hua, H., Hunter, J., Xu, H., Peng, Y., Kaufman, A.J., 2014b. A unifying model for Neoproterozoic-Palaeozoic exceptional fossil preservation through pyritization and carbonaceous compression. Nat. Commun. 5, 1–12. https://doi.org/10.1038/ncomms6754.
Schiffbauer, J.D., Xiao, S., Sen Sharma, K., Wang, G., 2012. The origin of intracellular structures in Ediacaran metazoan embryos. Geology 40, 223–226. https://doi.org/10.1130/G32546.1.
Schmid-Röhl, A., 2021. The lower Jurassic Posidonia Shale in the Swabian Alb Geopark—Geoeduction in an industrial environment. Geoconserv. Res. 4, 1–9. https://doi.org/10.30486/GCR.2021.1912251.1040.
Schmid-Röhl, A., Röhl, H.-J., 2003. Overgrowth on ammonite conchs: environmental implications for the lower Toarcian Posidonia Shale. Palaeontology 46, 339–352. https://doi.org/10.1111/1475-4983.00302.
Schmid-Röhl, A., Röhl, H.-J., Oschmann, W., Frimmel, A., Schwark, L., 2002. Palaeoenvironmental reconstruction of lower Toarcian epicontinental black shales (Posidonia Shale, SW Germany): Global versus regional control. Geobios 35, 13–20. https://doi.org/10.1016/S0016-6995(02)00005-0.
Schouten, S., van Kaam-Peters, H.M.E., Rijpstra, W.I.C., Schoell, M., Sinninghe Damste, J.S., 2000. Effects of an oceanic anoxic event on the stable isotopic composition of early Toarcian carbon. Am. J. Sci. 300, 1–22. https://doi.org/10.2475/ajs.300.1.1.
Schopf, T.J.M., 1978. Fossilization potential of an intertidal fauna: Friday Harbor, Washington. Paleobiology 4, 261–270. https://doi.org/10.1017/S0094837300005996.
Schulz, H.N., Brinkhoff, T., Ferdelman, T.G., Mariné, M.H., Teske, A., Jørgensen, B.B., 1999. Dense populations of a giant sulfur bacterium in namibian shelf sediments. Science 284, 493–495. https://doi.org/10.1126/science.284.5413.493.
Schulz, H.N., Schulz, H.D., 2005. Large sulfur bacteria and the formation of phosphorite. Science 307, 416–418. https://doi.org/10.1126/science.1103096.
Schweigert, G., 2013. A new record of the enigmatic lobster genus Stenodactylina Beurlen, 1928 (Crustacea: Decapoda: Erymidae) from the Middle Jurassic of South-Western Germany. Paläontol. Z. 87, 409–413. https://doi.org/10.1007/s12542-013-0163-7.
Schweigert, G., Garassino, A., Hall, R.L., Hauff, R.B., Karasawa, H., 2003. The lobster genus Uncina Quenstedt, 1851 (Crustacea: Decapoda: Astacidea: Uncinidae) from the lower Jurassic. Stuttgarter Beitr. Naturk. B332, 1–43.
Seilacher, A., 1970. Begriff und Bedeutung der Fossil-Lagerstätten. Neues Jb. Geol. Paläontol. Monat. 1970, 34–39.
Seilacher, A., 1980. Ammonite shells as habitats in the Posidonia Shales of Holzmaden—floats or benthic islands? Neues Jahrb. Geol. Palaontol. Abh. 159, 98–113. https://doi.org/10.1127/njgpm/1982/1982/98.
Seilacher, A., 2001. Concretion morphologies reflecting diagenetic and epigenetic pathways. Sediment. Geol. 143, 41–57. https://doi.org/10.1016/S0037-0738(01)00092-6.
Seilacher, A., Andalib, F., Dietl, G., Gocht, H., 1976. Preservational history of compressed Jurassic ammonites from Southern Germany. Neues Jahrb. Geol. Palaontol. Abh. 152, 307–356.
Seilacher, A., Reif, W.-E., Westphal, F., 1985. Sedimentological, ecological and temporal patterns of fossil Lagerstätten. Philos. Trans. R. Soc. B 311, 5–23. https://doi.org/10.1098/rstb.1985.0134.
Seilacher, A., Westphal, F., 1971. Fossil-Lagerstatten. In: Muller, G. (Ed.), Sedimentology of Parts of Central Europe, Guidebook 8. International Sedimentological Congress, Heidelberg, pp. 327–335.
Shaw, J.O., Briggs, D.E.G., Hull, P.M., 2021. Fossilization potential of marine assemblages and environments. Geology 49, 258–262. https://doi.org/10.1130/G47907.1.
Siebert, C., Nägler, T.F., von Blanckenburg, F., Kramers, J.D., 2003. Molybdenum isotope records as a potential new proxy for paleoceanography. Earth Planet. Sci. Lett. 211, 159–171. https://doi.org/10.1016/S0012-821X(03)00189-4.
Sinha, S., Muscente, A.D., Schiffbauer, J.D., Williams, M., Schweigert, G., Martindale, R. C., 2021. Global controls on phosphatization of fossils during the Toarcian Oceanic Anoxic Event. Sci. Rep. 11, 24087. https://doi.org/10.1038/s41598-021-03482-7.
Sinninghe Damsle, J.S., Wakeham, S.G., Kohnen, M.E.L., Hayes, J.M., de Leeuw, J.W., 1993. A 6,000-year sedimentary molecular record of chemocline excursions in the Black Sea. Nature 362, 827–829. https://doi.org/10.1038/362827a0.
Sperling, E.A., 2013. Tackling the 99%: can we begin to understand the paleoecology of the small and soft-bodied animal majority? In: Bush, A.M., Pruss, S.B., Payne, J.L. (Eds.), Paleontological Society Papers, Volume 19: Ecosystem Paleobiology and Geobiology. The Paleontological Society, pp. 77–86. https://doi.org/10.1017/S1089332600002692.
Sperling, E.A., Balthasar, U., Skovsted, C.B., 2018. On the edge of exceptional preservation: Insights into the role of redox state in Burgess Shale-type taphonomic windows from the Mural Formation, Alberta, Canada. Emerg. Top. Life Sci. 2, 311–323. https://doi.org/10.1042/etls20170163.
Sperling, E.A., Carbone, C., Strauss, J.V., Johnson, D.T., Narbonne, G.M., Macdonald, F. A., 2016. Oxygen, facies, and secular controls on the appearance of Cryogenian and Ediacaran body and trace fossils in the Mackenzie Mountains of northwestern Canada. Geol. Soc. Am. Bull. 128, 558–575. https://doi.org/10.1130/b31329.1.
Sperling, E.A., Wolock, C.J., Morgan, A.S., Gill, B.C., Kunzmann, M., Halverson, G.P., Macdonald, F.A., Knoll, A.H., Johnston, D.T., 2015. Statistical analysis of iron geochemical data suggests limited late Proterozoic oxygenation. Nature 523, 451–454. https://doi.org/10.1038/nature14589.
Spjeldnaes, N., 2002. Silurian bryozoans from Gotland fossilized in galena and sphalerite. GFF 124, 27–33. https://doi.org/10.1080/11035890201241027.
Suan, G., Nikitenko, B.L., Rogov, M.A., Baudin, F., Spangenberg, J.E., Knyazev, V.G., Glinskikh, L.A., Goryacheva, A.A., Adatte, T., Riding, J.B., Föllmi, K.B., Pittet, B., Mattioli, E., Lécuyer, C., 2011. Polar record of early Jurassic massive carbon injection. Earth Planet. Sci. Lett. 312, 102–113. https://doi.org/10.1016/j.epsl.2011.09.050.
Szpak, P., 2011. Fish bone chemistry and ultrastructure: Implications for taphonomy and stable isotope analysis. J. Archaeol. Sci. 38, 3358–3372. https://doi.org/10.1016/j.jas.2011.07.022.
Takashima, R., Nishi, H., Huber, B.T., Leckie, R.M., 2006. Greenhouse world and the Mesozoic Ocean. Oceanography 19, 82–92. https://doi.org/10.5670/oceanog.2006.07.
Tanabe, K., Kulicki, C., Landman, N.H., 2008. Development of the embryonic shell structure of Mesozoic Ammonoidea. Am. Mus. Novit. 3621, 1–19. https://doi.org/10.1206/588.1.
Them, T.R., Gill, B.C., Caruthers, A.H., Gerhardt, A.M., Gröcke, D.R., Lyons, T.W., Marroquín, S.M., Nielsen, S.G., Trabucho Alexandre, J.P., Owens, J.D., 2018. Thallium isotopes reveal protracted anoxia during the Toarcian (Early Jurassic) associated with volcanism, carbon burial, and mass extinction. Proc. Natl. Acad. Sci. 115, 6596–6601. https://doi.org/10.1073/pnas.1803478115.
Them, T.R., Gill, B.C., Caruthers, A.H., Gröcke, D.R., Tulsky, E.T., Martindale, R.C., Poulton, T.P., Smith, P.L., 2017a. High-resolution carbon isotope records of the

Toarcian Oceanic Anoxic Event (Early Jurassic) from North America and implications for the global drivers of the Toarcian carbon cycle. Earth Planet. Sci. Lett. 459, 118–126. https://doi.org/10.1016/j.epsl.2016.11.021.

Them, T.R., Gill, B.C., Selby, D., Gröcke, D.R., Friedman, R.M., Owens, J.D., 2017b. Evidence for rapid weathering response to climatic warming during the Toarcian Oceanic Anoxic Event. Sci. Rep. 7, 5003. https://doi.org/10.1038/s41598-017-05307-y.

Thies, D., Hauff, R.B., 2012. A speiballen from the lower Jurassic Posidonia Shale of South Germany. Neues Jahrb. Geol. Palaontol. Abh. 267, 117–124. https://doi.org/10.1127/0077-7749/2012/0301.

Thies, D., Waschkewitz, J., 2016. Redescription of Dapedium pholidotum (Agassiz, 1832) (Actinopterygii, Neopterygii) from the lower Jurassic Posidonia Shale, with comments on the phylogenetic position of Dapedium Leach, 1822. J. Syst. Palaeontol. 14 (4), 339–364. https://doi.org/10.1080/14772019.2015.1043361.

Thierry, J., 2000. Late Toarcian. In: Dercourt, J., Gaetani, M., Vrielynck, B., Barrier, E., Biju-Duval, B., Brunet, M.F., Cadet, J.P., Crasquin, S., Sandulescu, M. (Eds.), Atlas Peri-Tethys. Palaeogeographical Maps.

Tyson, R.V., Pearson, T.H., 1991. Modern and ancient continental shelf anoxia: an overview. In: Tyson, R.V., Pearson, T.H. (Eds.), Modern and Ancient Continental Shelf Anoxia, 58. Geological Society, London, pp. 1–24. https://doi.org/10.1144/GSL.SP.1991.058.01.01. Special Publications.

Ullmann, C., Boyle, R., Duarte, L., Hesselbo, S.P., Kasemann, S.A., Klein, T., Lenton, M., Piazza, V., Aberhan, M., 2020. Warm afterglow from the Toarcian Oceanic Anoxic Event drives the success of deep-adapted brachiopods. Sci. Rep. 10, 6549. https://doi.org/10.1038/s41598-020-63487-6.

Urlichs, M., 1977. The lower Jurassic in southwestern Germany. Stuttg. Beitr. Naturkunde B24, 1–41.

Urlichs, M., Wild, R., Ziegler, B., 1979. Fossilien aus Holzmaden. Stuttgarter Beiträge Naturkunde Ser. C 11, 1–34.

Valentine, J.W., 1989. How good was the fossil record? Clues from the Californian Pleistocene. Paleobiology 15, 83–94.

van Acken, D., Tütken, T., Daly, J.S., Schmid-Röhl, A., Orr, P.J., 2019. Rhenium-osmium geochronology of the Toarcian Posidonia Shale, SW Germany. Palaeogeogr. Palaeoclimatol. Palaeoecol. 534, 109294 https://doi.org/10.1016/j.palaeo.2019.109294.

van Gemerden, H., 1993. Microbial mats: a joint venture. Mar. Geol. 113, 3–25. https://doi.org/10.1016/0025-3227(93)90146-M.

van Loon, A.J., 2013. Ichthyosaur embryos outside the mother body: not due to carcass explosion but to carcass implosion. Palaeobiodivers. Palaeoenviron. 93, 103–109. https://doi.org/10.1007/s12549-012-0112-6.

Wang, Y., Ossa, F.O., Spangenberg, J.E., Wille, M., Schoenberg, R., 2021. Restricted oxygen-deficient basins on the northern european epicontinental shelf across the Toarcian carbon isotope excursion interval. Paleoceanogr. Paleoclimatol. 36, e2020PA004207 https://doi.org/10.1029/2020PA004207.

Waloszek, D., 2003. The "Orsten" window—a three-dimensionally preserved upper Cambrian meiofauna and its contribution to our understanding of the evolution of Arthropoda. Paleontol. Res. 7, 71–88. https://doi.org/10.2517/prpsj.7.71.

Wignall, P.B., Newton, R., 1998. Pyrite framboid diameter as a measure of oxygen deficiency in ancient mudrocks. Am. J. Sci. 298 (7), 537–552. https://doi.org/10.2475/ajs.298.7.537.

Wignall, P.B., Newton, R., Brookfield, M.E., 2005. Pyrite framboid evidence for oxygen-poor deposition during the Permian-Triassic crisis in Kashmir. Palaeogeogr. Palaeoclimatol. Palaeoecol. 216 (3–4), 183–188. https://doi.org/10.1016/j.palaeo.2004.10.009.

Wilby, P.R., 1993. The role of organic matrices in post-mortem phosphatization of soft tissues. Kaupia 2, 99–113.

Wilby, P.R., Whyte, M.A., 1995. Phosphatized soft tissues in bivalves from the Portland Roach of Dorset (Upper Jurassic). Geol. Mag. 132, 117–120. https://doi.org/10.1017/S001675680001147X.

Wilkin, R.T., Barnes, H.L., Brantley, S.L., 1996. The size distribution of framboidal pyrite in modern sediments: an indicator of redox conditions. Geochim. Cosmochim. Acta 60 (20), 3897–3912. https://doi.org/10.1016/0016-7037(96)00209-8.

Wilkin, R.T., Arthur, M.A., Dean, W.E., 1997. History of water-column anoxia in the Black Sea indicated by pyrite framboid size distributions. Earth Planet. Sci. Lett. 148 (3–4), 517–525. https://doi.org/10.1016/S0012-821X(97)00053-8.

Williams, M., Benton, M.J., Ross, A., 2015. The Strawberry Bank Lagerstätte reveals insights into early Jurassic life. J. Geol. Soc. 172, 683–692. https://doi.org/10.1144/jgs2014-144.

Xiao, S., Knoll, A.H., 1999. Fossil preservation in the Neoproterozoic Doushantuo phosphorite Lagerstätte, South China. Lethaia 32, 219–240. https://doi.org/10.1111/j.1502-3931.1999.tb00541.x.

Xiao, S., Schiffbauer, J.D., 2009. Microfossil phosphatization and its astrobiological implications. In: Seckbach, J., Walsh, M. (Eds.), From Fossils to Astrobiology: Record of Life on Earth and Search for Extraterrestrial Biosignatures. Springer, Netherlands, New York City, pp. 89–117.

Zabini, C., Schiffbauer, J.D., Xiao, S., Kowalewski, M., 2012. Biomineralization, taphonomy, and diagenesis of Paleozoic lingulide brachiopod shells preserved in silicified mudstone concretions. Palaeogeogr. Palaeoclimatol. Palaeoecol. 326–328, 118–127. https://doi.org/10.1016/j.palaeo.2012.02.010.

Zhang, Y., Yin, L., Xiao, S., Knoll, A.H., 1998. Permineralized fossils from the terminal Proterozoic Doushantuo Formation, South China. J. Paleontol. 72, 1–52. https://doi.org/10.1017/S0022336000059977.

Zhou, C., Jiang, S.Y., 2009. Palaeoceanographic redox environments for the lower Cambrian Hetang Formation in South China: evidence from pyrite framboids, redox sensitive trace elements, and sponge biota occurrence. Palaeogeogr. Palaeoclimatol. Palaeoecol. 271 (3–4), 279–286. https://doi.org/10.1016/j.palaeo.2008.10.024.